HAL
open science

A review of measurement-based assessment of aerosol direct radiative effect and forcing

H. Yu, Y. J. Kaufman, M. Chin, G. Feingold, L. A. Remer, T. L. Anderson, Yves Balkanski, N. Bellouin, O. Boucher, S. Christopher, et al.

To cite this version:

H. Yu, Y. J. Kaufman, M. Chin, G. Feingold, L. A. Remer, et al.. A review of measurement-based assessment of aerosol direct radiative effect and forcing. 2008. hal-00327959

HAL Id: hal-00327959

https://hal.science/hal-00327959v1

Preprint submitted on 18 Jun 2008

HAL is a multi-disciplinary open access archive for the deposit and dissemination of scientific research documents, whether they are published or not. The documents may come from teaching and research institutions in France or abroad, or from public or private research centers.

L'archive ouverte pluridisciplinaire **HAL**, est destinée au dépôt et à la diffusion de documents scientifiques de niveau recherche, publiés ou non, émanant des établissements d'enseignement et de recherche français ou étrangers, des laboratoires publics ou privés.

Atmos. Chem. Phys. Discuss., 5, 7647–7768, 2005
www.atmos-chem-phys.org/acpd/5/7647/
SRef-ID: 1680-7375/acpd/2005-5-7647
European Geosciences Union

Atmospheric Chemistry and Physics Discussions

A review of measurement-based assessment of aerosol direct radiative effect and forcing

H. Yu[1,2], Y. J. Kaufman[1], M. Chin[1], G. Feingold[3], L. A. Remer[1], T. L. Anderson[4], Y. Balkanski[5], N. Bellouin[6], O. Boucher[6,12], S. Christopher[7], P. DeCola[8], R. Kahn[9], D. Koch[10], N. Loeb[11], M. S. Reddy[12,13], M. Schulz[5], T. Takemura[14], and M. Zhou[15]

[1]Laboratory for Atmospheres, NASA Goddard Space Flight Center (GSFC), Greenbelt, USA
[2]Goddard Earth Science and Technology Center, University of Maryland, Baltimore County, Baltimore, USA
[3]NOAA Environmental Technology Laboratory (ETL), Boulder, USA
[4]University of Washington, Seattle, USA
[5]Laboratoire des Sciences du Climat et de l'Environnement, CEA/CNRS – LSCE, L'Orme des Merisiers, France
[6]Met Office, Exeter, UK
[7]University of Alabama, Huntsville, USA
[8]NASA Headquarters, Washington, D.C., USA
[9]NASA Jet Propulsion Laboratory (JPL), Pasadena, USA
[10]NASA Goddard Institute for Space Studies (GISS), New York, USA
[11]NASA Langley Atmospheric Research Center (LaRC), Hampton, USA

© 2005 Author(s). This work is licensed under a Creative Commons License.

[12] Laboratoire d'Optique Atmosphérique (LOA), Villeneuve d'Ascq, France
[13] NOAA Geophysical Fluid Dynamics Laboratory (GFDL), Princeton, USA
[14] Kyushu University, Fukuoka, Japan
[15] Georgia Institute of Technology, Atlanta, USA

Received: 27 May 2005 – Accepted: 27 June 2005 – Published: 30 August 2005

Correspondence to: H. Yu (hyu@climate.gsfc.nasa.gov)

Abstract

Aerosols affect the Earth's energy budget "directly" by scattering and absorbing radiation and "indirectly" by acting as cloud condensation nuclei and, thereby, affecting cloud properties. However, large uncertainties exist in current estimates of aerosol forcing because of incomplete knowledge concerning the distribution and the physical and chemical properties of aerosols as well as aerosol-cloud interactions. In recent years, a great deal of effort has gone into improving measurements and datasets. It is thus feasible to shift the estimates of aerosol forcing from largely model-based to increasingly measurement-based. Here we assess the aerosol optical depth, direct radiative effect (DRE) by natural and anthropogenic aerosols, and direct climate forcing (DCF) by anthropogenic aerosols, focusing on satellite and ground-based measurements supplemented by global chemical transport model (CTM) simulations. The multi-spectral MODIS measures global distributions of aerosol optical thickness (τ) on a daily scale, with a high accuracy of $\pm 0.03 \pm 0.05\tau$ over ocean. The annual average τ is about 0.14 over global ocean, of which about 21% is contributed by human activities, as determined by MODIS fine-mode fraction. The multi-angle MISR derives an annual average AOT of 0.23 over global land with an uncertainty of ~20% or ±0.05. These high-accuracy aerosol products and broadband flux measurements from CERES make it feasible to obtain observational constraints for the aerosol direct effect, especially over global ocean. A number of measurement-based approaches estimate the clear-sky DRE (on solar radiation) at the top-of-atmosphere (TOA) to be about $-5.5 \pm 0.2\,\mathrm{Wm^{-2}}$ (median ± standard error) over global ocean. Accounting for thin cirrus contamination of the satellite derived aerosol field will reduce the TOA DRE to $-5.0\,\mathrm{Wm^{-2}}$. Because of a lack of measurements of aerosol absorption and difficulty in characterizing land surface reflection, estimates of DRE over land and at the ocean surface are currently realized through a combination of satellite retrievals, surface measurements, and model simulations, and are less constrained. Over the ocean surface, the DRE is estimated to be $-8.8 \pm 0.4\,\mathrm{Wm^{-2}}$. Over land, an integration of satellite retrievals and model

simulations derives a DRE of $-4.9\pm0.7\,\mathrm{Wm}^{-2}$and $-11.8\pm1.9\,\mathrm{Wm}^{-2}$ at the TOA and surface, respectively. CTM simulations derive a wide range of DRE estimates that on average are smaller than the measurement-based DRE by about 30–40%, even after accounting for thin cirrus and cloud contamination.

Despite these achievements, a number of issues remain open and more efforts are required to address them. Current estimates of the aerosol direct effect over land are poorly constrained. Uncertainties of DRE estimates are also larger on regional scales than on a global scale and large discrepancies exist between different approaches. The characterization of aerosol absorption and vertical distribution remains challenging. The aerosol direct effect in the thermal infrared range and under cloudy condition remains relatively unexplored and quite uncertain, because of a lack of global systematic aerosol vertical profile measurements. A coordinated research strategy needs to be developed for integration and assimilation of satellite measurements into models to constrain model simulations. Hopefully, enhanced measurement capabilities in the next few years and high-level scientific cooperation, will further advance our knowledge.

1. Introduction

Aerosols participate in the Earth's energy budget "directly" by scattering and absorbing radiation (McCormick and Ludwig, 1967; Charlson and Pilat, 1969; Atwater, 1970; Mitchell Jr., 1971; Coakley et al., 1983) and "indirectly" by acting as cloud condensation nuclei and, thereby, affecting cloud properties (Twomey, 1977; Albrecht, 1989; Rosenfeld and Lensky, 1998). Moreover, the direct absorption of radiant energy by aerosols can influence the atmospheric temperature structure and, thereby, cloud formation - a phenomenon that has been labeled the "semi-direct effect" (Hansen et al., 1997; Ackerman et al., 2000; Koren et al., 2004). The addition of anthropogenic aerosols to the atmosphere may change the radiative fluxes at the top-of-atmosphere (TOA), at the surface, and within the atmospheric column. A positive radiative effect at the TOA indicates addition of the energy to the earth-atmosphere system (i.e., a warming

effect) whereas a negative effect indicates a net loss of energy (i.e., a cooling effect). Herein, we designate radiative perturbations by anthropogenic aerosols (both directly and indirectly) as "aerosol climate forcing (ACF)" and distinguish this from the "aerosol radiative effect (ARE) of the total aerosol (natural plus anthropogenic)". This review will focus on aerosol direct radiative effect (DRE) by the total aerosol and aerosol direct climate forcing (DCF) by the anthropogenic aerosol.

Recent reports summarize that the overall forcing by anthropogenic aerosols (ACF) is likely to be negative and may be comparable in magnitude to the positive forcing of about 2.4 Wm^{-2} by anthropogenic greenhouse gases (IPCC, 2001; Haywood and Boucher, 2001).Aerosol forcing assessments to date have been based largely on model calculations, although these models have been initialized and evaluated to some degree with satellite and surface measurements. Large uncertainties exist in current estimates of aerosol forcing because of incomplete knowledge concerning the distribution and the physical and chemical properties of aerosols as well as aerosol-cloud interactions. The uncertainty for the aerosol direct climate forcing (DCF) is about a factor of 2 to 3 whereas that for the indirect forcing is much larger and difficult to quantify (IPCC, 2001; Haywood and Boucher, 2001). These uncertainties raise questions about the interpretation of the 20th century temperature record (Anderson et al., 2003a) and complicate the assessment of aerosol impacts on surface-atmosphere interactions, the atmospheric boundary layer (Yu et al., 2002), global surface air temperatures (Charlson et al., 1992; Penner et al., 1992; Kiehl and Briegleb, 1993; Hansen et al., 1997), the hydrological cycle (Ramanathan et al., 2001a), photochemistry (Dickerson et al., 1997), and ecosystems (Chameides et al., 1999). Accordingly, the US Climate Change Research Initiative (CCRI) has specifically identified research on atmospheric concentrations and effects of aerosols as a top priority (NRC, 2001).

Reduction in these uncertainties requires a coordinated research strategy that will successfully integrate data from multiple platforms (e.g., ground-based networks, satellite, ship, and aircraft) and techniques (e.g., in-situ measurement, remote sensing, numerical modeling, and data assimilation) (Penner et al., 1994; Heintzenberg et al.,

1996; Kaufman et al., 2002a; Diner et al., 2004; Anderson et al., 2005). In recent years, a great deal of effort has gone into improving measurements and data sets, including the establishment of ground-based networks, the development and implementation of new and enhanced satellite sensors, and the execution of intensive field experiments in various aerosol regimes around the globe (e.g., Kahn et al., 2004a). As a result of these efforts it is now feasible to shift the estimates of DRE and DCF from largely model-based to increasingly measurement-based. In this new approach, satellite measurements provide the basis for the regional- to global-scale assessments and chemical transport models are used to interpolate and supplement the data in regions/conditions where observational data are not available. Measurements from ground-based networks and intensive field experiments are required for evaluating both the satellite retrievals and the model simulations. Model simulation is an indispensable tool for estimating past aerosol forcing and projecting future climate due to changes in atmospheric aerosols and observations can be used to improve and constrain model simulations of aerosol impacts through synthesis and integration (e.g., Collins et al., 2001; Yu et al., 2003). AEROCOM, an international initiative of scientists interested in aerosols and climate (http://nansen.ipsl.jussieu.fr/AEROCOM/), is documenting and intercomparing more than a dozen models and a large number of observations to identify and reduce the uncertainty in current global aerosol assessments (Kinne et al., 2005; Textor et al., 2005).

The US Climate Change Science Program (CCSP) is developing and extending its research activities to support policymaking and adaptive management. The present review is one of three aerosol-related reports being prepared for CCSP. The purposes of this review are (1) to review measurement-based understanding of tropospheric aerosol and their direct effects; (2) to estimate uncertainty associated with them through examining the differences among various estimates; and (3) to explore the use of recent measurements to improve the performance of model simulations. Specifically, we will:

– Assess the global aerosol distribution and DRE using satellites supplemented by

chemical transport models.

- Assess the anthropogenic component, using satellite data and models.
- Evaluate these assessments against surface network data and field experiments and compare them to model estimates.

Section 2 is an overview of factors determining DRE and DCF and of recent progress characterizing these factors. Global and regional comparisons among different measurements/simulations are presented in Sect. 3 for aerosol optical depth, DRE and DCF (solar and clear-sky). We discuss outstanding issues in Sect. 4. Our findings are summarized in Sect. 5.

2. Recent progress in characterizing tropospheric aerosols and assessing the aerosol direct effect

The aerosol direct radiative effect and its potential influences on climate were proposed and debated during the late 1960s and early 1970s (e.g., McCormick and Ludwig, 1967; Charlson and Pilat, 1969; Atwater, 1970; Mitchell Jr., 1971). The interactions between aerosols and solar radiation are determined by a combination of aerosol properties (loading, chemical composition, size distribution, shape), surface properties (e.g., spectral and angular variations of surface albedo), clouds (cloud fraction, optical depth, and vertical distribution), and geographical parameters (latitude, season). Assumptions associated with radiative transfer (RT) modeling also influence the assessment of the aerosol direct effect. For lack of data and computational resources, even the sign of the aerosol effect on global radiation (warming or cooling) was uncertain. Nevertheless, these pioneering studies highlighted the importance of acquiring better information concerning aerosols, and thereby inspired substantial research efforts in the intervening decades. Below is an overview of how a variety of factors determine the aerosol direct effect and how recent observations have advanced our knowledge.

2.1. Aerosol optical properties

The complex interaction of aerosols with radiation is usually understood using three optical parameters: aerosol optical thickness or depth (AOT, AOD, τ), the single-scattering albedo (SSA, ω_0), and the phase function. Aerosol optical thickness measures the magnitude of aerosol extinction (due to scattering and absorption) integrated in the vertical column. It is an e-folding length of the decrease of direct beam when traveling through the aerosol layer. Single-scattering albedo (SSA or ω_0) is the ratio of the scattering coefficient to the extinction coefficient, measuring the relative importance of scattering and absorption. The aerosol effect on the TOA radiative budget switches from net cooling to net warming at a certain value of SSA, depending on surface albedo (e.g., Charlson and Pilat, 1969; Atwater, 1970; Mitchell Jr., 1971; Hansen et al., 1997). The angular distribution of scattering radiation is described by the phase function, i.e., a ratio of the scattered intensity at a specific direction to the integral of the scattered intensity at all directions. In principle, given the size distribution of an assumed spherical aerosol, the phase function can be calculated from Mie theory (van de Hulst, 1981; Bohren and Huffman, 1983). In practice, approximations such as the Henyey-Greenstein (HG) phase function (Henyey and Greenstein, 1941) have been used in most radiative transfer models (e.g., Fu and Liou, 1993). The HG phase function is defined in terms of a single parameter – the asymmetry factor (g) – with g=1 for completely forward scattering and g=0 for symmetric (e.g. Rayleigh) scattering. Typical values of g range from 0.5 to 0.8.

These aerosol optical properties vary with the wavelength of radiation. The wavelength-dependence of optical depth is usually represented by the Ångström exponent (Ångström, 1929, 1930), with high values of Ångström exponent indicative of small particles and low values representative of large particles. Generally, at visible wavelengths, the single-scattering albedo decreases with wavelength for non-dust aerosols and increases for dust aerosols (Dubovik et al., 2002). The asymmetry factor g decreases with wavelength because of the decrease in the scattering-effective particle

size (e.g., Hansen and Travis, 1974).

Aerosol optical properties also depend strongly on the size distribution. Therefore any factors affecting the size distribution will impact the optical properties. One critical factor is the relative humidity (RH). Some aerosol types are hygroscopic, meaning that they grow as they take up water vapor. As a result, their size increases and their refractive indices change, in turn leading to changes in their optical properties. This effect is non-linear and varies with aerosol composition. For example, as RH increases from 40% to 80%, the scattering cross section of sulfate-dominated aerosol doubles, whereas it increases by only 10–40% for smoke over the same RH range (Hobbs et al., 1997; Kaufman et al., 1998). The response of the absorption coefficient to increasing RH is uncertain, although theoretical studies indicate it should be much smaller than that for the scattering coefficient (Redemann et al., 2001). Consequently, for hygroscopic aerosol, SSA increases with RH. In addition, g increases with increasing RH and particle size.

In contrast to greenhouse gases, aerosol loading and optical properties exhibit large spatial and temporal variability. Due to variability in sources and sinks, different aerosol components are associated with different geographical areas, and the residence time in the troposphere is relatively short (about 1 week). The vertical distribution of aerosol varies substantially, which is determined by injection height and a variety of atmospheric processes. Such variations complicate the estimate of aerosol direct effect under cloudy skies and in the thermal infrared region. The way of mixing of different species in aerosols can have a significant effect on aerosol optical properties. In reality, different chemical species can be in the same particles (internal mixing) or different particles (external mixing). While mixture state has little effect on the scattering and/or asymmetry factor (e.g., Chylek et al., 1995; Pilinis et al., 1995; McMurry et al., 1996; Malm and Kreidenweis, 1997), it can have a great effect on the absorption efficiency. Light absorption of a mixture of black carbon and transparent particles is significantly higher for internal mixing than for external mixing, resulting in a smaller SSA (Horvath, 1993; Chylek et al., 1995; Jacobson, 2000, 2001) and higher absorption efficiency

(Martins et al., 1998).

Errors in the estimation of aerosol optical properties can have a tremendous impact on the estimate of aerosol direct radiative effect. In recent years, the characterization of aerosols has been significantly improved through intensive field experiments, ground-based network, satellite remote sensing and its integration with model simulations, as summarized in the following.

2.1.1. Ground-based networks

AERONET: The AEROsol Robotic Network (AERONET) program is a federated remote sensing network of well-calibrated sun photometers and radiometers. AERONET includes about 200 sites around the world, covering all major tropospheric aerosol regimes (Holben et al., 1998, 2001). Spectral measurements of sun and sky radiance are calibrated and screened for cloud-free conditions (Smirnov et al., 2000). AERONET stations provide direct, calibrated measurements of spectral AOD (normally at wavelengths of 440, 670, 870, and 1020 nm) and provide inversion-based retrievals of a variety of effective, column-mean properties such as single-scattering albedo, and size distributions, phase function and asymmetry factor (Holben et al., 1998, 2001; Dubovik et al., 2000, 2002; Dubovik and King, 2001). Because of uniform calibration, cloud-screening, and retrieval methods, uniform data are available for all stations, some of which have operated for over 10 years. These data constitute a high-quality, ground-based aerosol climatology and, as such, have been widely used for aerosol process studies, as well as for evaluation and validation of model simulation and satellite remote sensing applications (e.g., Chin et al., 2002; Yu et al., 2003; Remer et al., 2005; Kahn et al., 2005a). It should be noted, however, that the inversion-based retrieval products have yet to be systematically validated by comparison to in situ measurements.

IMPROVE: The Interagency Monitoring of Protected Visual Environments (IMPROVE) network was established by the federal land management agencies and the Environmental Protection Agency in 1985 (Malm et al., 1994). The network has been expanded to 165 sites by 2003 and tracks spatial and temporal trends of visibility and

aerosols in rural areas and National Parks (Malm et al., 2004). Each site collects 24-h PM2.5 (particulate matter with aerodynamic diameter less than 2.5 μm) and PM10 (particulate matter with diameter less than 10 μm) samples every three days. The PM2.5 samples are analyzed for mass, elemental composition, ions, and organic and elemental carbon. These data are used to reconstruct the major aerosol species of fine particles, identifying sulfate, nitrate, organic mass by carbon, light-absorbing carbon, and fine soil. By assuming species-dependent mass extinction efficiencies and hygroscopic growth curves, the extinction coefficients can be calculated. While such near-surface extinction data can be readily compared with model simulations, assumptions of aerosol vertical profiles are needed to derive the columnar optical properties that lead to estimates of aerosol direct effects and forcings.

MFRSR: The multifilter rotating shadowband radiometer (MFRSR) has been widely used in recent years because of its automated operation and relatively low cost (Harrison et al., 1994). Several networks operate about a hundred instruments providing good geographical coverage of the United States. The MFRSR measures the direct solar beam extinction and horizontal diffuse flux at six visible and near-infrared wavelengths (nominally 415, 500, 615, 670, 870, and 940 nm) at 1-min intervals throughout the day. It uses an automated, objective, and computationally efficient cloud screening algorithm (Alexandrov et al., 2004a). The calibration-retrieval method has been developed to derive aerosol optical depth and particle size (Alexandrov et al., 2002a, b). Again, the retrieved size distributions have not been validated by comparison to in situ measurements.

NOAA/CMDL aerosol network: Aerosol measurements began at the NOAA Climate Modeling and Diagnostic Laboratory (CMDL) baseline observatories in the mid-1970's. In the 1990's, the research program expanded to establish regional stations for monitoring the influence of regional sources on the statistics and trends of aerosol optical properties (e.g., Sheridan and Ogren, 1999). Starting in March 2000, a similar instrument package has been operated from a light aircraft, obtaining in-situ aerosol profiles (IAP). Since then it has flown over the Southern Great Plain at altitudes be-

tween 500 m and 3500 m several times per week. In addition to the routine measurements at the long-term baseline and regional stations, short-term measurements have also been conducted in conjunction with several aerosol field experiments. The NOAA/CMDL network directly measures light absorption, total scattering and backscattering, particle number concentration and chemical composition (Quinn et al., 2000), making it feasible to link chemical measurements to physical measurements. These measurements are used to derive parameters required for aerosol forcing calculation (Delene and Ogren, 2002) and also to provide ground-truth for satellite remote sensing and input for global models.

Meteorological stations: Broadband direct solar radiation is measured at meteorological stations around the world. These long-term observations can be used to derive average aerosol optical depth over the solar spectrum, thus having the potential to detect changing atmospheric conditions on a decadal scale. For example, Luo et al. (2001) have applied a retrieval method to derive aerosol optical depth at 46 Class A solar radiation stations over China and analyzed the trend of aerosol optical depth from 1961 to 1990. The accuracy of such retrieved aerosol optical depth depends on the quality of the observations, including cloud-screening procedures and parameterizations of Rayleigh scattering, gaseous absorption, and aerosol extinction. These aerosol optical depth retrievals from meteorological stations still need to be evaluated using independent measurements from other surface observations, such as AERONET and MFRSR.

Lidar networks: In recent years, Raman Lidar and micro-pulse lidar (MPL) have been increasingly used to automatically and routinely retrieve profiles of aerosol backscattering and extinction during both day and night (e.g., Turner et al., 2001, 2002; Ferrare et al., 2001). The aerosol extinction profiles so-derived are pivotal to a better assessment of aerosol direct solar forcing under cloudy sky conditions, aerosol thermal infrared forcing and aerosol-cloud interactions (Feingold et al., 2003). Several regional aerosol lidar networks are emerging, including EARLINET, MPLNET, REALM, and AD-Net.

a. EARLINET: The European Aerosol Research Lidar Network (EARLINET) was established in 2002 to build a quantitative, comprehensive, and statistical database of the horizontal, vertical, and temporal distribution of aerosols on a continental scale. The observations are used in conjunction with back-trajectory analysis to characterize the transport and evolution of air pollution events (Matthias et al., 2004). The dataset collected over the past three years is being used to validate and improve model simulations under the framework of AEROCOM.

b. MPLNET: The NASA Micro Pulse Lidar Network (MPLNET) consists of ground-based micro-pulse lidar systems, co-located with sun/sky photometer sites of AERONET. Such a compact lidar is capable of acquiring long-term observations of aerosol and cloud vertical structures continuously and in an autonomous fashion (Welton et al., 2001, 2002). In conjunction with AERONET sunphotometer measurements, they are able to produce quantitative aerosol and cloud products, such as optical depth, sky radiance, vertical structure, and extinction profiles. The data have contributed to studies of aerosol properties of key aerosol types and have been used to validate and help interpret results from satellite sensors. MPLNET also serves as a ground calibration network for space-based lidars such as GLAS and CALIPSO.

c. REALM: The Regional East Atmospheric Lidar Mesonet (REALM) is a lidar network designed to monitor regional air pollution and transport from multiple locations (currently 12) in the eastern United States (Hoff and McCann, 2002).

d. AD-Net: The Asian Dust Network (AD-Net) was established to monitor the transport of Asian dust through distributed lidar systems in Japan, China and Korea. The network has been expanded to include observations of radiation and chemical and physical properties of near-surface aerosols (Murayama et al., 2001).

2.1.2. Satellite remote sensing

A measurement-based characterization of aerosols on a global scale can only be realized through satellite remote sensing, due to aerosols' short lifetime, complex chemical composition and interaction in the atmosphere. Monitoring aerosols from space has

been performed for over two decades (King et al., 1999). Early aerosol monitoring from space used data from sensors that were designed for other purposes, e.g., Advanced Very High Resolution Radiometer (AVHRR), and Total Ozone Mapping Spectrometer (TOMS), among others. However, they have provided multi-decadal climatology of aerosol optical thickness that has significantly advanced the understanding of aerosol distributions (e.g., Husar et al., 1997; Mishchenko et al., 1999, 2003; Geogdzhayev et al., 2002; Herman et al., 1997; Torres et al., 1998, 2002). The AVHRR, intended as a weather satellite, provides radiance observations in the visible and near infrared wavelengths that are sensitive to aerosol properties over the ocean. Originally intended for ozone monitoring, the UV channels used for TOMS are sensitive to aerosol absorption and not too sensitive to surface interferences, even over land (Torres et al., 1998). TOMS has proved to be extremely successful in monitoring biomass burning smoke and dust (Herman et al., 1997) and retrieving aerosol single-scattering albedo from space (Torres et al., 2005). A new sensor, OMI aboard Aura, has improved on such advantages. In recent years, satellite aerosol retrievals have become increasingly sophisticated. Now, satellites measure the angular dependence of polarization and radiance in multiple wavelengths in the UV through the IR, at fine temporal and spatial resolution. From these observations, retrieved aerosol products now include not only optical depth at one wavelength, but spectral optical depth and particle size both over ocean and land, as well as more direct measurements of polarization and phase function. In addition, cloud screening is much more robust than before. Examples of such new and enhanced sensors include POLDER, MODIS, and MISR, among others. Aerosol profiling from space is also making promising progress. In the following, a brief description of such new sensors is given. Readers are encouraged to refer to King et al. (1999) for details.

POLDER: The Polarization and Directionality of the Earth's Reflectance (POLDER) is a unique aerosol sensor that consists of a wide field-of-view imaging spectroradiometer capable of measuring multi-spectral, multi-directional, and polarized radiances. The observed multi-angle polarized radiances can be exploited to better sep-

arate the atmospheric contribution from the surface contribution over both land and ocean (Déuzé et al., 2001). The POLDER onboard the Japanese Advanced Earth Observation Satellite (ADEOS-1 and -2) has collected aerosol data over both land and ocean (e.g., Boucher and Tanré, 2000). A similar POLDER instrument flies on the PARASOL satellite launched in December 2004. A limitation of POLDER is the rather coarse spatial resolution of about 6 km, which affects the ability to account for scene heterogeneity. In addition, larger aerosol particles, such as desert dust, do not polarize sunlight and therefore can not be retrieved quantitatively.

MODIS: The MODerate resolution Imaging Spectroradiometer (MODIS) aboard NASA's twin satellites, namely Terra and Aqua (crossing the equator in opposite directions at about 10:30 and 13:30 local time, respectively), performs near global daily observations of atmospheric aerosols. MODIS has 36 channels ranging from 0.44 to 15 μm. Seven of these channels between 0.47 and 2.13 μm are used to retrieve aerosol properties over cloud and surface-screened areas (identified by using other channels and examining spatial variability (Martins et al., 2002; Li et al., 2004). The MODIS retrieval uses separate algorithms over land and ocean (Kaufman et al., 1997; Tanré et al., 1997; Remer et al., 2005). Over vegetated land, MODIS retrieves aerosol optical thickness at three visible channels with high accuracy, i.e., $\pm 0.05 \pm 0.2\tau$ (Chu et al., 2002; Remer et al., 2005). It also derives a fraction of small particles in terms of aerosol extinction (the so-called fine-mode fraction). This parameter over land should be treated as a qualitative measure only. Because of its wide spectral range over ocean and the greater simplicity of the ocean surface, MODIS has the unique capability of retrieving not only aerosol optical thickness with greater accuracy, i.e., $\pm 0.03 \pm 0.05\tau$ (Remer et al., 2002, 2005), but also quantitative aerosol size parameters (e.g., effective radius, fine-mode fraction) (Kaufman et al., 2002a; Remer et al., 2005).

MISR: The Multi-angle Imaging SpectroRadiometer (MISR) aboard the sun-synchronous polar orbiting satellite Terra measures upwelling solar radiance in four spectral bands (centered at 446, 558, 672, and 866 nm) and at nine view angles spread out in the forward and aft directions along the flight path (at nadir, ±70.5°, ±60.0°,

±45.6°, and ±26.1° of nadir) (Diner et al., 2002). It acquires global coverage about once per week. A wide range of along-track view angles makes it feasible to more accurately evaluate the surface contribution to the TOA radiances and hence retrieve aerosols over all kinds of ocean surfaces and especially over land surfaces, including bright desert aerosol source regions (Diner et al., 1998; Martonchik et al., 1998a, 2002; Kahn et al., 2005a). Evaluation studies show that for the early post-launch algorithm (Version 12) overall, about two thirds of MISR AOTs are within 20% or ±0.05 of coincident AERONET measurements. Over dark ocean, the MISR early post-launch AOTs overall have a high bias of 0.038 (Kahn et al., 2005a; Abdou et al., 2005). New low-light level calibration, applied to aerosol product Versions 16 and higher, improve the accuracy of the dark water MISR AOT retrievals compared to sun photometer results (Kahn et al., 2005b; Bruegge et al., 2004). (Re-runs of the multi-year MISR data records with the Version 16 algorithm were not available in time for this assessment, but should be complete by early 2006.)

The MISR multi-angle data also sample scattering angles ranging from about 60° to 160° in midlatitudes, yielding information about particle size (Kahn et al., 1998, 2001, 2005a) and shape (Kalashnikova et al., 2005a, b[1]). These quantities are of interest in–and-of themselves for identifying aerosol airmass types, and should also help further refine the accuracy of space-based AOT retrievals and particle property determinations.

CERES: The Clouds and the Earth's Energy System (CERES) measures broadband solar and terrestrial radiances at three channels with a large footprint (e.g., 20 km for CERES/Terra) (Wielicki et al., 1996). It is collocated with MODIS and MISR aboard Terra and with MODIS on Aqua. The observed radiances are converted to the TOA irradiances or fluxes using the Angular Distribution Models (ADMs) as a function of viewing angle, sun angle, and scene type (Loeb and Kato, 2002; Zhang et al., 2005a).

[1]Kalashnikova, O. V., Kahn, R. A., and Li, W.-H.: The ability of multi-angle remote sensing observations to identify and distinguish mineral dust types: Part 2. Sensitivity data analysis, J. Geophys. Res., submitted, 2005b.

Such estimates of TOA solar flux under clear-sky conditions can be compared to the expected flux for an aerosol-free atmosphere, in conjunction with aerosol measurements from other sensors (e.g., MODIS and MISR) to derive the aerosol direct effect (Christopher and Zhang, 2002a, 2004; Loeb and Kato, 2002; Loeb and Manalo-Smith, 2005; Zhang and Christopher, 2003; Zhang et al., 2005b). The derived instantaneous value is then scaled to obtain a daily average. Broadband flux measurements from the Earth Radiation Budget Experiment (ERBE) have also been used in a similar way (e.g., Hsu et al., 2000). Note that a direct use of the coarse spatial resolution CERES measurements would exclude aerosol distributions in partly cloudy CERES scenes and some approaches should be employed to overcome this limitation.

Aerosol profiling: Profiling global aerosols using satellite-borne lidar is another emerging capability. Following a demonstration of U.S. Space Shuttle mission in 1994 (Winker et al., 1996), the Geoscience Laser Altimeter System (GLAS) was launched in early 2003 to become the first polar orbiting satellite lidar (Schutz, 1998; Zwally et al., 2002). It provides global aerosol extinction (at 532 nm) profiling for a one-month period out of every three to six months. Some scientific results are going to be published soon (e.g., Spinhirne et al., 2005; Hart et al., 2005; Hlavka, et al., 2005). The Cloud-Aerosol Lidar and Infrared Pathfinder Satellite Observations (CALIPSO), scheduled to launch in July 2005, will carry a lidar instrument (CALIOP) that will collect profiles of the attenuated backscatter at visible and near-infrared wavelengths along with polarized backscatter in the visible channel (Winker et al., 2003). Flying in formation with the Aqua, AURA, POLDER, and CloudSat satellites, this vertically resolved information is expected to greatly improve passive aerosol and cloud retrievals as well as allow the development of new retrieval products (see, e.g. Kaufman et al., 2003; Léon et al., 2003).

The high accuracy of aerosol products (mainly aerosol optical depth) from these new-generation sensors, together with improvements in characterizing the surface and cloud (see Sect. 2.2), can help reduce the uncertainties associated with the aerosol direct radiative effect, as discussed in several recent studies (Boucher and Tanré, 2000;

Christopher and Zhang, 2002, 2004; Loeb and Kato, 2002; Bellouin et al., 2003; Yu et al., 2004; Remer and Kaufman, 2005; Loeb and Manalo-Smith, 2005; Zhang et al., 2005a, b). The retrieved aerosol size parameters can help distinguish anthropogenic aerosols from natural aerosols and hence help assess the anthropogenic aerosol radiative forcing (Kaufman et al., 2002a, 2005a; Christopher and Zhang, 2004). As discussed earlier, individual sensors have their own strengths and weakness. No single sensor is adequate for characterizing the complex aerosol system and they are usually complementary to each other. Therefore, the best strategy for characterizing global aerosols is to integrate measurements from different sensors. Furthermore, some sensors will fly in formation with other aerosol and cloud sensors (including OMI on Aura, CALIOP on CALIPSO) in the coming years. The constellation of these new-generation sensors, also called the A-Train (Stephens et al., 2002) provides an unprecedented opportunity to improve the characterization of global aerosols, clouds, and surface properties and hence the quantification of aerosol radiative forcing (Anderson et al., 2005). These global measurements of aerosols can also be used to improve the performance of aerosol model simulations and hence the assessment of the aerosol direct radiative effect through assimilation or integration process (e.g., Collins et al., 2001; Yu et al., 2003, 2004; Matsui et al., 2004; Liu et al., 2005). Finally, algorithms are being developed to retrieve aerosol absorption or single-scattering albedo from satellite observations (e.g., Kaufman et al., 2001; Torres et al., 2005).

2.1.3. Intensive field campaigns

Over the past decade, more than a dozen intensive field experiments have been conducted to study physical, chemical, and optical properties and radiative effects of aerosols in a variety of aerosol regimes around the world, as depicted in Fig. 1. These experiments have either been designed mainly for aerosol research or have included aerosol characterization as one of their major themes as part of interdisciplinary research efforts. A brief description of them is given in Table 1.

One of the main scientific goals of both TARFOX and ACE-2 was to examine how the

North Atlantic is influenced by pollution outflows from North America and West Europe during the summer season (Russell et al., 1999; Raes et al., 2000). Aerosol processes and properties have also been a major theme in air quality and atmospheric chemistry experiments, such as NEAQS in New England (Quinn and Bates, 2003), MINOS in the Mediterranean region (Lelieveld et al., 2002), INTEX-NA (2004), and ICARTT (2004).

South and East Asia have been of great interest to the atmospheric chemistry community because of the rapid and persistent increase in emissions in recent decades and complexity of aerosol composition and properties in the region. As observed by INDOEX, brown hazes blanketing large areas of northern Indian Ocean in the pre-monsoon season can significantly influence the atmospheric radiative budget, climate, and hydrological cycles (Ramanathan et al., 2001b). Such research is being extended to the broader Asia regions under the framework of ABC (Ramanathan and Crutzen, 2003). In East Asia, a mixture of industrial pollution and mineral dust influences large areas of the North Pacific and may even reach the North American continent, especially during the spring season. In the 1990s, several missions, under the framework of NASA's global tropospheric experiment (GTE), have been conducted, including PEM-West A and B (Hoell et al., 1996, 1997). A decade of data describing Pacific aerosols is summarized in Clarke and Kapustin (2002). More recently, TRACE-P and ACE-Asia were conducted in the spring of 2001 to document and characterize such intercontinental transport and its regional and hemispheric impacts. In particular, ACE-Asia was designed specifically for comprehensive aerosol research (Huebert et al., 2003; Seinfeld et al., 2004).

In the tropics, biomass burning comprises a major source of atmospheric aerosols and several international missions have been conducted to investigate how the emissions of gases and particles from biomass burning influence atmospheric chemistry, radiative budget, and climate, including BASE-A (Kaufman et al., 1992), SCAR-B (Kaufman et al., 1998) and LBA-SMOCC (Andreae et al., 2004) over South America, SAFARI2000 (King et al., 2003a), SAFARI92 (Lindesay et al., 1996), and TRACE-A (Fishman et al., 1996) over South Africa and the South Atlantic Ocean.

The largest sources of mineral dust come from North Africa and the Arabian Peninsula. They impose pronounced impacts over the tropical and subtropical Atlantic Ocean, Arabian Sea and as far as Southeastern US, as documented by observations during SHADE (Tanré et al., 2003), PRIDE (Reid et al., 2003), and UAE2 (http://uae2.gsfc.nasa.gov/). The ACE-1experiment was conducted over remote southern oceans to characterize the aerosols over the remote region least influenced by human activities (Quinn and Coffman, 1998).

During each of these comprehensive missions, aerosols were studied in great detail, using combinations of in-situ and remote sensing observations of physical and chemical properties from various platforms (e.g., aircraft, ship, satellite, ground-network), and numerical modeling (e.g., Seinfeld et al., 2004). In spite of their relatively short duration, these missions have acquired comprehensive data sets of regional aerosol properties that can be compared and compiled to understand the complex interactions of aerosols within the earth and atmosphere system. For such data comparison and compilation, it is required that different observations are sampling the same air mass. Nevertheless, where aerosol properties are "over-determined" by coordinated deployment of multiple platforms and instruments, they can be used to identify inconsistencies and quantify uncertainties. Column closure studies are an example of using this approach to improve knowledge of aerosol radiative forcing (e.g., Russell et al., 1997).

2.2. Surface albedo and clouds

2.2.1. Surface albedo

Surface albedo and reflectance properties are key factors in the solar energy budget, and accurate portrayal of the surface is important for determining how aerosols perturb this budget (Atwater, 1970; Mitchell Jr., 1971; Coakley et al., 1983). Multiple reflections between the surface and aerosols cause a non-linear surface influence in addition to the aerosol radiative effect. In general, the larger the surface albedo, the smaller the

aerosol radiative effects are (for the same non-absorbing aerosol). However, even weak aerosol absorption above a highly reflective surface (deserts or snow) would cause warming at the TOA. As such, inadequate characterization of surface reflection will introduce additional uncertainties in the estimate of the aerosol direct radiative effect.

The characterization of surface albedo is challenging. Over ocean, the surface albedo depends primarily on wavelength, but also on solar and viewing angles, wind-speed, and chlorophyll concentration. The oceanic surface reflectance can be adequately calculated using an adequate coupled atmosphere-ocean radiative transfer model (Jin et al., 2002, 2004). However, reflectance by a land surface is much more complicated. Often the land surface is highly heterogeneous, having highly anisotropic and wavelength-dependent optical properties (e.g., Dickinson, 1984). Therefore its characterization is even more difficult, leading to additional uncertainty in the aerosol direct effect. Until recently, aerosol radiative forcing calculations have assumed surface albedos that have been determined based on empirical parameterizations of vegetation and soils (Dickinson et al., 1993; Sellers et al., 1996). New satellite-borne instruments, such as MODIS and MISR, can much better characterize surface optical properties because they measure at multiple wavelengths and angles at spatial resolutions as fine as 1 km (Moody et al., 2005; Schaaf et al., 2002; Martonchik et al., 1998b). Their albedo products include both global black- and white-sky albedos, which represent respectively the directional hemispheric reflectance contributed by the direct beam and the bihemispherical reflectance contributed from reflection of diffuse light. These and other new datasets can provide better lower boundary conditions to the radiative transfer model and reduce the uncertainty in the estimate of aerosol direct effect (e.g., Yu et al., 2004).

The MODIS/MISR retrieved angular dependence of the surface albedo, i.e., a separation of direct beam and diffuse light contribution, also provides an unprecedented dataset for examining the complex interaction of aerosol extinction with surface reflectance (Yu et al., 2004). In principle, the determination of global albedo requires

integrating the angular dependence of the surface reflectance, over a diurnal cycle of solar zenith angles with appropriate fractions of spectral direct and diffuse solar beam radiances. Because aerosols modify the directional composition of incident solar radiation (by increasing the diffuse light and decreasing the direct beam), they alter the surface albedo as well. As a result of the spectral dependence of aerosol extinction, the spectral dependence of the surface albedo changes as well. In other words the interaction of aerosol and the surface complicates the calculation of the aerosol TOA forcing (Yu et al., 2004).

The left panel of Fig. 2 shows that the white-sky albedo is larger than the black-sky albedo at high solar zenith angles and smaller at low angles. A reduction of direct beam fraction (as would be caused by aerosols) increases the effective reflection at high Sun but decreases it at low Sun. The right panel of Fig. 2 shows this effect over grassland. Although this aerosol effect is negligible when considering monthly or daily averages, the inclusion of land surface anisotropy is necessary for capturing diurnal aerosol effects. Magnitudes of aerosol effects strongly depend on both the aerosol properties and land classifications (Yu et al., 2004). Bellouin et al. (2004) showed that the inclusion of anisotropy is also necessary over the ocean.

2.2.2. Clouds

Clouds can profoundly modify the aerosol radiative effects. The extent of their modification depends on both the aerosol and cloud properties, their relative positioning in the atmosphere, and on their diurnal variation with respect to the solar illumination. (e.g., Liao and Seinfeld, 1998; Haywood and Shine, 1997). Cloud properties that must be accounted for include cloud fraction and cloud optical depth. For absorbing aerosols, the vertical profile of clouds is also desired (Keil and Haywood, 2003). For a first-order approximation (as assumed in box models), the direct aerosol radiative effect is negligible under overcast skies, but is a cloud-fraction weighted product of clear and cloudy sky effects under partly cloudy skies (e.g., Charlson et al., 1992). Such an assumption only holds for optically thick clouds residing above the aerosol layer, where the solar

radiation is sufficiently diffused by the cloud. For optically thin clouds, a significant amount of solar radiation is transmitted to, and will interact with the underlying aerosol layer. If absorbing aerosol lies above the cloud layer (in essence a very bright surface) then the aerosol absorption effect tends to be magnified. Thus, aerosols over bright surfaces tend to induce a warming effect at the TOA.

MODIS uses multiple spectral bands at 250 m, 500 m, and 1 km resolution to detect clouds, and retrieve cloud properties recorded at 1 and 5 km horizontal resolution (Platnick et al., 2003). From the pressure dependence of thermal emission bands, MODIS infers cloud top pressure and temperature. Using six visible and near-infrared bands, MODIS retrieves drop effective radius (weighted towards cloud top), columnar optical depth, and water path for different cloud thermodynamic phases (i.e., water, ice, and mixed) at 1 km resolution. Such retrievals are only performed for overcast pixels as determined by the two highest confidence bits of the cloud mask. The combination of MODIS/Terra and MODIS/Aqua allows for some indication of cloud evolution from late morning to early afternoon. Figure 3 shows the annual cycle (2001) of cloud fraction and total (water plus ice) cloud optical depth averaged over the entire globe, land, and ocean. On global and annual average, the cloud fraction is about 0.63 and cloud optical depth is 10.8. Compared with clouds over ocean, clouds over land are optically thicker and have smaller cloud fraction,

The International Satellite Cloud Climatology Project (ISCCP), a part of the World Climate Research Program (WCRP), has been collecting radiance measurements from the international constellation of weather satellites and analyzing cloud properties and variations since July 1983 (Schiffer and Rossow, 1983; Rossow and Schiffer, 1991, 1999). It has provided information on variations of cloud fraction, optical thickness, cloud-top temperature for various types of cloud at a time scale of 3 h, daily, and monthly for two decades. Such information can be exploited to better constrain the estimate of the aerosol direct effect under cloudy sky conditions and to study interannual variations of the aerosol radiative effect.

2.3. Radiative transfer modeling

The early box model or one-line formula (e.g., Charlson et al., 1991; Chylek and Wong, 1995) represents aerosol-radiation interactions with a number of simplifications. While the calculations are straightforward, the simplifications cause large uncertainties in estimates of aerosol radiative forcing (e.g., Wendisch et al., 2001). In such box models, the aerosol properties are almost assumed for a single wavelength (e.g., 550 nm). However, the optical properties at 700 nm may be more representative for the whole solar spectrum than those at 550 nm (Blanchet, 1982). Box models do not adequately account for the spectral dependence of aerosol/Rayleigh scattering interactions, especially at short wavelengths and at low Sun where Rayleigh scattering is strong. In addition, multiple scattering effects become stronger at high aerosol loadings. Therefore, such simple box models should only be applied to optically thin atmospheres.

With the substantially enhanced computational capability of modern computers, it is now feasible to carry out sophisticated radiative transfer modeling. Most recent studies have used plane-parallel radiative transfer (RT) models numerically solved with a discrete-ordinate method, with varying levels of complexity depending on spectral resolution and streams (e.g., Fu and Liou, 1993; Chou et al., 1993). Boucher et al. (1998) compare sulfate radiative effects calculated from a dozen such radiative transfer models. Recently, a few studies have used more sophisticated Monte-Carlo RT models (e.g., Podgorny et al., 2000; Podgorny and Ramanathan, 2001). Such modeling is capable of better characterizing the complex particle-radiation interactions in heterogeneous media, including aerosols in the vicinity of broken clouds.

Simplified phase function parameterizations such as HG functions employed by most RT models cannot adequately represent backward scattering (van de Hulst, 1980), thereby introducing errors in the estimate of aerosol radiative forcing. Errors vary in magnitude, depending on the solar zenith angle, aerosol size distribution and refractive index (Boucher, 1998; Marshall et al., 1995). Aerosol direct solar effects change appreciably with the solar zenith angle (SZA). For purely scattering sulfate aerosol,

the largest cooling occurs around a SZA of ~70° because of the angular dependence of both aerosol upscattering fraction and Rayleigh scattering (Nemesure et al., 1995; Boucher et al., 1998; Russell et al., 1999). Aerosol absorption decreases with increasing SZA, nearly compensating for the SZA-dependence of aerosol backscattering (Yu et al., 2002). The SZA-dependence of the aerosol direct effect is relatively weak for absorbing aerosols. Accurately modeling the SZA-dependence of aerosol radiative effect requires that the time step for radiative calculations be adequately small, e.g., less than 30 min, in order to sample a range of solar zenith angles and calculate the unbiased daily average aerosol direct effect (Yu et al., 2004).

As a summary, we present here an example that demonstrates how the aerosol direct solar effect is determined by a combination of aerosol and surface properties. Figure 4a and b show respectively the AERONET measured aerosol optical properties, and the corresponding clear-sky aerosol direct effect of various aerosol types (biomass burning smoke, mineral dust, and industrial/urban pollution) for different geographical regions (Zhou et al., 2005). The monthly aerosol direct effect is normalized with respect to the corresponding monthly optical depth at 550 nm. This normalized aerosol direct radiative effect (DRE/τ) has been referred to as "radiative efficiency" (E_τ) (Anderson et al., 2005). This quantity is mainly governed by aerosol size distribution and chemical composition (determining aerosol single-scattering albedo and phase function), surface reflectivity, and solar irradiance, and also to some degree depends on optical depth because of multiple scattering. Black vertical bars represent one standard deviation of AOT, SSA, and E_τ for individual aerosol regimes. Both all-mode (total) and fine-mode aerosols are considered.

Due to stronger absorption of smoke in South Africa (SSA ~0.862±0.027) as compared to South America (SSA~0.940±0.025) (Dubovik et al., 2002; Eck et al., 2003), biomass burning aerosols in South Africa are found to have an average E_τ that is smaller by ~35% at the TOA but larger by ~38% at the surface. For industrial pollution, the aerosol absorption and hence the radiative efficiency are inbetween South Africa biomass burning smoke and South America smoke. On average, the TOA and surface

E_τ are relatively large in North America.

Mineral dust dominates over North Africa and the Arabian Peninsula. Here the surface reflectivity is high and has considerable spatial variability, ranging from about 0.2 to 0.4 for albedo in the solar spectrum (Tsvetsinskaya et al., 2002). Dust outflow also influences nearby oceans substantially where the surface albedo is less than 0.1. Such large variations of surface albedo could be the major reason for the large differences of aerosol solar effect shown in the plots. The radiative efficiency ranges from −44 to $-17\,\mathrm{Wm}^{-2}\tau^{-1}$ at the TOA and from −80 to $-48\,\mathrm{Wm}^{-2}\tau^{-1}$ at the surface when the surface albedo changes from less than 0.1 to 0.3∼0.35.

It also shows that the radiative efficiency of fine-mode aerosol is larger at the TOA but smaller at the surface than that of all-mode aerosol, due to a larger single-scattering albedo and smaller asymmetry factor of fine-mode aerosol retrieved from AERONET measurements.

3. Assessment of global and regional aerosols and their direct effect

3.1. Description of assessments

In this review, we concentrate on measurement-based assessments (e.g., from ground-based networks, satellite remote sensing, and intensive field experiments) of tropospheric aerosols and their direct radiative effect, supplemented by five global aerosol model simulations. We assess the aerosol properties and resulting estimates of the DRE derived from these different approaches, both globally (in Sect. 3.2) and regionally (in Sect. 3.3). DCF by anthropogenic aerosols is assessed in Sect. 3.4. In this section, the assessments concentrate on aerosol optical depth and influences on solar radiation under clear sky conditions. In Sect. 4, we will briefly discuss DRE in the thermal infrared range and under cloudy conditions. Because satellite sensors generally do not retrieve aerosols with good accuracy at high latitudes (due to weak sunlight and high surface reflectance of snow and ice), the global assessments are actually con-

fined to areas between 60° N and 60° S. The regional assessments are conducted over the 13 zones shown in Fig. 5.

Here, we have compared retrievals of aerosol optical depth from a number of datasets. These include derivations from different satellite sensors (e.g., Terra-MODIS, MISR), model simulations (e.g., GOCART, SPRINTARS, GISS, LMDZ-INCA, LOA, MPI-HAM), and satellite-model integrations (MO_GO, MI_GO, and MO_MI_GO), and are listed in Table 2. Aerosol retrievals from MODIS and MISR have previously been described in Sect. 2.1. All MODIS values of AOT or DRE shown in this paper are from Terra Collection 4 retrievals.

Five global aerosol models are included in our comparisons, namely GISS (Koch and Hansen, 2005; Koch et al., 2005[2]; Miller et al., 2005[3]; Schmidt et al., 2005[4]), GOCART (Chin et al., 2000a, b, 2002, 2003, 2004; Ginoux et al., 2001, 2004), LMDZ-INCA (Schulz et al., 2005[5]; Textor et al., 2005), LMDZ-LOA (Boucher et al., 2002; Boucher and Pham, 2002; Reddy et al., 2004, 2005a, b), and SPRINTARS (Takemura et al., 2000, 2002, 2005). All models simulate major components of tropospheric aerosols, including sulfate (natural and anthropogenic separately), organic carbon (natural and anthropogenic separately), black carbon, and size-resolvable dust and sea-salt. On the other hand, individual models differ in emissions inventories, parameterizations of

[2]Koch, D., Schmidt, G., and Field, C.: Sulfur, sea salt and radionuclide aerosols in GISS ModelE, J. Geophys. Res., submitted, 2005.

[3]Miller, R. L., Cakmur, R. V., Perlwitz, J. A., Koch, D., Schmidt, G. A., Geogdzhayev, I. V., Ginoux, P., Prigent, C., and Tegen, I.: Mineral dust aerosols in the NASA Goddard Institute for Space Sciences ModelE atmospheric general circulation model, J. Geophys. Res., submitted, 2005.

[4]Schmidt, G. A., Ruedy, R., Hansen, J. E., et al.: Present day atmospheric simulations using GISS ModelE: Comparison to in-situ, satellite and reanalysis data, J. Clim., submitted, 2005.

[5]Schulz, M., Balkanski, Y., Textor, C., Guibert, S., Generoso, S., Boucher, O., Breon, F.-M., Hauglustaine, D., and Hourdin, F.: The LMDzT-INCA Global Aerosol Model and its, Evaluation with Surface, Lidar and Satellite Aerosol Observations, in preparation, 2005.

physical and chemical processes of aerosols, radiative transfer schemes, and spatial resolution. Some models are driven by assimilated/nudged climatology, whereas others are coupled with atmospheric general circulation model. All models provide the total aerosol optical depth under whole sky conditions. In addition, SPRINTARS and GISS provide the clear-sky AOT (denoted as SPRINTARS_clr and GISS_clr, respectively). For deriving SPRINTARS_clr AOT, clear sky is defined as a condition where the grid-average cloud fraction (maximum-random overlapping) is less than 0.2 at each time step of model integration (e.g., 8 min). GISS_clr is derived by weighting the simulated AOT with clear-sky fraction.

Both satellite retrievals and model simulations have uncertainties and data assimilation or objective analysis should form an optimal estimate of aerosol distributions by combining them with weights inversely proportional to the square of the errors of individual descriptions. An optimum interpolation approach with the Kalman-Bucy filter can fill gaps in satellite retrievals and generate global distributions of aerosols in better agreement with ground-based measurements than are either the satellite retrievals or model simulations alone (Yu et al., 2003). MO_GO and MI_GO denote, respectively, an integration of GOCART simulations with MODIS (land and ocean) and MISR (land and ocean). We also integrate GOCART simulations with MODIS retrievals over ocean and MISR retrievals over land, denoted as MO_MI_GO. By doing so, we take advantage of the high accuracy of MODIS over-ocean retrievals and high accuracy of MISR retrievals over bright as well as darker land surfaces.

Table 3 lists the estimates of aerosol direct solar effect included in the comparison. A brief description of each is presented in the table and readers are encouraged to refer to the relevant literature for more details. The assessments fall into three broad categories:

The first category is satellite based that includes MODIS, MODIS_A, CERES_A, CERES_B, CERES_C.

The MODIS approach is to use the MODIS aerosol retrievals consistently in conjunction with the CLIRAD-SW radiative transfer model (Chou et al., 1992) to calculate

TOA fluxes and aerosol direct radiative effects. The MODIS retrieval returns a linked set of AOT, ω_0, and phase function that best matches spectral radiances observed at the TOA. Using these three retrieved parameters consistently with CLIRAD-SW results in fluxes that best match the observed radiances, and is preferable to inferring ω_0 and phase function from non-MODIS sources that may be inconsistent with the MODIS-retrieved AOT (Remer and Kaufman, 2005).

The MODIS_A approach splits the total MODIS observed AOT into three components, namely mineral dust, sea salt, and biomass-burning+pollution. AERONET measurements are used to derive the size distribution and single-scattering albedo for these individual components. These parameters are then used to derive the 24-h average direct radiative effect of individual components at the TOA and surface (Bellouin et al., 2005[6]). The land surface albedo is taken from MODIS observations. Both AOT and the direct effect are weighted by the MODIS pixel counts and averaged over $1^{\circ}\times 1$ boxes. Here the total aerosol direct effect is assumed to be a sum of individual components. Since the compositional direct effects are not additive, this assumption may lead to an overestimation of the aerosol direct effect, especially when one of the components is strongly absorbing. Over bright surfaces, MODIS observations and hence the direct effect are not available.

For the CERES related assessments in this category, the aerosol direct effect is derived using CERES/Terra measured radiances/fluxes along with aerosol and cloud distributions from MODIS/Terra (e.g., Loeb and Manalo-Smith, 2005; Zhang et al., 2005a, b). Because of the coarse spatial resolution of CERES measurements (i.e., 20 km for CERES/Terra), a direct use of CERES flux measurements would exclude aerosol distributions in partly cloudy CERES scenes. Several approaches have been employed to overcome this limitation (Loeb and Manalo Smith, 2005; Zhang et al., 2005b). Loeb and Manalo-Smith (2005) combine CERES radiances and fluxes with scene information from coincident high spatial and spectral resolution MODIS measurements. Aerosol

[6]Bellouin, B., Boucher, O., Haywood, J., and Reddy, S.: Global estimates of aerosol direct radiative forcing from satellite measurements, Nature, in revision, 2005.

properties are determined from two sources: (1) directly from the MOD04 aerosol product (Remer et al., 2005); and (2) by applying the NOAA-NESDIS algorithm (Ignatov and Stowe, 2002) to the MODIS measurements determined to be cloud-free. Correspondingly, the derived aerosol direct effect is denoted here as CERES_A and CERES_B, respectively. In Zhang et al. (2005a, b), aerosol direct effects are derived from 20 km-resolution CERES measurements by using empirical aerosol angular models. The aerosol effect are then scaled by the ratio of the MODIS average AOT to the AOT in CERES cloud-free pixels to include the aerosol direct effect at sub-CERES footprint (e.g., CERES_C).

The second category is a hybrid of satellite retrievals and model simulations, in which satellite retrieved optical depths are used to conduct radiative transfer modeling in conjunction with model simulations of other parameters (MODIS_G, MISR_G, MO_GO, MO_MI_GO) (Yu et al., 2004) or use of prescribed aerosol models (POLDER, and SeaWiFS) (Boucher and Tanré, 2000; Bellouin et al., 2003; Chou et al., 2002). For MO_GO and MO_MI_GO cases, satellite retrieved optical depths are also adjusted by GOCART simulations through the use of optimum interpolation with a Kalman filter (Yu et al., 2003; Matsui et al., 2004).

The third category is purely model based, including five model calculations namely GOCART (Chin et al., 2001, 2002; Yu et al., 2004), SPRINTARS (Takemura et al., 2002, 2005), GISS (Koch and Hansen, 2005; Koch et al., 2005[2]), LMDZ-INCA (Balkanski et al., 2005[7]; Balkanski and Schulz, 2005[8]; Kinne et al., 2005), and LMDZ-LOA (Reddy et al., 2005a, b). For GOCART estimates, similar to satellite-based estimates, radiative transfer calculations driven by monthly average GOCART aerosols are performed every 30 min with the solar insolation condition of 15th day of each month. Surface albedos are taken from MODIS observations over land and a look up table over

[7]Balkanski, Y., Schulz, M., and Boucher, O.: Dust radiative forcing revisited, in preparation, 2005.

[8]Balkanski, Y. and Schulz, M.: The aerosol direct radiative effect: Global model integrations of uncertainties on mixing, size and humidity growth, in preparation, 2005.

ocean. GISS calculates the instantaneous DRE by assuming clear sky. The instantaneous DRE weighted by clear-sky fraction is summed up during a month, which is then divided by monthly average clear-sky fraction to derive monthly average clear-sky DRE. For the other four model-based estimates, radiative transfer models are driven by model calculated aerosol properties every 2 or 3 h. Clouds are switched off in RT calculations to derive the clear-sky aerosol direct effect. Feedbacks of aerosol radiative effects on meteorology and hence aerosol simulations are not taken into account in these online calculations. Major sources of uncertainty in model calculated aerosol direct effect include uncertainties in emissions of individual aerosol types and their precursors, parameterizations of a variety of aerosol processes, and assumptions on aerosol size, absorption and humidification of particles (Kinne et al., 2003).

Finally, assessments from AERONET climatology (Sect. 2.1.1) and previous field experiments (above) are also incorporated in appropriate regional comparisons. We compile AERONET measurements of aerosols and their direct effect by averaging them over seasons and in the individual zones defined in Fig. 5. Field experiments were usually conducted in different years and only covered a portion of individual zones defined in Fig. 5. Because of mesoscale variations of aerosols (Anderson et al., 2003b), aerosol loading during the field experiments may not be representative of the seasonal climatology over a defined zone. Here, we normalize the DRE assessments with the observed aerosol optical depth τ at 550 nm and then compare such a normalized DRE or radiative efficiency E_τ ($\mathrm{Wm}^{-2}\tau^{-1}$). Note that the aerosol direct effect increases with τ nonlinearly because of multiple scattering, with the slope depending on latitude, season, and aerosol properties. Nevertheless such scaling or normalization would remove much of the influence of aerosol loading and so allows us to do a more fair intercomparison and see more clearly how the internal optical properties determined by aerosol size distributions and chemical compositions and environmental parameters (e.g., surface albedo) impact the direct radiative effect.

3.2. Assessment of the global aerosol direct effect

3.2.1. Global patterns of aerosol optical depth and direct radiative effect

Figure 6 shows global distributions of aerosol optical depth (left panel) and clear-sky direct radiative effect at the TOA (right panel) for March-April-May (MAM). The direct effect at the surface follows the same pattern as that at the TOA but is significantly larger in magnitude because of aerosol absorption. It appears that different approaches agree on large-scale patterns of aerosol optical thickness and the direct effect on solar radiation. In this season, the aerosol impacts in the Northern Hemisphere are much larger than those in the Southern Hemisphere. Dust outbreaks and biomass burning elevate the optical thickness to more than 0.3 in large parts of North Africa and the tropical Atlantic. In the tropical Atlantic, TOA cooling as large as $-10\,\mathrm{Wm}^{-2}$ extends westward to Central America. In highly polluted eastern China, the optical depth is as high as 0.6–0.8, resulting from the combined effects of pollution, biomass burning in the south, and dust outbreaks in the north. The impacts from Asia also extend to the North Pacific, with a TOA cooling of more than $-10\,\mathrm{Wm}^{-2}$. Other areas with large aerosol impacts include Western Europe, mid-latitude North Atlantic, and much of South Asia and the Indian Ocean. Over the "roaring forties" in the Southern Hemisphere, high winds generate a large amount of sea-salt. Such elevation of optical depth, along with high solar zenith angle and hence large backscattering to space, results in a band of TOA cooling of more than $-4\,\mathrm{Wm}^{-2}$. Some differences exist between different approaches. For example, the early post-launch MISR retrieved optical depths over the southern hemisphere oceans are higher than MODIS retrievals and GOCART simulations. Over the "roaring forties", the MODIS derived TOA solar flux perturbations are larger than the estimates from other approaches.

Tables 4 and 5 show seasonal (MAM and JJA) and annual (ANN) averages of optical depth and the direct effect over 13 oceanic and continental regions, respectively. Note that the AOT values in Table 4 (MODIS) are weighted with the number of aerosol retrieval that roughly corresponds to the clear-sky fraction. Because aerosol optical depth

increases with cloud fraction, these weighted values are smaller than un-weighted CERES_A AOT values, especially in the North Pacific. Various assessments differ in magnitude, depending on regions. Generally, model simulations of aerosol optical depth and the direct effect are smaller than satellite measurements. The integration of satellite measurements of aerosol optical depth into model simulations improves the agreement of the model simulated direct effect with measurements.

3.2.2. Intercomparisons of global average aerosol optical depths

Tables 6a, b, c show the intercomparison of seasonal and annual aerosol optical depth at 550 nm, averaged over globe, land, and ocean, respectively (all limited to 60° S–60° N for reasons discussed earlier). Here gaps in MODIS retrievals (over deserts and snow-melting regions) and to a lesser extent in MISR retrievals are filled with the GOCART simulations. MODIS and MISR retrievals give a comparable average AOT on the global (land and ocean) scale, with MISR greater than MODIS by 0.01∼0.02 depending on the season. However, differences between MODIS and MISR are much larger when land and ocean are examined separately. On the one hand, over land seasonal average AOTs from MODIS are larger than their MISR counterparts by 0.024∼0.067, with an annual average of 0.054 (see also Abdou et al., 2005). On the other hand, over ocean MISR AOTs are larger than their MODIS counterparts by 0.030∼0.036. These differences are much reduced by improved low-light-level calibration of MISR radiance measurements (Kahn et al., 2005b; Bruegge et al., 2004; MISR aerosol products Version 16 and higher) and by improving land characterization for the MODIS retrieval. Satellite aerosol retrievals can be contaminated by thin cirrus and clouds in general, resulting in an overestimate of aerosol optical depth (Kaufman et al., 2005b[9]). It is estimated that, on average, residual cirrus causes 0.015±0.003 high bias in the MODIS

[9]Kaufman, Y. J., Remer, L. A., Tanre, D., Li, R.-R., Kleidman, R., Mattoo, S., Levy, R., Eck, T., Holben, B. N., Ichoku, C., Martins, J., and Koren, I.: A critical examination of the residual cloud contamination and diurnal sampling effects on MODIS estimates of aerosol over ocean, IEEE Trans. on Geoscience & Remote Sensing, submitted, 2005b.

AOT at 550 nm over the oceans. Correlation of the difference between the MODIS AOT and that of AERONET with cloud fraction measured from MODIS shows that for average cloud conditions the total cloud contamination (including cirrus) of the AOT is about 0.02±0.005. Note that the MODIS oceanic and annual average of 0.15 in the table is larger than the 0.13 derived from 1°×1° grid data, weighted by the number of retrievals within the 1° grid square. The latter weighted value already has reduced cloud contamination (Remer and Kaufman, 2005).

Under whole-sky conditions, the annual and global average AOT from five models is 0.191±0.017 (mean ± standard deviation) over land and 0.126±0.046 over ocean, respectively. On a seasonal basis, the standard deviation accounts for 9–13% and 32–40% of the corresponding mean AOT over land and ocean, respectively. Over land, no model gives consistently high or low AOT values and differences between models depend on season. Over ocean, GISS derives the largest AOTs. In general, GOCART and LMDZ-INCA give comparable AOT values that are larger than LMDZ-LOA and SPRINTARS simulations. Clearly, the model-based mean AOT is smaller than MISR retrieval over land by 0.034 (or 15%) and MODIS retrieval over ocean by 0.028 (or 18%), respectively. These differences could be attributed partially to cloud contamination in satellite retrievals. The satellite and model integrations are generally inbetween the satellite retrievals and the model simulations.

A separation of clear-sky and whole-sky aerosol optical depth in SPRINTARS and GISS allows us to examine cloud impacts on aerosol optical depth. Clouds can increase aerosol optical depth through water vapor uptake in the humid regions adjacent to clouds. If in-cloud aqueous sulfate production in a cloud-rich airmass occurs, then this air mass contains at a later moment more sulfate aerosol, which is correlated with cloud occurrence if the airmass did not change its equilibrium of humidity and temperature profile. New particle formation in the vicinity of clouds produces nanometer-sized particles that do not immediately contribute significantly to AOT, although coagulation of these particles could eventually make a significant contribution. Stronger upward transport associated with low-pressure systems and cloudy skies may also increase

aerosol lifetime. On the other hand, clouds remove aerosols from the atmosphere through scavenging and rainout. Meteorological conditions (e.g., relative humidity, wind speed) would be different in clear- and cloudy skies, resulting in different hygroscopic growth and mechanical generation of aerosols (dusts, sea-salt). The net effects of cloud on aerosol optical depth should depend on aerosol types. For SPRINTARS simulations, the clear-sky aerosol optical depth is smaller than the all-sky values by 14–17% on global average, with the difference somewhat larger over land than over ocean. The largest differences occur over regions dominated by sulfate (e.g., East US, West Europe, and East Asia) and over the "roaring forties" belt dominated by sea-salt aerosols. Such differences may suggest the importance of sulfate production through cloud processes and the hygroscopic growth of particles. Differences in wind speed would also contribute to different sea-salt production. Because different models parameterize aerosol processes differently and use or simulate different meteorological fields, cloud effects on optical depth are model-dependent. For example, the GISS clear-sky AOT is 42–53% smaller than the all-sky value on global average, with much larger differences over ocean than over land.

3.2.3. Intercomparions of global and seasonal average aerosol direct effect

Ocean: Table 7 summarizes estimates of the clear-sky aerosol direct radiative effect over 60° S–60° N oceans on a seasonal basis. For the aerosol direct effect at the TOA, 8 of 11 measurement-based and satellite-model integration-based estimates agree with each other within about 10%, giving the annual average DRE at the TOA of $-5.1 \sim -5.7\,\mathrm{Wm}^{-2}$. By comparisons, the CERES_B estimate is 25-33% smaller (less negative), whereas MODIS_A and MISR_G estimates are 15–40% larger (more negative). Given that CERES_B and CERES_A have used the same flux and radiance measurements but with different algorithms for clear pixel identification and aerosol retrieval, their DRE difference emphasizes a need for more effort on clear-sky identification and improvement of aerosol retrieval algorithms and ADMs (Loeb and Manalo-Smith, 2005; Zhang et al., 2005a, b). The large MODIS_A estimate may result from

adding the DRE of individual components to derive the total DRE, because the aerosol direct effect is not additive and a simple summation would introduce a high bias of up to 50% in some regions, depending on aerosol absorption (Bellouin et al., 2005[6]). The high bias in the MISR_G estimate should result from an overall overestimate of 20% in early post-launch MISR optical depth retrievals (Kahn et al., 2005). Seasonal variations derived from these approaches are generally small, with a ratio of the largest to the smallest TOA cooling no more than 1.2. On annual average, the median and standard error ε ($\varepsilon=\sigma/(n-1)^{1/2}$, where σ is standard deviation and n is the number of measurements or simulations) of these TOA DRE estimates are $-5.5\,\mathrm{Wm}^{-2}$ and $0.19\,\mathrm{Wm}^{-2}$, respectively.

Seven measurement-based estimates give the DRE at the surface of $-8.8\pm0.40\,\mathrm{Wm}^{-2}$ (median $\pm$ ε) on an annual basis. This suggests that the ocean surface cooling is about 60% larger than the cooling at the TOA. Note that the SeaWiFS estimates (Chou et al., 2002) of sea surface cooling are much smaller than other measurement-based estimates, possibly resulting from biases/uncertainties in its assumed aerosol models. We notice that Chou et al. (2002) assume the spectral-independent SSA of 0.9955 for maritime aerosols, 0.9 for $\tau>0.3$ (representing dust and smoke), and a linear interpolation in between. Such oversimplification has perhaps underestimated the aerosol absorption over ocean. The notion is somewhat corroborated by comparisons with available measurement-based calculations. For example, Chou et al. (2002) derive the surface to TOA DRE ratio of 2.5 in Southeast Asia due to the 1997 Indonesian fires, which is smaller than the value of 3.3 reported by Podgorny et al. (2003) on the basis of radiometric observations of aerosol single-scattering albedo in the region (e.g., Nakajima et al., 1999; von Hoyningen-Huene et al., 1999).

Model simulations give wide ranges of DRE estimates at both the TOA and surface. In particular, the SPRINTARS estimated DRE values at both the TOA and surface differ substantially from other models. Possible reasons for such large discrepancies include smaller optical depth, stronger absorption, and potential uncertainties in other

optical parameters of SPRINTARS simulations (Yu et al., 2004). Estimates from GOCART and LMDZ-INCA are generally 30–60% larger than those from LMDZ-LOA and GISS. The ensemble of five models gives the annual average DRE (median $\pm\ \varepsilon$) of $-3.5\pm0.64\,\mathrm{Wm}^{-2}$ and $-4.8\pm0.8\,\mathrm{Wm}^{-2}$ at the TOA and surface, respectively. On average, the surface cooling is about 37% larger than the TOA cooling, slightly smaller than the measurement-based estimate of 60%. Large DRE differences between models result from a combination of differences in parameterizations of various aerosol processes, which are being documented under the AEROCOM framework (Kinne et al., 2005; Textor et al., 2005).

The model-based ensemble estimates of DRE are 30–50% smaller than the measurement-based estimates. As discussed earlier, MODIS retrieved optical depths tend to be overestimated by about 10–15% due to the contamination of thin cirrus and clouds in general. Such overestimation of optical depth would result in a comparable overestimate of the aerosol direct radiative effect. Other satellite AOT data may have similar contamination, which however has not yet been quantified. Note also that the cloud contamination in the MODIS value probably already has been reduced by the weighting with the number of aerosol retrievals (Remer and Kaufman, 2005). For simplicity, we assume a cloud contamination of 10–15% in the measurement-based average DRE. With this correction of cloud contamination, the discrepancy between the measurement-based and model-based estimates would be reduced to 20–40%.

Land: Currently, satellite measurements alone are not adequate to characterize complex aerosol properties and hence can not derive the aerosol direct effect over land with good accuracy. As such DRE estimates over land rely on model simulations and satellite-model or satellite-AERONET integrations, as listed in Table 8. For the measurement-based estimates, MODIS_A using MODIS AOT in conjunction with AERONET retrieved size distribution and single-scattering albedo gives the largest DRE at both the surface and TOA. Significant DRE differences between MODIS_A and MODIS_G should result from differences in size distribution and single-scattering albedo between GOCART simulations and AERONET retrievals and in RT parame-

terizations, given that the two approaches use the same albedo dataset and AOT differences between 2001 and 2002 are small. On global and annual average, these measurement-based approaches derive a DRE (median ± ε) of $-4.9\pm0.66\,\mathrm{Wm^{-2}}$ at the TOA and $-11.8\pm1.87\,\mathrm{Wm^{-2}}$ at the surface respectively. The surface cooling is about 2.4 times larger than the TOA cooling because of aerosol absorption.

For model simulations, again SPRINTARS gives the lowest DRE of $-1.7\,\mathrm{Wm^{-2}}$ at the TOA and $-5.1\,\mathrm{Wm^{-2}}$ at the surface on annual average. In addition to possible reasons discussed previously for ocean DRE, differences in land surface albedo parameterizations should also contribute. On annual and global land average, SPRINTARS derives an albedo of 0.29 in the visible and 0.26 in the near-infrared, respectively. The seemingly high visible albedo would reduce the aerosol direct effect at both the TOA and surface. GOCART and LMDZ-INCA derive larger DRE than LMDZ-LOA and GISS do. An ensemble of five model simulations derives a DRE (median ± ε) of $-2.8\pm0.59\,\mathrm{Wm^{-2}}$ at the TOA and $-7.2\pm0.93\,\mathrm{Wm^{-2}}$ at the surface, respectively. These are about 40% smaller than the measurement-based estimates. However, the model-derived surface/TOA DRE ratio of about 2.6 is not inconsistent with the value of 2.4 derived from the measurement-based estimates. The measurement-model differences are a combination of differences in aerosol amount (optical depth), single-scattering albedo, phase function, surface albedo, and radiative transfer schemes. We also find that seasonal variations of DRE over land, as derived from both measurements and models, are larger than that over ocean as discussed earlier.

3.3. Assessment of the regional aerosol direct effect

3.3.1. Intercomparisons over ocean

Table 9 compares individual assessments of the clear-sky average aerosol direct effect at the TOA for MAM, JJA, and ANN over five zones (excluding land), i.e., zone 2, 4, 6, 7, and 9 as defined in Fig. 5. These zones are chosen to represent regions significantly influenced by pollution (zone 2 and zone 4) and dust (zone 4 in MAM and zone 6 and 7)

and the most pristine region (zone 9). Clearly, model simulations are generally smaller than measurement-based estimates by 30–50%. Differences between measurement-based estimates are generally moderate, with the standard deviation accounting for about 15–25% of the average. Differences among various approaches are generally much larger than the detected seasonal variations. While the different approaches tend to agree on the global distribution of aerosol impacts in MAM, they tend to disagree in JJA. In MAM all approaches show the Northwest Pacific (zone 4) having the largest impact followed by the North Atlantic (zone 2 and 6) and the Arabian Sea (zone 7). In JJA the measurement-based assessments indicate that the Arabian Sea (zone 7) has the greatest impact, while the model-satellite integrated assessments indicate zones 4, 6, and 7 are more or less equivalent. Different model simulations appear to suggest different patterns. For example, GOCART simulations suggest that zone 6 has the greatest aerosol effect, whereas LMDZ-INCA suggests that zone 4 and zone 7 have a comparable and greatest effect.

To further examine pattern differences (e.g., peak, broadness, and skewness) between different approaches, we also calculate the probability density function (PDF) for DRE in individual zones for six approaches, as shown in Figs. 7 and 8 for MAM and JJA, respectively. Our sensitivity tests show that differences in the spatial resolution between individual approaches will not introduce any significant difference in the PDF. The following discussion focuses on major characteristics as revealed by satellite observations.

Zone 2: The region is perturbed by pollution outflows from North America and to a lesser extent from West Europe. In MAM, the largest TOA cooling of -8.5 to $-9.4\,\mathrm{Wm^{-2}}$ is estimated by MODIS_A, MODIS, CERES_C, and MISR_G. As evidenced in Fig. 7a, MODIS and MISR_G have a similar PDF, except that MISR_G is biased slightly toward less negative DRE. CERES_A, MODIS_G, and MO_MI_GO derive less negative DRE values of around $-8\,\mathrm{Wm^{-2}}$ because of a less frequent occurrence at more negative DRE ranges. The GOCART simulation peaks at a relatively less negative DRE, giving an average of $-6.8\,\mathrm{Wm^{-2}}$ that is smaller than other estimates discussed above but

greater than CERES_B estimate of $-5.6\,Wm^{-2}$. In JJA, MODIS has a relatively constant PDF from -3 to $-14\,Wm^{-2}$, while GOCART simulations give a narrow PDF that is well within -4 to $-8\,Wm^{-2}$. Other methods give comparable PDFs that fall inbetween MODIS and GOCART. The largest DRE of $\sim-8.5\,Wm^{-2}$ is estimated by MODIS and MISR_G, though their PDFs are different.

Zone 4: In MAM, the region is profoundly influenced by continental outflows from East Asia and aerosols in the region are a complex mixture of Asian pollution, mineral dust, and sea-salt. Various methods derive the TOA DRE ranging from -8.7 (CERES_B) to $-17.3\,Wm^{-2}$ (CERES_C), which is the largest among the regions examined. In JJA, the impacts from Asian continental outflow become weaker. The aerosol direct effect can reduce from MAM to JJA by as much as 50% for CERES_B. For other approaches, such reductions generally range from 8 to 30%, which is comparable to the differences among different approaches. Note that in both seasons, the PDF of GOCART simulation is narrower than other PDFs and peaks at a less negative DRE.

Zone 6: The region is influenced by dust outflow from North Africa throughout the year, and by biomass burning smoke in winter and early spring. Different approaches, except CERES_C, yield more negative DRE in JJA than in MAM. The PDFs exhibit a larger breadth and peak at a more negative DRE in JJA than in MAM. However, such seasonal variations are smaller by as much as a factor of 2 than differences existing among different approaches. Note also that the model-satellite integration-based assessments in the region are generally larger than both the measurement-based and model-based estimates.

Zone 7: The region is influenced by dust from the Arabian Peninsula and North Africa, and pollution from the Indian subcontinent. While pollution impacts occur mainly in the Northern Indian Ocean and in winter and spring, dust impacts dominate in the Arabian Sea and in summer. Different approaches derive broad PDFs in both seasons. In summer, the DRE ranges from about $-6.9\,Wm^{-2}$ (GOCART) to as much as $-17.5\,Wm^{-2}$ (MODIS), larger than those in spring (e.g., -5.1 to $-12.7\,Wm^{-2}$). Such seasonal variations are comparable to those in zone 4 and somewhat smaller than

differences among various approaches.

Zone 9: The tropical Southeast Pacific is the most pristine region in the world and has the smallest ADRE of −2 to −6 Wm^{-2} without significant seasonal variations. Various approaches give PDFs with similar breadth but with somewhat different peak. While GOCART simulates the lowest DRE (∼−2 Wm^{-2}) in this remote region, MISR derives the largest DRE (−5 to −6 Wm^{-2}) because of the high bias of aerosol optical depth in the early post-launch version of MISR aerosol data (pre-Version 16).

Figure 9a shows scatterplots of seasonal and regional (zonal) average DRE estimates at the TOA and over ocean versus the MODIS estimate. Each data point represents a seasonal average ADRE in one of 13 zones defined in Fig. 5. Table 10a summarizes some statistical measures of individual DRE estimates (Y) with respect to the MODIS assessment (X), including linear correlation coefficient (r), mean ratio ($B=\frac{1}{N}\sum_{i=1}^{N}\frac{Y_i}{X_i}$, where i denotes a specific season for a specific zone, N=39 for CERES_C and N=52 for the other estimates), and the standard deviation of the ratio (σ_B). A value of 1 for B denotes no difference of an individual assessment with respect to MODIS. B<1 and B>1 indicates less and more negative DRE, respectively. Clearly, CERES_A, CERES_C, and MODIS_G compare very well with MODIS estimate, with the ratios of 0.99±0.23, 1.03±0.21 and 1.03±0.28, respectively. The correlation coefficient for CERES_A and CERES_C (0.93) is higher than 0.86 for MODIS_G. CERES_B also has a high correlation of 0.91 but is smaller in magnitude with a ratio of 0.77±0.19. Due to the overall high bias of the early post-launch aerosol optical depth over ocean as discussed earlier, the MISR-derived DRE has a high bias of 1.20±0.42 with a moderate correlation of 0.68. MODIS_A also shows a high ratio of 1.28±0.33 but with a higher correlation of 0.88. The two satellite-model integration-based assessments (MO_GO and MO_MI_GO) have a correlation of 0.82-0.86, comparable to GOCART simulations. However they are much closer in magnitude to the MODIS estimate than GOCART simulations. All model simulations are lower than the MODIS estimate. Among them, LMDZ-INCA and GOCART are relatively close to the MODIS estimate with a mean

ratio of 0.7~0.8, followed by GISS and LMDZ-INCA with the mean ratio of 0.4~0.5. SPRINTARS simulations have the weakest correlation (0.57) and lowest DRE (with a ratio of 0.32±0.14) with respect to the MODIS estimate.

Figure 9b shows scatterplots similar to Fig. 9a, but for seasonal and regional average DRE estimates at the surface with respect to the MODIS_A estimate. Corresponding statistical measures are listed in Table 10b. It appears that all satellite-GOCART integration-based estimates (i.e., MO_MI_GO, MO_GO, MODIS_G, MISR_G) correlate well with the MODIS_A estimate (r=0.82~0.89). On average, MODIS_G and MISR_G are higher by 10–20%. MO_MI_GO and MO_GO are lower by less than 10%, suggesting a significant reduction of lower bias (B=0.74) for GOCART estimates. A large majority of model-based estimates are lower than the MODIS_A estimate, with SPRINTARS showing the largest deviations.

3.3.2. Comparisons with AERONET derived DRE over land

Monthly mean values of observed aerosol optical depth, retrieved single scattering albedo, and derived aerosol direct solar effect based on the AERONET measurements (Zhou et al., 2005) are compiled to seasonal averages in individual zones, as shown in Table 11. There are 8 zones (i.e., zone 1–4, 6–7, and 10–11), in which 3–25 AERONET sites are available in individual seasons. Since most AERONET sites are established over land, the regional averages so derived are not representative of conditions over ocean. Note also that regional representativeness of AERONET measurements may be undermined by the limited number of stations and/or possibly their general proximity to source regions (e.g., urban areas, biomass burning regions) in some zones. Nevertheless, these averages do show some seasonal variations and geographical differences that are consistent with previous studies. In the US (zone 1 and zone 2), the aerosol effect is greatest in summer and least in winter, with magnitudes larger by 36–113% for the TOA DRE and 27–66% for the surface DRE in the Eastern US than in the Western US, depending on season. In the Western Europe (zone 3), the TOA DRE has no significant seasonal variations, while the surface DRE is greatest in summer

and least in winter. The TOA/surface ratios from spring to autumn are smaller than those over East US, due to stronger absorption in West Europe than in East US. In East Asia (zone 4), the aerosol impacts are greatest in summer and spring and least in winter. The surface cooling of about $-30\,\mathrm{Wm}^{-2}$ in summer and spring is much greater than that in the US and West Europe. Zone 6 and zone 7 are significantly influenced by mineral dust from the Saharan region and Arabian Peninsula during the whole year and by biomass burning from tropical Africa in winter. The aerosol optical depth is among the largest but the absorption of dust is weaker than pollution, resulting in a larger TOA cooling and smaller surface cooling than those in East Asia. South America and South Africa (zone 10 and zone 11) are greatly influenced by absorptive smoke from biomass burning in the austral spring (SON) and winter (JJA). Such a heavy smoke cools the surface by more than $30\,\mathrm{Wm}^{-2}$ in SON and by about $23\,\mathrm{Wm}^{-2}$ in JJA, a factor of 2–3 more than that in wet seasons.

These AERONET measurements are used to evaluate a variety of DRE estimates from satellite (MODIS_A), model simulations (GOCART, SPRINTARS, GISS, LMDZ-INCA, LMDZ-LOA), and model-satellite integrations (MODIS_G, MISR_G, MO_GO, MO_MI_GO), as shown in Fig. 10. The MODIS_A estimates, at both the TOA and surface, are greater (i.e., more negative) than AERONET measurements. DRE estimates from GOCART and LMDZ-INCA simulations and the integrations of GOCART simulations and satellite data sets generally agree reasonably well with AERONET measurements at relatively weak cooling regimes (e.g., DRE$>-7\,\mathrm{Wm}^{-2}$ at the TOA and DRE$>-20\,\mathrm{Wm}^{-2}$ at the surface), but are biased toward less cooling otherwise. Further examination indicates that those underestimates of DRE generally occur in South Africa and South America (zone 10 and 11) during the austral spring and winter (biomass burning season), North Africa and mid-East (zone 6 and 7) around a year, East Asia (zone 4) during non-summer seasons, and Europe in winter. Such discrepancies may result from inadequacies in both model simulations and satellite retrievals. They would also come from the poor regional representativeness of AERONET stations due to the limited number of sites (zones 4, 6, 7) and/or proximity to biomass

burning and dust storm areas (zones 6–7, 10–11). Other model simulations generally show much larger deviations from the AERONET measurements.

3.3.3. Comparisons of the radiative efficiency with results from the literature

In the following, we discuss aerosol direct radiative effect in several distinct aerosol regimes where results from intensive field experiments and/or independent satellite analyses have been published. We will concentrate on comparisons of the radiative efficiency E_τ from different measurement-based methods collected in this review (see Table 3) with ranges of five models and those from the literature. We also convert published E_τ values with respect to the AOT at wavelengths other than 550 nm to that with respect to AOT at 550 nm by using aerosol Angström exponents either from available observations or from the MODIS retrievals. In all cases, E_τ is calculated as the mean DRE divided by the mean AOT.

A. East US and mid-latitude North Atlantic

In the Eastern US and mid-latitude North Atlantic (zone 2), the aerosol optical depth in spring and summer is larger than that in fall and winter (Malm et al., 2004; Bergstrom and Russell, 1999). A number of field campaigns have been conducted in summer (see Table 1). Table 12 compares various E_τ estimates in the region. In the Eastern US, MODIS_A derives E_τ of $-43\sim-46\,\mathrm{Wm^{-2}}\tau^{-1}$ at the TOA, greater than AERONET values by 15–25%. These TOA E_τ values are much greater than measurement-based estimates ($\sim-25\,\mathrm{Wm^{-2}}\tau^{-1}$) from Kinne and Pueschel (2001) and Delene and Ogren (2002). Ranges of model simulations are generally inbetween. For E_τ at the surface, MODIS_A values are ~14% less than AERONET measurements of $-80\sim-84\,\mathrm{Wm^{-2}}\tau^{-1}$, but 10–60% greater than model ranges. Over the mid-latitude North Atlantic, MODIS and MODIS_A derive E_τ values at the TOA that are greater than CERES estimates and model ranges. Nevertheless, all these TOA values fall into

a wide range of estimates (−30 to −60 $Wm^{-2}\tau^{-1}$) from field experiments in the region (Hignett et al., 1999; Russell et al., 1999; Kinne and Pueschel, 2001). The model estimates of surface E_τ are generally less than observations.

B. Europe

Europe is influenced by regional pollution and dust from the Saharan Desert. In spring, Arctic haze also influences the region with a TOA DRE comparable to values in heavily polluted regions, as documented by measurements in Leipzig, Germany in April 2002 (Heintzenberg et al., 2003). Comparisons of E_τ estimates in Europe are summarized in Table 13. Clearly, there is good agreement between AERONET, MODIS_A, and observations during the MINOS experiment (Markowicz et al., 2002), for E_τ at both TOA and surface. However, these values are much greater than observations in urban and coastal areas (Horvath et al., 2002) and model estimates.

C. East Asia and Northwest Pacific

The regions are perturbed by a mixture of Asian pollution and dust, particularly in spring and summer. Comparisons of radiative efficiency estimates are summarized in Table 14. Over Northwest Pacific, the TOA E_τ estimates from MODIS and MODIS_A are greater than the observations during ACE-Asia (Seinfeld et al., 2004), calculations based on several SKYNET sites in East China Sea and Korean Peninsula (Kim et al., 2005), CERES measurements and model simulations. For surface DRE, MODIS_A derived E_τ agrees well with the observations in the ACE-Asia region (Seinfeld et al., 2004) but is much less than measurements in Korea (Bush and Valero, 2003) and all SKYNET measurements (Kim et al., 2005). The model-derived surface E_τ values are much smaller than MODIS_A estimate. Over land, AERONET measurements give E_τ of −28 Wm^{-2} at the TOA, which agrees well with MODIS_A estimate and an independent sunphotometer measurement in November at a background air

monitoring station sitting in the Yangtze delta region (Linan, China) (Xu et al., 2003). However, these TOA E_τ values are much greater than SKYNET observations (Kim et al., 2005). At the surface, the E_τ from AERONET measurements is generally larger than MODIS_A estimate, other observations (Xu et al., 2003; Kim et al., 2005).

D. Tropical North Atlantic and coastal North Africa

The region is influenced by biomass burning from tropical Savanna in winter and early spring, and mineral dust year round. Some measurements using CERES and ERBE fluxes in conjunction with MODIS and TOMS aerosols (Li et al., 2004; Hsu et al., 2000) show that the TOA E_τ in winter is smaller than in summer, as shown in Table 15, presumably because biomass burning smoke is more absorbing than mineral dust. Such seasonal variations are shown in MODIS_A measurements but not in others. In winter, both MODIS and MODIS_A give a much greater value of E_τ than other measurements and model estimates. In summer, MODIS_A gives a TOA cooling that is much greater than other measurements and model estimates. For the surface E_τ and in both seasons, MODIS_A values are consistent with the results from Li et al. (2004), but are greater than the model estimates.

E. Arabian Sea and Northern Indian Ocean

The Northern Indian Ocean and Arabian Sea are influenced by anthropogenic aerosols from South and Southeast Asia (Ramanathan et al., 2001b) and by local sea-salt and dust transported from the Arabian and Saharan regions (Satheesh and Srinivasan, 2002), with compositional contributions changing with season. While during the premonsoon period (January–March) pollution dominates (Ramanathan et al., 2001b), the dust contribution becomes larger in April-May, as documented by the observations that show larger near-infrared aerosol optical depth in April-May than during Februray-March (Satheesh and Srinivasan, 2002). This, along with weaker absorp-

tion of dust than pollution, results in a more negative TOA DRE in May (Satheesh and Srinivasan, 2002). The aerosol direct solar effect also has large spatial variations over the tropical Indian Ocean (Rajeev and Ramanathan, 2001). The observed TOA solar effect north of the equator is about a factor of 2 greater than that south of the equator, with the minimum effect occurring around the Inter-Tropical Convergence Zone (ITCZ). The aerosol radiative effect also shows as much as a factor of 2 of interannual variation (Satheesh et al., 2002; Satheesh and Srinivasan, 2002) in the region.

Table 16 summarizes assessments of radiative efficiency in the region and field measurements in the Arabian Sea, northern Indian Ocean, and Bay of Bengal. In all seasons, MODIS and MODIS_A produce radiative efficiencies in zone 7 that are greater than CERES measurements and model estimates, both at the TOA and surface. The values of E_τ at the TOA derived from MODIS and MODIS_A are consistently greater than a number of field experiments conducted in the northern Indian Ocean. Such differences may result from contrasts in aerosol compositions between the Arabian Sea (i.e., dust dominated) and the northern Indian Ocean (a mix of pollution and dust).

F. South America and South Africa

During the austral winter and spring, biomass burning smoke significantly influences South America, Southern Africa and the South Atlantic. Table 17 summarizes the E_τ assessments in South America. The AERONET and MODIS_A measurements give E_τ of $-25\sim-27\,\mathrm{Wm}^{-2}\tau^{-1}$ and $-71\sim-76\,\mathrm{Wm}^{-2}\tau^{-1}$ at the TOA and at the surface, respectively. Model estimates cover a wide range of $-14\sim-44\,\mathrm{Wm}^{-2}\tau^{-1}$ at the TOA and $-43\sim-80\,\mathrm{Wm}^{-2}\tau^{-1}$ at the surface. Several studies demonstrate that the TOA radiative effect depends strongly on surface land cover (Ross et al., 1998; Christopher et al., 2000).

3.4. Estimating anthropogenic aerosol direct climate forcing

Estimates of anthropogenic aerosol optical depth and direct forcing so far have been predominantly model-based. The determination of anthropogenic aerosols requires a quantification of biomass burning ignited by lightning (natural origin) and mineral dust due to human induced changes of land cover change and climate (anthropogenic origin), which remains uncertain. Recent modeling (Tegen et al., 2004) suggests that the anthropogenic sources of dust contribute less than 10% of the total dust optical depth, although early studies speculated the fraction to be between 0% (Ginoux et al., 2001) and 50% (Tegen and Fung, 1995). Three global chemical transport models, namely GOCART, LMDZ-LOA, and SPRINTARS, consistently give the anthropogenic aerosol optical depth of 0.030~0.036 over global oceans (Kaufman et al., 2005a).

Satellite instruments do not measure the aerosol chemical composition needed to discriminate anthropogenic from natural aerosol components. Because anthropogenic aerosols are predominately sub-micron, the fine-mode fraction derived from new-generation satellite sensors like POLDER, MODIS, or MISR, might be used as a surrogate for deriving anthropogenic aerosol optical depths. This could provide a feasible way to conduct measurement-based estimates of anthropogenic aerosol forcing (Kaufman et al., 2002a; Christopher and Zhang, 2004). Kaufman et al. (2005a) show that the fraction of the aerosol originating from anthropogenic activity can be estimated from MODIS measurements with an uncertainty of ±30% over the oceans. The so-derived average anthropogenic aerosol optical thickness is about 0.033, consistent with assessments of 0.030~0.036 from three global chemical transport models even though the total AOT from MODIS is 25–40% higher than the models (Kaufman et al., 2005a). This accounts for 21±7% of the MODIS observed total aerosol optical thickness, compared with about 33% of anthropogenic contributions estimated by the three models.

There have been some estimates of DCF by anthropogenic aerosols. Bellouin et al. (2005)[6] decompose MODIS total AOT into four generic aerosol types , namely ma-

rine aerosol, mineral dust, biomass burning and pollution, by using the MODIS fine-mode fraction in combination with TOMS aerosol index (a semi-quantitative measure of UV-absorbing aerosol loading) and SSM/I wind speed (for estimating the marine AOT). They estimate that on a global and annual average, the clear-sky DCF is −2.7 and $-6.0\,\mathrm{Wm}^{-2}$ at the TOA and surface, respectively, accounting for about 37% and 47% of DRE by all aerosols. Yu et al. (2004) combine MODIS retrievals and GOCART simulations to yield the clear-sky DFC of −1.4 and $-4.2\,\mathrm{Wm}^{-2}$ at the TOA and surface, respectively. These respectively account for about 31% and 42% of the DRE. Recent model simulations by Reddy et al. (2005b) estimate that the clear-sky DCF by fossil fuel and biomass burning is about $-0.64\,\mathrm{Wm}^{-2}$ or 31% of the DRE. It appears that these independent studies estimate that the anthropogenic aerosol DCF at the TOA accounts for about 31–37% of the DRE by both natural and anthropogenic aerosols, although the absolute values differ by as much as a factor of 4. In comparison, the surface DFC accounts for 42–47% of the DRE.

Anderson et al. (2005) establish a conceptual framework for achieving an observationally based quantification of DCF through the use of satellite observations coordinated with suborbital remote and in situ measurements and with chemical transport models. The whole-sky DCF at a specific time and location can be expressed as:

$$DCF = (1 - A_c)\tau f_f f_{af} E_a \tag{1}$$

Its integration over time and space (weighted by surface area) gives the regional or global average DCF. In this conceptual model, the clear-sky DCF is determined by optical depth (τ), fine-mode fraction of τ (f_f), anthropogenic fraction of fine-mode τ (f_{af}), and forcing efficiency with respect to anthropogenic τ (E_a). It is assumed here that the whole-sky DCF is a product of the clear-sky DCF and clear-sky fraction ($1 - A_c$) where A_c is cloud cover. This assumption will introduce large uncertainties in regions where absorbing aerosols stay above low clouds. The uncertainty analysis can therefore be approached in terms of our knowledge of the global-mean value of each parameter and their complex correlations. Table 18 presents an uncertainty analysis for land and ocean separately, in which observational constraints derived from this review are

imposed and for other parameters that lack observational constraints, assumptions are made based on model simulations. Given the absence of knowledge about correlations between the deterministic parameters of DCF, the current calculation is framed in terms of mean values only. Assignment of these values is detailed in the table footnote. The analysis shows that the DCF over land is about a factor of 2 larger than that over ocean. Its uncertainty is also larger over land than over ocean. On global and annual average, DCF is estimated to be about $-0.5\,\mathrm{W/m^2}$ with an uncertainty of about 67%. The uncertainty partitions 60% to the land and 40% to the ocean. The parameter uncertainty contribution to DCF further suggests that five parameters, namely f_f and f_{af} over both land and ocean, and τ over ocean, introduce about 80% of the overall uncertainty in the DCF estimate, with individual shares ranging from 10–20%.

4. Discussion: outstanding issues

Despite substantial progresses in the assessment of the aerosol direct effect as summarized above, several important issues remain, and significant efforts are required to address them. As discussed earlier, most measurement-based studies so far have concentrated on the influences by the sum of natural and anthropogenic aerosols on solar radiation under clear sky conditions. Current DCF estimates are poorly constrained by observations. Because of a lack of measurements of aerosol absorption and difficulty in characterizing land surface reflection, estimates of DRE over land and at the ocean surface are currently realized through a combination of satellite retrievals, surface measurements, and model simulations, and are less constrained. There is also a need to quantify aerosol impacts on the thermal infrared radiation and characterize the cloud modulation of aerosol-radiation interactions. In addition, quantifying aerosol absorption remains a pressing issue. It is also essential to adequately characterize diurnal variations of the aerosol radiative effect. Finally, aerosol measurements from different platforms generally are not consistent in terms of their spatial and temporal representativeness. Great efforts are necessary to account for such inconsistency when

comparing and integrating different aerosol measurements. However, the patterns in the relative behavior of models and observations suggest that once these differences are fully understood and accounted for, a unified picture would emerge (e.g., Diner et al., 2004).

4.1. Direct effect in the thermal infrared range and under cloudy conditions

Due to their large size, mineral dust and sea-salt aerosols can cause warming in the thermal infrared, both at the TOA and at the surface. Such a warming effect could be significant, as suggested by a few observational studies summarized in Table 19. The thermal infrared effect of Saharan dust could account for 10% (Highwood et al., 2003) to 30% (Hsu et al., 2000) of the observed instantaneous solar effect. Haywood et al. (2005) demonstrate that mineral dust in July can exert a longwave radiative forcing by as much as 50 $\mathrm{Wm^{-2}}$ in the monthly mean for 1200 UTC in cloud-free regions, which accounts for the discrepancy between model calculations and the satellite observations. Zhang and Christopher (2003) derived a thermal infrared warming of 15 $\mathrm{Wm^{-2}}\tau^{-1}$ at the satellite overpassing time over the Saharan desert that would cancel ~40% of the solar cooling at the TOA. Satheesh and Lubin (2003) show that aerosols in the northern Indian Ocean, a mixture of dust, sea-salt and pollution, would impose a thermal infrared warming that could reduce the solar radiative effect by about 45% at modest winds (4–6 $\mathrm{ms^{-1}}$) and by more than 70% at high winds (>10 $\mathrm{ms^{-1}}$), because sea-salt production increases with wind speed. Nevertheless, current estimates of aerosol warming effects in the thermal infrared remain highly uncertain, because its assessment requires vertical distributions of aerosol extinction and atmospheric temperature that are not well characterized by either observations or simulations (Sokolik et al., 2001; Lubin et al., 2002). Aerosol optical properties in the thermal infrared range are rarely measured directly, hence the estimates of the thermal infrared effect depend largely on assumed aerosol models. In addition, the scattering effect in the thermal infrared domain is generally neglected in most GCMs, which may lead to an underestimate of the thermal infrared aerosol effect (Dufresne et al., 2002).

Most studies so far have focused on the clear-sky direct effect. Calculations of the cloudy-sky aerosol direct effect require an adequate characterization of vertical distributions of aerosols and three-dimensional fields of clouds, especially for absorbing aerosols (Haywood and Shine, 1997; Liao and Seinfeld, 1998; Podgorny and Ramanathan, 2001; Zhou et al., 2005). Neglect of aerosol impacts under cloudy conditions generally would introduce large errors to the aerosol direct effect, as documented by observations. In the tropical Indian Ocean, the surface cooling under climatological cloud conditions is comparable to that under clear conditions, while the TOA effect could switch from cooling under clear conditions to warming under overcast conditions (Podgorny and Ramanathan, 2001). Observations over the South Atlantic show a clear separation between the elevated smoke layer from southern Africa (2–4 km) and low-level stratiform clouds (below 1 km) during the SAFARI 2000 experiment. In the presence of clouds, the smoke causes a net TOA warming of 12 Wm^{-2}, compared to a cooling of $-13\,Wm^{-2}$ under clear conditions for average smoke conditions and at a SZA of 60° (Keil and Haywood, 2003). Note that substantial differences currently exist in aerosol vertical distributions simulated by different models (Penner et al., 2002) and limited measurements do not suffice for the estimate of the cloudy-sky effect. Hopefully, the emerging ground-based aerosol lidar network (as discussed in Sect. 2.1) and launch of spaceborne lidars (Stephens et al., 2001) will help improve the understanding of the aerosol direct effect under cloudy conditions and the thermal infrared range.

4.2. Deriving aerosol direct effect over land from satellite

It has been easier to estimate the aerosol direct effect from satellite measurements over ocean than over land because the dark ocean surface reflection is easier to characterize for this purpose. The land surface reflection is large, heterogeneous, and anisotropic, which complicates the determination of the aerosol direct effect. For example, Hsu et al. (2000) detect a significant impact of Saharan dust on solar radiation over the Atlantic Ocean but no clear signal over the nearby Saharan deserts. Apparently the lack of a dust signal over the deserts is attributable to the large heterogeneity of surface

reflectance as documented by high-resolution MODIS land albedo retrievals (Tsvetsinskaya et al., 2002). The new-generation satellite sensors like MODIS and MISR are improving the characterization of land surface reflection by measuring its wavelength dependence and angular distribution at high resolution. This offers a promising opportunity for inferring the aerosol direct effect over land from satellite measurements of radiative fluxes (e.g., CERES).

4.3. Aerosol single-scattering albedo and absorption

A characterization of aerosol absorption or SSA is complicated by instrumental errors and modeling inadequacies, and hence these associated uncertainties/biases are major sources of uncertainty in studying aerosol radiative forcing and climate response (e.g., Heintzenberg et al., 1997). The theoretical uncertainty of the AERONET retrieval of SSA is 0.03 for AOD greater than 0.3 (Dubovik et al., 2002). Similarly, at large AOD the estimated AERONET uncertainty for absorptive optical depth is 0.01 (Dubovik and King, 2000; Dubovik et al., 2001). These estimated accuracies have yet to be validated by independent measurements. It is important to pursue such validation because a recent study has shown a factor of 2–4 discrepancy between the AERONET retrievals and the simulated absorptive optical depths from tow models (Sato et al., 2003). This discrepancy would imply significant errors in the global burden of black carbon and/or the absorptive efficiency of black carbon (perhaps related to aerosol mixing state, morphology, or size distribution) (Sato et al., 2003; Martins et al., 1998; Jacobson, 2000, 2001). On the other hand, a recent comparison of in situ to AERONET absorption over the Chesapeake Bay indicated that the latter may be biased high (Magi et al., 2005). Satellite methods for quantifying SSA and absorption have been developed and partially validated at UV wavelengths (Torres et al., 1998, 2002, 2005), although the retrieval has large uncertainties associated with its sensitivity to the height of the aerosol layer and it is unclear at present how these UV results can be extended to visible wavelengths. Kaufman et al. (2002b) developed an algorithm using views in and out of sunglint to retrieve total aerosol extinction and scattering, respectively, thus con-

straining aerosol absorption over oceans. The technique is going to be applied to the collocated MODIS and PARASOL data in the A-Train. Clearly, the global assessment of aerosol absorption and SSA represents a major challenge in efforts to quantify direct forcing. Note that the MODIS and CERES methods described here bypass the need for estimates of aerosol single-scattering albedo and other aerosol characteristics to calculate DRE at the TOA. Instead aerosol characteristics are intrinsically included in the basic satellite retrieval.

4.4. Diurnal cycle

Significant efforts are demanded to capture the diurnal cycle of aerosol direct forcing in order to better assess aerosol impacts on climate. In this context, diurnal variability of aerosol and cloud needs to be adequately characterized. AERONET measurements show that the daytime variability depends on location and aerosol type, with the variation as large as 40% for biomass burning smoke and urban/industrial pollution near the sources, and essentially negligible for dust (Smirnov et al., 2002). From the perspective of satellite remote sensing, the diurnal variation of aerosols can be better characterized by geostationary satellites (GOES) (Christopher and Zhang, 2002; Wang et al., 2003a, b). However, these satellites generally lack the information required to characterize aerosol types. Costa et al. (2004a, b) developed a method based on the synergistic use of low earth orbit and geostationary earth orbit satellite data for aerosol-type characterization, AOT retrieval and aerosol monitoring over the ocean. They use multiple spectral measurements from the low earth orbit satellite to characterize aerosol types dynamically. The derived aerosol type information is then used for retrieving aerosols from geostationary satellite measurements. By so doing, the diurnal variation of aerosols can be monitored. MODIS flying with EOS twin satellites, namely Terra and Aqua, can also be used to some extent to characterize aerosol diurnal variations, i.e., from late morning (10:30 LT) to early afternoon (13:30 LT) (Ichoku et al., 2005). Clouds can modulate the aerosol direct solar effect significantly and daytime variations of clouds need to be adequately characterized.

The aerosol direct effect depends on surface reflection and the anisotropy of surface reflection further complicates the calculation of the diurnal cycle of the aerosol radiative effect. A neglect of anisotropy of surface reflection could lead to significant overestimation of the diurnal range of the aerosol direct effect (Yu et al., 2004). With satellite remote sensing providing angular and spectral variations of surface reflection (e.g., Moody et al., 2005; Martonchik et al., 1998, 2002), it is feasible to better characterize the complexity of surface reflection and its interaction with aerosol extinction through the use of the black-sky and white-sky albedo for direct beam and diffuse light respectively (Yu et al., 2004; Bellouin et al., 2004).

4.5. Spatial and temporal scaling

Aerosol measurements from different platforms provide information representing different spatial and temporal scales. Polar-orbiting satellites can only observe global aerosols once a day. The geostationary satellites can monitor evolutions of aerosols at an hourly scale but usually cover limited regions. Aerosols can be substantially under-sampled by satellite sensors in regions with a high frequency of cloud presence. Ground-based sun photometers sample aerosols only during daylight hours, without clouds. Such point-type measurements may not be representative of 10^2 km^2 grid boxes of current global aerosol models. These inconsistencies complicate intercomparison and integration of aerosol products from different sources because aerosols generally show significant variability over meso-scales (e.g., 40–400 km and 2–48 h) (Anderson et al., 2003b). Several studies have examined these spatial and temporal scaling issues. For example, Kaufman et al. (2000) demonstrate that MODIS measurements onboard Terra and Aqua on average well represent the daily aerosols by analyzing the daytime variations of AERONET optical depth. New results from MODIS on Terra and Aqua confirm this analysis (Kaufman et al., 2005b[9]). High-resolution satellite retrievals prove to be extremely useful for examining spatial variability of aerosols and comparing satellite retrieved or model simulated grid-box averages with point measurements from ground-based networks (Ichoku et al., 2002). Alexandrov et al. (2004b) de-

rives statistics of temporal and spatial variations of aerosols based on high-frequency MFRSR measurements at two ARM sites located in Oklahoma and Kansas. However, the aerosol variability controlled by emissions and meteorological conditions should depend on location and time, making it challenging to account for these variations in regional- and global-scale intercomparisons and in data assimilation/integration.

5. Concluding remarks

5.1. Summary of findings from this review

Since the proposal of conceptual aerosol-radiation-climate interactions around 1970, substantial progress has been made, particularly in the last ten years. Such advancement has greatly benefited from significant improvements in aerosol measurements and increasing sophistication of model simulations. In particular, the establishment of ground-based aerosol networks such as AERONET and the execution of intensive field experiments in a variety of aerosol regimes have collected invaluable datasets that have been serving as a baseline for constraining and evaluating satellite retrievals and model simulations. New and enhanced satellite sensors, such as POLDER, MODIS, and MISR, are measuring aerosols on a global scale and with good accuracy. CERES measures broadband solar and thermal infrared fluxes that are used to derive aerosol radiative effect and forcing.

As a result of these improvements, we now have a much improved knowledge of aerosol properties and the interaction with solar radiation on the global scale. The multi-spectral MODIS measures global distributions of aerosol optical thickness (τ) on a daily scale, with high accuracy of $\pm 0.03 \pm 0.05\tau$ over ocean. The annual average τ is about 0.140 over global ocean, of which about 21% is estimated to be contributed by human activities based on the MODIS fine-mode and background aerosol fraction. The multi-angle MISR can evaluate the surface reflectance and retrieve aerosols simultaneously over all kinds of surfaces, including bright deserts. MISR derives an annual

average AOT of 0.225 over global land with an uncertainty of ∼20% or ±0.05. A combination of MODIS over-ocean and MISR over-land retrievals gives a global average of aerosol optical depth of about 0.167, which is 16% larger than an ensemble average 0.144 of five global aerosol models. It is possible that such discrepancy can be largely reduced by correcting cloud contamination in satellite retrievals.

The high-accuracy MODIS and MISR aerosol products and broadband flux measurements from CERES, together with simultaneous improvements in surface and cloud characterizations in these sensors, make it feasible to obtain observational constraints for the aerosol direct effect. Figure 11 summarizes the measurement- and model-based estimates of clear-sky annual average DRE at both the TOA and surface. A number of measurement-based approaches consistently estimate the clear-sky DRE (on solar radiation) at the top-of-atmosphere to be about $-5.5\pm0.19\,\mathrm{Wm}^{-2}$ (median ± standard error ε) over global ocean. At the ocean surface, the DRE is estimated to be $-8.8\pm0.40\,\mathrm{Wm}^{-2}$ with a combination of MODIS optical depth, AERONET measurements, and CTM simulations. Over land, deriving the aerosol direct effect from the flux measurements such as that from CERES is complicated by large and highly heterogeneous surface reflection. An integration of satellite retrievals and model simulations yields a DRE of $-4.9\pm0.66\,\mathrm{Wm}^{-2}$and $-11.8\pm1.87\,\mathrm{Wm}^{-2}$ at the TOA and surface, respectively. Overall, in comparison to that over ocean, the DRE estimates over land are more poorly constrained by observations and have larger uncertainties. An ensemble of five model simulations gives a DRE that is about 40–50% smaller than the measurement-based estimate. Such discrepancy could be reduced to 30–40% after accounting for cloud contamination in satellite retrievals. The integration of satellite and surface measurements into CTM proves to be a promising and essential approach to producing an optimal description of global aerosol distributions.

5.2. Future research

Despite these achievements several issues associated with measurement-based assessments remain open. We hope new developments in the next few years will further

advance our knowledge. Measurements of aerosol single-scattering albedo remain challenging (Heintzenberg et al., 1997). It would appear that uncertainty in current aerosol single-scattering albedo measurements constitutes the largest source of uncertainty in aerosol forcing and climate response. Measurement-based assessment of direct forcing by anthropogenic aerosol has been only applied to oceans because of the limited capability of satellite sensors in retrieving aerosol size information over land. Estimating aerosol direct effects in cloudy conditions requires measurements of diurnal cycle and vertical profile of aerosols and clouds. A few measurements suggest that aerosol effects on the thermal infrared radiation seemingly are not negligible but are highly uncertain because of scarcity of observations of aerosol profiles and aerosol properties in the thermal infrared region. The constellation of new-generation satellite sensors (e.g., A-Train) provides an unprecedented opportunity to improve aerosol characterization. In particular, satellite-borne lidar systems in ICESat and CALIPSO will improve aerosol profiling and assessment of the aerosol direct effect in the thermal infrared and under cloudy conditions. A synergistic use of multiple sensors would improve the characterization of global aerosols, clouds and land properties, and hence the assessment of aerosol forcing. For example, a combination of polar-orbiting and geostationary satellites would monitor the daytime cycle of aerosols with a better accuracy than a geostationary satellite alone, because multi-spectral measurements from a polar-orbiting satellite can provide an important constraint to aerosol retrievals from a geostationary satellite.

Aerosol models are a unique tool for estimating the past aerosol forcing and projecting future climate change. However model uncertainties are still large. It is important to use satellite measurements to improve model performance, such as integration and assimilation of satellite measurements with global models. Progress is promising but more effort is needed. Schemes of surface albedo characterization in global models also need to be evaluated and constrained with emerging measurements from new-generation satellite sensors. Finally, aerosol indirect effects on clouds continue to be an enormous challenge from both the observational and modeling perspectives and

progress is crucial if we are to improve our ability to predict climate change.

Acronyms and symbols:

	A
ABC:	Atmospheric Brown Cloud
ACE:	Aerosol Characterization Experiment
AD-Net:	Asian Dust Network
ADEOS:	Advanced Earth Observation Satellite
ADM:	Angular Distribution Models
AERONET:	Aerosol Robotic Network
AOD (AOT, τ):	Aerosol optical depth (thickness)
AVHRR:	Advanced Very High Resolution Radiometer
	B
BASE-A:	Biomass Burning Airborne and Spaceborne Experiment Amazon and Brazil
BRDF:	Bidirectional Reflectance Distribution Function
	C
CALIPSO:	Cloud Aerosol Infrared Pathfinder Satellite Observations
CCRI:	Climate Change Research Initiative
CCSP:	Climate Change Science Program
CERES:	Clouds and the Earth's Radiant Energy System
CLAMS:	Chesapeake Lighthouse and Aircraft Measurements for Satellite campaign
CMDL:	Climate Modeling and Diagnostic Laboratory (NOAA)
	D
DAAC:	Distributed Active Archive Center
DCF:	Direct climate forcing (anthropogenic aerosols)
DRE:	Direct radiative effect (total aerosols)
	E
EARLINET:	European Aerosol Research Lidar Network
ERBE:	Earth Radiation Budget Experiment
E_τ:	Radiative efficiency (DRE normalized by τ)
	G
GEOS:	Goddard Earth Observing System
GFDL:	Geophysical Fluid Dynamics Laboratory (NOAA)
GISS:	Goddard Institute for Space Studies (NASA)
GLAS:	Geoscience Laser Altimeter System
GOCART:	Goddard Global Ozone Chemistry Aerosol Radiation and Transport
GOES:	Geostationary Operational Environmental Satellite
GSFC:	Goddard Space Flight Center (NASA)
	H
HG phase function:	Henyey-Greenstein phase function
	I
ICARTT:	International Consortium for Atmospheric Research on Transport and Transformation
ICESat:	Ice, Cloud, and Land Elevation Satellite

IMPROVE:	Interagency Monitoring of Protected Visual Environments
INCA:	INteractions between Chemistry and Aerosol (LMDz model)
INDOEX:	Indian Ocean Experiment
INTEX-NA:	Intercontinental Transport Experiment – North America
IPCC:	Intergovermental Panel on Climate Change
ISCCP:	International Satellite Cloud Climatology Project
	L
LACE 98:	Lindenberg Aerosol Characterization Experiment 1998 (Germany)
LBA:	Large-Scale Biosphere-Atmosphere Experiment in Amazonia
LMDZ:	Laboratoire de Météorologie Dynamique with Zoom
LOA:	Laboratoire d' Optique Atmosphérique
	M
MFRSR:	Multifilter Rotating Shadowband Radiometer
MINOS:	Mediterranean Intensive Oxidant Study
MISR:	Multi-angle Imaging SpectroRadiometer
MODIS:	Moderate Resolution Imaging Spectroradiometer
MPLNET:	Micro Pulse Lidar Network
	N
NASA:	National Aeronautics and Space Administration
NEAQS:	New England Air Quality Study
NOAA:	National Oceanography and Atmosphere Administration
NRL:	Naval Research Laboratory
	O
OMI:	Ozone Monitoring Instrument
	P
PEM-West:	Western Pacific Exploratory Missions
POLDER:	Polarization and Directionality of the Earth's Reflectance
PRIDE:	Puerto Rico Dust Experiment
	R
REALM:	Regional East Atmospheric Lidar Mesonet
RH:	Relative Humidity
RT:	Radiative Transfer
	S
SAFARI:	South African Regional Science Experiment
SCAR-A:	Smoke, Clouds, and Radiation – America
SCAR-B:	Smoke, Clouds, and Radiation – Brazil
SeaWiFS:	Sea-viewing Wide Field-of-view Sensor
SHADE:	SaHAran Dust Experiment
SMOCC	Smoke, Aerosols, Clouds, Rainfall and Climate
SPRINTARS:	Spectral Radiation-Transport Model for Aerosol Species
SSA (ϖ_0):	aerosol Single-Scattering Albedo

	T
TARFOX:	Tropospheric Aerosol Radiative Forcing Observational Experiment
TOA:	Top-Of-Atmosphere
TOMS:	Total Ozone Mapping Spectrometer
TRACE-A:	Transport and Chemical Evolution over the Atlantic
TRACE-P:	Transport and Chemical Evolution over the Pacific
	U
UAE^2:	United Arab Emirates Unified Aerosol Experiment

Acknowledgements. The paper is derived from a report being prepared for the US Climate Change Science Program (CCSP). M. Chin would like to acknowledge NASA Atmospheric Chemistry Modeling and Analysis Program (ACMAP) and Radiation Science Program (RSP) for supporting the GOCART model. G. Feingold acknowledges funding from NOAA's Climate Goal. T. L. Anderson acknowledges support from NASA's CALIPSO Mission (contract NAS1-99105) and the National Science Foundation (grants ATM-0138250 and ATM-0205198). The work of N. Bellouin and O. Boucher forms part of the Climate Prediction Programme of the UK Department for the Environment, Food and Rural Affairs (DEFRA) under contract PECD 7/12/37. S. A. Christopher was supported by NASA's Radiation Sciences, Interdisciplinary sciences and ACMAP programs. The work of R. Kahn is supported in part by the NASA Earth Observing System MISR Project, and in part by the NASA Earth Sciences Climate and Radiation Program, under H. Maring. His work was performed at the Jet Propulsion Laboratory, California Institute of Technology, under contract with NASA. D. Koch acknowledges support from the NASA Radiation Science and Climate Modeling Programs. M. Zhou's work is in part supported by NASA NNG04GB89G. H. Yu thanks R. Levy for editorial assistance.

References

Abdou, W. A., Diner, D. J., Martonchik, J. V., Bruegge, C. J., Kahn, R. A., Gaitley, B. J., and Crean, K. A.: Comparison of conincident MISR and MODIS aerosol optical depths over land and ocean scenes containing AERONET sites, J. Geophys. Res., 110, D10S07, doi:10.1029/2004JD004693, 2005.

Ackerman, A. S., Toon, O. B., Stevens, D. E., Heymsfield, A. J., Ramanathan, V., and Welton, E. J.: Reduction of tropical cloudiness by soot, Science, 288, 1042–1047, 2000.

Albrecht, B. A.: Aerosols, cloud microphysics, and fractional cloudiness, Science, 245, 1227–1230, 1989.

Alexandrov, M. D., Lacis, A., Carlson, B. E., and Cairns, B.: Remote sensing of atmospheric aerosols and trace gases by means of Multifilter Rotating Shadowband Radiometer. Part I: Retrieval Algorithm, J. Atmos. Sci., 59(3), 524–543, 2002a.

Alexandrov, M. D., Lacis, A., Carlson, B. E., and Cairns, B.: Remote sensing of atmospheric aerosols and trace gases by means of Multifilter Rotating Shadowband Radiometer. Part II: climatological applications, J. Atmos. Sci., 59(3), 544–566, 2002b.

Alexandrov, M. D., Marshak, A., Cairns, B., Lacis, A., and Carlson, B. E.: Automatic cloud screening algorithm for MFRSR data, Geophys. Res. Lett., 31(4), L04118, doi:10.1029/2003GL019105, 2004a.

Alexandrov, M. D., Marshak, A., Cairns, B., Lacis, A., and Carlson, B. E.: Scaling properties of aerosol optical thickness retrieved from ground-based measurements, J. Atmos. Sci., 61, 1024–1039, 2004b.

Anderson, T. L., Charlson, R. J., Schwartz, S. E., Knutti, R., Boucher, O., Rodhe, H., and Heintzenberg, J.: Climate forcing by aerosols – A hazy picture, Science, 300, 1103–1104, 2003a.

Anderson, T. L., Charlson, R. J., Winker, D. M., Ogren, J. A., and Holmén, K.: Mesoscale variations of tropospheric aerosols, J. Atmos. Sci., 60, 119–136, 2003b.

Anderson, T. L., Charlson, R. J., Bellouin, N., Boucher, O., Chin, M., Christopher, S. A., Haywood, J., Kaufman, Y. J., Kinne, S., Ogren, J. A., Remer, L. A., Takemura, T., Tanre, D., Torres, O., Trepte, C. R., Wielicki, B. A., Winker, D. M., and Yu, H.: An "A-Train" strategy for quantifying direct aerosol forcing of climate, Bull. Am. Met. Soc., accepted, 2005.

Andreae, M. O., Rosenfeld, D., Artaxo, P., Costa, A. A., Frank, G. P., Longo, K. M., and Silva-Dias, M. A. F.: Smoking Clouds over the Amazon, Science 303(5662), 1337–1342, doi:10.1126/science.1092779, 2004.

Ångström, A.: On the atmospheric transmission of sun radiation and on dust in the air, Geogr. Ann. H., 12, 130–159, 1929.

Ångström, A.: On the atmospheric transmission of Sun radiation, II, Geogr. Ann., 2, 156–165, 1930.

Ansmann, A., Wandinger, U., Wiedensohler, A., and Leiterer, U.: Lindenderg Aerosol Characterization Experiment 1998 (LACE 98): Overview, J. Geophys. Res., 107, 8129, doi:10.1029/2000JD000233, 2002.

Atwater, M. A.: Planetary albedo changes due to aerosols, Science, 170(3953), 64–66, 1970.

Bates, T. S., Huebert, B. J., Gras, J. L., Griffiths, F. B., and Durkee, P. A.: International Global

Atmospheric Chemistry (IGAC) Project's First Aerosol Characterization Experiment (ACE 1): Overview, J. Geophys. Res., 103, 16 297–16 318, 1998.
Bates, T. S., Quinn, P. K., Coffman, D. J., Johnson, J. E., Miller, T. L., Covert, D. S., Wiedensohler, A., Leinert, S., Nowak, A., and Neusüb, C.: 2001: Regional Physical and Chemical Properties of the Marine Boundary Layer Aerosol across the Atlantic during Aerosols99: An overview, J. Geophys. Res., 106, 20 767–20 782, 2001.
Bellouin, N., Boucher, O., Tanré, D., and Dubovik, O.: Aerosol absorption over the clear-sky oceans deduced from POLDER-1 and AERONET observations, Geophys. Res. Lett., 30, 1748, doi:10.1029/2003GL017121, 2003.
Bellouin, B., Boucher, O., Vesperini, M., and Tanré, D.: Estimating the direct aerosol radiative perturbation: Impact of ocean surface representation and aerosol non-sphericity, Q. J. Roy. Met. Soc., 130(601), 2217–2232, 2004.
Bergstrom, R. W. and Russell, P. B.: Estimation of aerosol direct radiative effects over the mid-latitude North Atlantic from satellite and in-situ measurements, Geophys. Res. Lett., 26, 1731–1734, 1999.
Blanchet, J.-P.: Application of the Chandrasekhar mean to aerosol optical parameters, Atmosphere-Ocean, 20, 189–206, 1982.
Bohren, C. F. and Huffman, D. R.: Absorption and Scattering of Light by Small Particles, 530 pp., Wiley, New York, 1983.
Boucher, O., Schwartz, S. E., Ackerman, T. P., et al.: Intercomparison of models representing shortwave radiative forcing by sulfate aerosols, J. Geophys. Res., 103, 16 979–16 998, 1998.
Boucher, O.: On aerosol direct shortwave forcing and the Henyey-Greenstein phase function, J. Atmos. Sci., 55, 128–134, 1998.
Boucher, O. and Tanré, D.: Estimation of the aerosol perturbation to the Earth's radiative budget over oceans using POLDER satellite aerosol retrievals, Geophys. Res. Lett., 27, 1103–1106, 2000.
Boucher, O. and Pham, M.: History of sulfate aerosol radiative forcings, Geophys. Res. Lett., 29(9), 1308, doi:10.1029/2001GL014048, 2002.
Boucher, O., Pham, M., and Venkataraman, C.: Simulation of the atmospheric sulfur cycle in the Laboratoire de Meteorologie Dynamique General Circulation Model. Model description, model evaluation, and global and European budgets, IPSL scientific Note, 23, 27 pp., (available at http://www.ipsl.jussieu.fr/poles/Modelisation/NotesSciences.htm), July, 2002.

Bruegge, C. J., Abdou, W. A., Diner, D. J., Gaitley, B. J., Helmlinger, M. C., Kahn, R. A., and Martonchik, J. V.: Validating the MISR radiometric scale for the ocean aerosol science communities, in: Post-launch calibration of satellite sensors, edited by: Morain, S. A. and Budge, A. M., A.A. Balkema Publishers, Leiden, Netherlands, pp. 103–115, 2004.

Bush, B. C. and Valero, F. P. J.: Surface aerosol radiative forcing at Gosan during the ACE-Asia campaign, J. Geophys. Res., 108(D23), 8660, doi:10.1029/2002JD003233, 2003.

Chameides, W. L., Yu, H., Liu, S. C., et al.: A case study of the effects of atmospheric aerosols and regional haze on agriculture: An opportunity to enhance crop yields in China through emission controls?, Proc. Natl. Acad. Sci., 96, 24, 13 626–13 633, 1999.

Charlson, R. J. and Pilat, M. J.: Climate: The influence of aerosols, J. Appl. Meteorol., 8, 1001–1002, 1969.

Charlson, R. J., Langner, J., Rodhe, H., Leovy, C. B., and Warren, S. G.: Perturbation of the Northern Hemisphere radiative balance by backscattering from anthropogenic sulfate aerosols, Tellus, 43AB, 152–163, 1991.

Charlson, R. J., Schwartz, S. E., Hales, J. H., Cess, R. D., Coakley Jr., J. A., Hansen, J. E., and Hofmann, D. J.: Climate forcing by anthropogenic aerosols, Science, 255, 423–430, 1992.

Chin, M., Rood, R. B., Lin, S.-J., Muller, J.-F., and Thompson, A. M.: Atmospheric sulfur cycle simulated in the global model GOCART: Model description and global properties, J. Geophys. Res., 105, 24 671–24 687, 2000a.

Chin, M., Savoie, D. L., Huebert, B. J., Bandy, A. R., Thornton, D. C., Bates, T. S., Quinn, P. K., Saltzman, E. S., and De Bruyn, W. J.: Atmospheric sulfur cycle simulated in the global model GOCART: Comparison with field observations and regional budgets, J. Geophys. Res., 105, 24 689–24 712, 2000b.

Chin, M., Ginoux, P., Holben, B., et al.: The GOCART model study of aerosol composition and radiative forcing, paper presented at 12th Symposium on Global Change and Climate Variations, Am. Meteorol. Soc., Albuquerque, New Mexico, 2001.

Chin, M., Ginoux, P., Kinne, S., Torres, O., Holben, B., Duncan, B. N., Martin, R. V., Logan, J. A., Higurashi, A., and Nakajima, T.: Tropospheric aerosol optical thickness from the GOCART model and comparisons with satellite and sun photometer measurements, J. Atmos. Sci., 59, 461–483, 2002.

Chin, M., Ginoux, P., Lucchesi, R., Huebert, B., Weber, R., Anderson, T., Masonis, S., Blomquist, B., Bandy, A., and Thornton, D.: A global aerosol model forecast for the ACE-Asia field experiment, J. Geophys. Res., 108(D23), 8654, doi:10.1029/2003JD003642, 2003.

Chin, M., Chu, D. A., Levy, R., Remer, L. A., Kaufman, Y. J., Holben, B. N., Eck, T., and Ginoux, P.: Aerosol distribution in the northern hemisphere during ACE-Asia: Results from global model, satellite observations, and sunphotometer measurements, J. Geophy. Res., 109, D23S90, doi:10.1029/2004JD004829, 2004.

Chou, M. D., Suarez, M. J., Ho, C. H., Yan, M. M. H., and Lee, K. T.: Parameterizations for cloud overlapping and shortwave single-scattering properties in the Goddard GCM, J. Clim., 11, 201–214, 1998.

Chou, M.-D., Chan, P.-K., and Wang, M.: Aerosol radiative forcing derived from SeaWiFS-retrieved aerosol optical properties, J. Atmos. Sci., 59, 748–757, 2002.

Christopher, S. A., Li, X., Welch, R. M., et al.: Estimation of surface and top-of-atmosphere shortwave irradiance in biomass-burning regions during SCAR-B, J. Appl. Meteorol., 39, 1742–1753, 2000.

Christopher, S. A. and Zhang, J.: Shortwave aerosol radiative forcing from MODIS and CERES observations over the oceans, Geophys. Res., Lett., 29, 1859, doi:10.1029/2002GL014803, 2002a.

Christopher, S. A. and Zhang, J.: Daytime Variation of Shortwave Direct Radiative Forcing of Biomass Burning Aerosols from GOES-8 Imager, J. Atmos. Sci., 59(3), 681–691, 2002b.

Christopher, S. A., Wang, J., Ji, Q., and Tsay, S.-C.: Estimation of Shortwave Dust Aerosol Radiative forcing during PRIDE, J. Geophys. Res., 108(D19), 8956, doi:10.1029/2002JD002787, 2003.

Christopher, S. A. and Zhang, J.: Cloud-free shortwave aerosol radiative effect over oceans: Strategies for identifying anthropogenic forcing from Terra satellite measurements, Geophys. Res. Lett., 31, L18101, doi:10.1029/2004GL020510, 2004.

Chu, D. A., Kaufman, Y. J., Ichoku, C., Remer, L. A., Tanré, D., and Holben, B.: Validation of MODIS aerosol optical depth retrieval over land, Geophys. Res. Lett., 29(12), doi:10.1029/2001/GL013205, 2002.

Chylek, P., Videen, G., Ngo, D., Pinnick, R. G., and Klett, J. D.: Effects of black carbon on the optical properties and climate forcing of sulfate aerosols, J. Geophys. Res., 100, 16 325–16 332, 1995.

Chylek, P. and Wong, J.: Effect of absorbing aerosol on global radiation budget, Geophys. Res. Lett., 22, 929–931, 1995.

Clarke, A. D. and Kapustin, V.: A Pacific aerosol survey: Part I: A decade of data on production, transport, evolution, and mixing in the troposphere, J. Atmos. Sci., 59, 363–382, 2002.

Coakley Jr., J. A., Cess, R. D., and Yurevich, F. B.: The effect of tropospheric aerosols on the earth's radiation budget: A parameterization for climate models, J. Atmos. Sci., 40, 116–138, 1983.

Collins, W. D., Rasch, P. J., Eaton, B. E., Khattatov, B. V., Lamarque, J., and Zender, C. S.: Simulating aerosols using a chemical transport model with assimilation of satellite aerosol retrievals: Methodology for INDOEX, J. Geophys. Res., 106(D7), 7313–7336, 2001.

Conant, W. C.: An observational approach for determining aerosol surface radiative forcing: results from the first field phase of INDOEX, J. Geophys. Res., 105, 15 347–15 360, 2000.

Costa, M. J., Silva, A. M., and Levizzani, V.: Aerosol characterization and direct radiative forcing assessment over the ocean. Part I: Methodology and sensitivity analysis, J. Appl. Meteorol., 43(12), 1799–1817, 2004a.

Costa, M. J., Silva, A. M., and Levizzani, V.: Aerosol characterization and direct radiative forcing assessment over the ocean. Part II: Application to test cases and validation, J. Appl. Meteorol., 43(12), 1818–1833, 2004b.

Delene, D. J. and Ogren, J. A.: Variability of aerosol optical properties at four North American surface monitoring sites, J. Atmos. Sci., 59, 1135–1150, 2002.

Deuzé, J. L., Bréon, F. M., Devaux, C., Goloub, P., Herman, M., Lafrance, B., Maignan, F., Marchand, A., Nadal, F., Perry, G., and Tanré, D.: Remote sensing of aerosols over land surfaces from POLDER-ADEOS-1 polarized measurements, J. Geophys. Res., 106, 4913–4926, 2001.

Dickerson, R. R., Kondragunta, S., Stenchikov, G., et al.: The impacts of aerosols on solar ultraviolet radiation and photochemical smog, Science, 278, 827–830, 1997.

Dickinson, R. E.: Land surface processes and climate – surface albedos and energy balance, Adv. Geophys., 25, 305–353, 1983.

Dickinson, R. E., Henderson-Seller, A., and Kennedy, P. J.: Biosphere-Atmosphere Transfer Scheme (BATS) version 1e as Coupled to the NCAR Community Model, Tech. Note NCAR/TN-387+STR, 72pp., Natl. Cent. of Atmos. Res., Boulder, Colo., 1993.

Diner, D. J., Beckert, J. C., Reilly, T. H., et al.: Multiangle Imaging SptectrRadiometer (MISR) description and experiment overview, IEEE Trans. Geosci. Remote. Sens., 36, 1072–1087, 1998.

Diner, D. J., Beckert, J. C., Bothwell, G. W., and Rodriguez, J. I.: Performance of the MISR instrument during its first 20 months in Earth orbit, IEEE Trans. Geosci. Remote Sens., 40, 1449–1466, 2002.

Diner, D. J., Ackerman, T. P., Anderson, T. L., et al.: Progressive Aerosol Retrieval and Assimilation Global Observing Network (PARAGON): An integrated approach for characterizing aerosol climatic and environmental interactions, Bull. Amer. Meteo. Soc., 85(10), 1491–1501, 2004.

Dubovik, O., Smirnov, A., Holben, B. N., King, M. D., Kaufman, Y. J., and Slutsker, I.: Accuracy assessments of aerosol optical properties retrieved from AERONET sun and sky radiance measurements, J. Geophys. Res., 105, 9791–9806, 2000.

Dubovik, O. and King, M. D.: A flexible inversion algorithm for retrieval of aerosol optical properties from Sun and sky radiance measurements, J. Geophys. Res., 105, 20 673–20 696, 2000.

Dubovik, O., Holben, B. N., Eck, T. F., Smirnov, A., Kaufman, Y. J., King, M. D., Tanré, D., and Slutsker, I.: Variability of absorption and optical properties of key aerosol types observed in worldwide locations, J. Atmos. Sci., 59, 590–608, 2002.

Dufresne, J., Gautier, C., Ricchizzi, P., and Fouquart, Y.: Longwave scattering effects of mineral aerosols, J. Atmos. Sci., 59(12), 1959–1966, 2002.

Eck, T. F., Holben, B. N., Reid, J. S., et al.: High aerosol optical depth biomass burning events: A comparison of optical properties for different source regions, Geophys. Res. Lett., 30, 2035, doi:10.1029/2003GL017861, 2003.

Feingold, G., Eberhard, W. L., Veron, D. E., and Previdi, M.: First measurements of the Twomey aerosol indirect effect using ground-based remote sensors, Geophys. Res. Lett., 30(6), 1287, doi:10.1029/2002GL016633, 2003.

Ferrare, R. A., Turner, D. D., Brasseur, L. H., Feltz, W. R., Dubovik, O., and Tooman, T. P.: Raman lidar measurements of the aerosol extinction-to-backscatter ratio over the Southern Great Plains, J. Geophys. Res., 106(D17), 20 333–20 347, 2001.

Fishman, J., Hoell Jr., J. M., Bendura, R. D., McNeal, R. J., and Kirchhoff, V.: NASA GTE TRACE A experiment (Septemner–October 2002): Overview, J. Geophys. Res., 101, 23 865–23 880, 1996.

Fu, Q. and Liou, K. N.: Parameterization of the radiative properties of cirrus clouds, J. Atmos. Sci., 50, 2008–2025, 1993.

Geogdzhayev, I. V., Mishchenko, M. I., Rossow, W. B., Cairns, B., and Lacis, A.: Global Two-Channel AVHRR Retrievals of Aerosol Properties over the Ocean for the Period of NOAA-9 Observations and Preliminary Retrievals Using NOAA-7 and NOAA-11 Data, J. Atmos. Sci., 59(3), 262–278, 2002.

Ginoux, P., Chin, M., Tegen, I., Prospero, J., Holben, B., Dubovik, O., and Lin, S.-J.: Sources and distributions of dust aerosols simulated with the GOCART model, J. Geophys. Res., 106, 20 225–20 273, 2001.

Ginoux, P., Prospero, J., Torres, O., and Chin, M.: Long-term simulation of dust distribution with the GOCART model: Correlation with the North Atlantic Oscillation, Environ. Modeling and Software, 19, 113–128, 2004.

Gras, J. L., Jensen, J. B., Okada, K., Ikegami, M., Zaizen, Y., and Makino, Y.: Some optical properties of smoke aerosol in Indonesia and tropical Australia, Geophys. Res. Lett., 26(10), 1393–1396, 1999.

Hansen, J. and Travis, L. D.: Light scattering in planetary atmospheres, Space Sci. Rev., 16, 527–610, 1974.

Hansen, J., Sato, M., and Ruedy, R.: Radiative forcing and climate response, J. Geophys. Res., 102, 6831–6864, 1997.

Harrison, L., Michalsky, J., and Berndt, J.: Automated Multifilter Rotating Shadowband Radiometer: An Instrument for Optical Depth and Radiation Measurements, Appl. Opt., 33, 5118–5125, 1994.

Hart, W. D., Spinhirne, J. D., Palm, S. P., and Hlavka, D.: Height Distribution Between Cloud And Aerosol Layers in the Indian Ocean Region from the GLAS Spaceborne Lidar, Geophys. Res. Lett., in press, 2005.

Haywood, J. M. and Shine, K. P.: Multi-spectral calculations of the radiative forcing of tropospheric sulfate and soot aerosols using a column model, Q. J. R. Meteorol. Soc., 123, 1907–1930, 1997.

Haywood, J., Ramaswamy, V., and Soden, B.: Tropospheric aerosol climate forcing in clear-sky satellite observations over the oceans, Science, 283, 1299–1303, 1999.

Haywood, J. and Boucher, O.: Estimates of the direct and indirect radiative forcing due to tropospheric aerosols: A review, Rev. Geophys., 38, 513–543, 2000.

Haywood, J., Francis, P., Osborne, S., Glew, M., Loeb, N., Highwood, E., Tanré, D., Myhre, E., Formenti, P., and Hirst, E.: Radiative properties and direct radiative effect of Saharan dust measured by the C-130 aircraft during SHADE: 1.Solar spectrum, J. Geophys. Res., 108(D18), 8577, doi:10.1029/2002JD002687, 2003.

Haywood, J., Allan, R., Culverwell, I., Slingo, T., Milton, S., Edwards, J., and Clerbaux, N.: Can desert dust explain the outgoing longwave radiation anomaly over the Sahara during July 2003?, J. Geophys. Res., 110, D05105, doi:10.1029/2004JD005232, 2005.

Heintzenberg, J., Graf, H.-F., Charlson, R. J., and Warneck, P.: Climate forcing and the physico-chemical life cycle of the atmospheric aerosol – Why do we need an integrated, interdisciplinary global research programme?, Beitr. Phys. Atmosph., 69, 261–271, 1996.

Heintzenberg, J., Charlson, R. J., Clarke, A. D., et al.: Measurements and modeling of aerosol single-scattering albedo: progress, problems and prospects, Beitr. Phys. Atmosph., 70, 249–263, 1997.

Heintzenberg, J., Tuch, T., Wehner, B., et al.: Arctic haze over central Europe, Tellus, 55B, 796–807, 2003.

Henyey, L. G. and Greenstein, T. L.: Diffuse radiation in the galaxy, Astrophys. J., 93, 70–83, 1941.

Herman, J. R., Bhartia, P. K., Torres, O., Hsu, C., Seftor, C., and Celarier, E.: Global distribution of UV-absorbing aerosols from Nimbus-7/TOMS data, J. Geophys. Res., 102, 16 911–16 922, 1997.

Highwood, E. J., Haywood, J. M., Silverstone, M. D., Newman, S. M., and Taylor, J. P.: Radiative properties and direct effect of Saharan dust measured by the C-130 aircraft during Saharan Dust Experiment (SHADE): 2. Terrestrial spectrum, J. Geophys. Res., 108(D18), 8578, doi:10.1029/2002JD002552, 2003.

Hignett, P., Taylor, J. P., Francis, P. N., and Glew, M. D.: Comparison of observed and modeled direct aerosol forcing during TARFOX, J. Geophys. Res., 104, 2279–2287, 1999.

Hlavka, D. L., Palm, S. P., Hart, W. D., Spinhirne, J. D., McGill, M. J., and Welton, E. J.: Aerosol and cloud optical depth from GLAS: Results and verification for an October 2003 California fire smoke case, Geophys. Res. Lett., in press, 2005.

Hobbs, P. V., Reid, J. S., Kotchenruther, R. A., Ferek, R. J., and Weiss, R.: Direct radiative forcing by smoke from biomass burning, Science, 275, 1776–1778, 1997.

Hoell, J. M., Davis, D. D., Liu, S. C., Newell, R., Shipham, M., Akimoto, H., McNeal, R. J., Bemdura, R. J., and Drewry, J. W.: Pacific Exploratory Mission-West A (PEM-WEST A): September–October, 1991, J. Geophys. Res.,101, 1641–1653, 1996.

Hoell, J. M., Davis, D. D., Liu, S. C., Newell, R., Shipham, M., Akimoto, H., McNeal, R. J., Bemdura, R. J., and Drewry, J. W.: The Pacific Exploratory Mission-West Phase B: February–March, 1994, J. Geophys. Res., 102, 28 223–28 239, 1997.

Hoff, R. M. and McCann, K. J.: A Regional East Atmospheric Lidar Mesonet (REALM), EOS Trans. Amer. Geophys. Union, 83 (Fall Meeting Suppl. A22C-0147), 2002.

Holben, B. N., Eck, T. F., Slutsker, I., et al.: AERONET – A federated instrument network and

data archive for aerosol characterization, Remote Sens. Environ., 66, 1–16, 1998.
Holben, B. N., Tanre, D., Smirnov, A., et al.: An emerging ground-based aerosol climatology: aerosol optical depth from AERONET, J. Geophys. Res., 106, 12 067–12 098, 2001.
Horvath, H.: Atmospheric light absorption – A review, Atmos. Environ., 27A, 293–317, 1993.
Horvath, H., Arboledas, L. A., Olmo, F. J., Jovanovic, O., Gangl, M., Kaller, W., Sanchez, C., Sauerzopf, H., and Seidl, S.: Optical properties of the aerosol in Spain and Austria and its effect on radiative forcing, J. Geophys. Res., 107(D19), 4386, doi:10.1029/2001JD001472, 2002.
Hsu, N. C., Herman, J. R., and Weaver, C. J.: Determination of radiative forcing of Saharan dust using combined TOMS and ERBE data, J. Geophys. Res., 105, 20 649–20 661, 2000.
Huebert, B. J., Bates, T., Russell, P. B., Shi, G., Kim, Y. J., Kawamura, K., Carmichael, G., and Nakajima, T.: An overview of ACE-Asia: Strategies for quantifying the relationships between Asian aerosols and their climatic impacts, J. Geophys. Res., 108(D23), 8633, doi:10.1029/2003JD003550, 2003.
Husar, R. B., Prospero, J. M., and Stowe, L. L.: Characterization of tropospheric aerosols over the oceans with the NOAA advanced very high resolution radiometer optical thickness operational product, J. Geophys. Res., 102, 16 889–16 909, 1997.
Ichoku, C., Chu, D. A., Chu, S., Kaufman, Y. J., Remer, L. A., Tanré, D., Slutsker, I., and Holben, B. N.: A spatio-temporal approach for global validation and analysis of MODIS aerosol products, Geophys. Res. Lett., 29(12), 8006, doi:10.1029/2001GL013206, 2002.
Ichoku, C., Remer, L. A., and Eck, T. F.: Quantitative evaluation and intercomparison of morning and afternoon MODIS aerosol measurements from Terra and Aqua satellites, J. Geophys. Res., 110, D10S03, doi:10.1029/2004JD004987, 2005.
Ignatov, A. and Stowe, L. L.: Aerosol retrievals from individual AVHRR channels: I. Retrieval algorithm and transition from Dave to 6S radiative transfer model, J. Atmos. Sci., 59, 313–334, 2002.
Intergovernmental Panel on Climate Change (IPCC): Radiative forcing of climate change, in: Climate Change 2001, Cambridge Univ. Press, New York, Cambridge University Press, 2001.
Jacob, D. J., Crawford, J. H., Kleb, M. M., Connors, V. S., Bendura, R. J., Raper, J. L., Sachse, G. W., Gille, J. C., Emmons, L., and Heald, C. L.: The Transport and Chemical Evolution over the Pacific (TRACE-P) aircraft mission: design, execution, and first results, J. Geophys. Res., 108, 9000, doi:10.1029/2002JD003276, 2003.

Jacobson, M. Z.: A physically-based treatment of elemental carbon optics: Implications for global direct forcing of aerosols, Geophys. Res. Lett, 27, 217–220, 2000.
Jacobson, M. Z.: Strong radiative heating due to the mixing state of black carbon in atmospheric aerosols, Nature, 409, 695–697, 2001.
Jin, Z., Charlock, T. P., and Rutledge, K.: Analysis of broadband solar radiation and albedo over the ocean surface at COVE, J. Atmos. Oceanic Technol., 19, 1585–1601, 2002.
Jin, Z., Charlock, T. P., Smith Jr., W. L., and Rutledge, K.: A parameterization of ocean surface albedo, Geophys. Res. Lett., 31, L22301, doi:10.1029/2004GL021180, 2004.
Kahn, R., Gaitley, R., Martonchik, J. V., Diner, D. J., Crean, K. A., and Holben, B. N.: MISR global aerosol optical depth validation based on two years of coincident AERONET observations, J. Geophys. Res., 110, D10S04, doi:10.1029/2004JD004706, 2005a.
Kahn, R., Li, W.-H., Martonchik, J. V., Bruegge, C., Diner, D. J., Gaitley, B., Abdou, W., Dubovik, O., Holben, B., Smirnov, A., Jin, Z., and Clark, D.: MISR low-light-level calibration, and implications for aerosol retrieval over dark water, J. Atmos. Sci., 62(4), 1032–1052, 2005b.
Kahn, R., Ogren, J. A., Ackerman, T. P., et al.: Aerosol data sources and their roles within PARAGON, Bull. Amer. Meteor. Soc., 85, 1511–1522, 2004a.
Kahn, R., Anderson, J., Anderson, T. L., Bates, T. S., Brechtel, F., Carrico, C. M., Clarke, A., Doherty, S. J., Dutton, E., Flagan, R., Frouin, R., Fukushima, H., Holben, B., Howell, S., Huebert, B., Jefferson, A., Jonsson, H., Kalashnikova, O., Kim, J., Kim, S.-W., Kus, P., Li, W.-H., Livingston, J. M., McNaughton, C., Merrill, J., Mukai, S., Murayama, T., Nakajima, T., Quinn, P., Redemann, J., Rood, M., Russell, P., Sano, I., Schmid, B., Seinfeld, J., Sugimoto, N., Wang, J., Welton, E. J., Won, J.-G., and Yoon, S.-C.: Environmental snapshots from ACE-Asia, J. Geophys. Res., doi:10.1029/2003JD004339, 2004b.
Kahn, R., Banerjee, P., and McDonald, D.: The Sensitivity of Multiangle Imaging to Natural Mixtures of Aerosols Over Ocean, J. Geophys. Res., 106, 18 219–18 238, 2001.
Kalashnikova, O. V., Kahn, R., Sokolik, I. N., and Li, W.-H.: The ability of multi-angle remote sensing observations to identify and distinguish mineral dust types: Optical models and retrievals of optically thick plumes, J. Geophys. Res., 110, D18S14, doi:10.1029/2004JD004550, 2005a.
Kaufman, Y. J., Setzer, A., Ward, D., Tanre, D., Holben, B. N., Menzel, P., Pereira, M. C., and Rasmussen, R.: Biomass Burning Airborne and Spaceborne Experiment in the Amazonas (BASE-A), J. Geophys. Res., 97, 14 581–14 599, 1992.
Kaufman, Y. J., Tanre, D., Remer, L. A., Vermote, E. F., Chu, A., and Holben, B. N.: Operational

remote sensing of tropospheric aerosol over land from EOS moderate resolution imaging spectroradiometer, J. Geophys. Res., 102, 17 051–17 067, 1997.
Kaufman, Y. J., Hobbs, P. V., Kirchhoff, V., et al.: Smoke, Clouds, and Radiation-Brazil (SCAR-B) Experiment, J. Geophys. Res., 103(D24), 31 783–31 808, 1998.
Kaufman, Y. J., Holben, B. N., Tanre, D., Slutsker, I., Smirnov, A., and Eck, T. F.: Will aerosol measurements from Terra and Aqua polar orbiting satellites represent daily aerosol abundance and properties?, Geophys. Res. Lett., 27, 3861–3864, 2000.
Kaufman, Y. J., Tanre, D., Dubovik, O., Karnieli, A., and Remer, L. A.: Absorption of sunlight by dust as inferred from satellite and ground-based measurements, Geophys. Res., Lett., 28, 1479–1482, 2001.
Kaufman, Y. J., Tanre, D., and Boucher, O.: A satellite view of aerosols in the climate system, Nature, 419, doi:10.1038/nature01091, 2002a.
Kaufman, Y. J., Martins, J. V., Remer, L. A., Schoeberl, M. R., and Yamasoe, M. A.: Satellite retrieval of aerosol absorption over the oceans using sunglint, Geophys. Res. Lett., 29(19), 1928, doi:10.1029/2002GL015403, 2002b.
Kaufman, Y. J., Haywood, J. M., Hobbs, P. V., Hart, W., Kleidman, R., and Schmid, B.: Remote sensing of vertical distributions of smoke aerosol off the coast of Africa, Geophys. Res. Lett., 30(16), 1831, doi:10.1029/2003GL017068, 2003.
Kaufman, Y. J., Boucher, O., Tanré, D., Chin, M., Remer, L. A., and Takemura, T.: Aerosol anthropogenic component estimated from satellite data, Geophys. Res. Lett., in press, 2005a.
Keil, A. and Haywood, J.: Solar radiative forcing by biomass burning aerosol particles during SAFARI-2000: A case study based on measured aerosol and cloud properties, J. Geophys. Res., 108(D13), 8467, doi:10.1029/2002JD002315, 2003.
Kiehl, J. T. and Briegleb, B. P.: The relative role of sulfate aerosols and greenhouse gases in climate forcing, Science, 260, 311–314, 1993.
Kim, D., Sohn, B. J., Nakajima, T., and Takemura, T.: Aerosol radiative forcing over east Asia determined from ground-based solar radiation measurements, J. Geophys. Res., 110, D10S22, doi:10.1029/2004JD004678, 2005.
King, M. D., Kaufman, Y. J., Tanré, D., and Nakajima, T.: Remote sensing of tropospheric aerosols: Past, present, and future, Bull. Am. Meteorol. Soc., 80, 2229–2259 1999.
King, M. D., Platnick, S., Moeller, C. C., Revercomb, H. E., and Chu, D. A.: Remote sensing of smoke, land, and clouds from the NASA ER-2 during SAFARI 2000, J. Geophys. Res., 108(D13), 8502, doi:10.1029/2002JD003207, 2003a.

King, M. D., Menzel, W. P., Kaufman, Y. J., et al.: Cloud and aerosol properties, precipitable water and profiles of temperature and water vapor from MODIS, IEEE Trans. Geosci. Remote Sens., 41, 442–458, 2003b.

Kinne, S. and Pueschel, R.: Aerosol radiative forcing for Asian continental outflow, Atmos. Environ., 35, 5019–5028, 2001.

Kinne, S., Lohmann, U., Feichter, J., et al.: Monthly averages of aerosol properties: A global comparison among models, satellite data, and AERONET ground data, J. Geophys. Res., 108(D20), 4634, doi:10.1029/2001JD001253, 2003.

Kinne, S., Schulz, M., Textor, C., et al.: An AeroCom initial assessment – optical properties in aerosol component modules of global models, Atmos. Chem. Phys. Discuss., accepted, 2005.

Koch, D. and Hansen, J.: Distant origins of Arctic black carbon: A Goddard Institute for Space Studies ModelE experiment, J. Geophys. Res., 110, D04204, doi:10.1029/2004JD005296, 2005.

Koren, I. Y., Kaufman, Y. J., Remer, L. A., and Martins, J. V.: Measurement of the effect of Amazon smoke on inhibition of cloud formation, Science, 303, 1342–1345, 2004.

Lelieveld, J., Berresheim, H., Borrmann, S., et al.: Global air pollution crossroads over the Mediterranean, Science, 298, 794–799, 2002.

Léon, J.-F., Tanré, D., Pelon, J., Kaufman, Y. J., Haywood, J. M., and Chatenet, B.: Profiling of a Saharan dust outbreak based on a synergy between active and passive remote sensing, J. Geophys. Res., 108(D18), 8575, doi:10.1029/2002JD002774, 2003.

Li, F., Vogelmann, A. M., and Ramanathan, V.: Dust aerosol radiative forcing measured from space over the Western Africa, J. Clim., 17(13), 2558–2571, 2004.

Liu, H., Pinker, R., and Holben, B. N.: A global view of aerosols from merged transport models, satellite, and ground observations, J. Geophys. Res., 110, D10S15, doi:10.1029/2004JD004695, 2005.

Li, R.-R., Kaufman, Y. J., Hao, W.-M., Salmon, J. M., and Gao, B.-C.: A Technique for Detecting Burn Scars Using MODIS Data, IEEE Trans. on Geoscience & Remote Sensing, 42(6), 1300–1308, 2004.

Liao, H. and Seinfeld, J. H.: Effects of clouds on direct aerosol radiative forcing of climate, J. Geophys. Res., 103, 3781–3788, 1998.

Lindesay, J. A., Andreae, M. O., Goldammer, J. G., Harris, G., Annegarn, H. J., Garstang, M., Scholes, R. J., and van Wilgen, B. W.: International Geosphere Biosphere Pro-

gramme/International Global Atmospheric Chemistry SAFARI-92 field experiment: Background and overview, J. Geophys. Res., 101, 23 521–23 530, 1996.
Loeb, N. G. and Kato, S.: Top-of-atmosphere direct radiative effect of aerosols over the tropical oceans from the Clouds and the Earth's Radiant Energy System (CERES) satellite instrument, J. Clim., 15, 1474–1484, 2002.
Loeb, N. G. and Manalo-Smith, N.: Top-of-Atmosphere direct radiative effect of aerosols over global oceans from merged CERES and MODIS observations, J. Clim., in press, 2005.
Lubin, D., Satheesh, S. K., McFarquar, G., and Heymsfield, A. J.: Longwave radiative forcing of Indian Ocean tropospheric aerosol, J. Geophys. Res., 107(D19), 8004, doi:10.1029/2001JD001183, 2002.
Luo, Y. F., Lu, D., Zhou, X., Li, W., and He, Q.: Characteristics of the spatial distribution and yearly variation of aerosol optical depth over China in last 30 years, J. Geophys. Res., 106(D13), 14501, doi:10.1029/2001JD900030, 2001.
Magi, B. I., Hobbs, P. V., Kirchstetter, T. W., Novakov, T., Hegg, D. A., Gao, S., Redemann, J., and Schmid, B.: Aerosol properties and chemical apportionment of aerosol optical depth at locations off the United States East Coast in July and August 2001, J. Atmos. Sci., 62, 919–933, 2005.
Malm, W. C., Sisler, J. F., Huffman, D., Eldred, R. A., and Cahill, T. A.: Spatial and seasonal trends in particle concentration and optical extinction in the United States, J. Geophys. Res., 99, 1347–1370, 1994.
Malm, W. C. and Kriedenweiss, S. M.: The effects of models of aerosol hygroscopicity on the apportionment of extinction, Atmos. Environ., 31, 1965–1976, 1997.
Malm, W. C., Schichtel, B. A., Pitchford, M. L., Ashbaugh, L. L., and Eldred, R. A.: Spatial and monthly trends in speciated fine particle concentration in the United States, J. Geophys. Res., 109, D03306, doi:10.1029/2003JD003739, 2004.
Markowicz, K. M., Flatau, P. J., Ramana, R. V., Crutzen, P. J., and Ramanathan, V.: Absorbing mediterranean aerosols lead to a large reduction in the solar radiation at the surface, Geophys. Res. Lett., 29, 1968, doi:10.1029/2002GL015767, 2002.
Markowicz, K. M., Flatau, P. J., Vogelmann, A. M., Quinn, P. K., and Welton, E. J.: Clear-sky infrared aerosol radiative forcing at the surface and the top of the atmosphere, Q. J. R. Meteorol. Soc., 129, 2927–2947, 2003.
Marshall, S., Covert, D. S., and Charlson, R. J.: Relationships between asymmetry parameter and hemispheric backscatter ratio: Implications for climate forcing by aerosols, Appl. Opt.,

34, 6306–6311, 1995.
Martins, J. V., Artaxo, P., Liousse, C., Reid, J. S., Hobbs, P. V., and Kaufman, Y. J.: Effects of black carbon content, particle size, and mixing on light absorption by aerosols from biomass burning in Brazil, J. Geophys. Res., 103, 32 041–32 050, 1998.
Martins, J. V., Tanré, D., Remer, L. A., Kaufman, Y. J., Mattoo, S., and Levy, R.: MODIS Cloud screening for remote sensing of aerosol over oceans using spatial variability, Geophys. Res. Lett., 29(12), doi:10.1029/2001GL013252, 2002.
Martonchik, J. V., Diner, D. J., Kahn, R., Verstraete, M. M., Pinty, B., Gordon, H. R., and Ackerman, T. P.: Techniques for the Retrieval of aerosol properties over land ocean using multiangle data, IEEE Trans. Geosci. Remt. Sensing, 36, 1212–1227, 1998a.
Martonchik, J. V., Diner, D. J., Pinty, B., Verstraete, M. M., Myneni, R. B., Knjazikhin, Y., and Gordon, H. R.: Determination of land and ocean reflective, radiative, and biophysical properties using multiangle imaging, IEEE Trans. Geosci. Remote Sens., 36, 1266–1281, 1998b.
Martonchik, J. V., Diner, D. J., Crean, K. A., and Bull, M. A.: Regional aerosol retrieval results from MISR, IEEE Trans. Geosci. Remote Sens., 40, 1520–1531, 2002.
Matsui, T., Kreidenweis, S., Pielke Sr., R. A., Schichtel, B., Yu, H., Chin, M., Chu, A., and Niyogi, D.: Regional comparison and assimilation of GOCART and MODIS aerosol optical depth across the eastern U.S., Geophys. Res. Lett., 31, L21101, doi:10.1029/2004GL021017, 2004.
Matthis, I., Ansmann, A., Müller, D., Wandinger, U., and Althausen, D.: Multiyear aerosol observations with dual-wavelength Raman lidar in the framework of EARLINET, J. Geophys. Res., 109, D13203, doi:10.1029/2004JD004600, 2004.
McCormick, R. A. and Ludwig, J. H.: Climate modification by atmospheric aerosols, Science, 156(3780), 1358–1359, 1967.
McMurry, R. H., Zhang, X., and Lee, C.-T.: Issues in aerosol measurement for optical assessments, J. Geophys. Res., 101, 19 189–19 197, 1996.
Mishchenko, M. I., Geogdzhayev, I. V., Cairns, B., Rossow, W. B., and Lacis, A. A.: Aerosol retrievals over the ocean by use of channels 1 and 2 AVHRR data: Sensitivity analysis and preliminary results, Appl. Opt., 38, 7325–7341, 1999.
Mishchenko, M. I., Geogdzhayev, I. V., Liu, L., Ogren, J. A., Lacis, A. A., Rossow, W. B., Hovenier, J. W., Volten, H., and Muñoz, O.: Aerosol retrievals from AVHRR radiances: Effects of particle nonsphericity and absorption and an updated long-term global climatology of aerosol properties, J. Quant. Spectrosc. Radiat. Transfer, 79–80, 953–972, doi:10.1016/S0022-

4073(02)00331-X, 2003.
Mitchell Jr., J. M.: The effect of atmospheric aerosols on climate with special reference to temperature near the Earth's surface, J. Appl. Meteorol., 10, 703–714, 1971.
Moody, E. G., King, M. D., Platnick, S., Schaaf, C. B., and Gao, F.: Spatially complete global spectral surface albedos: value-added datasets derived from Terra MODIS land products, IEEE Trans. Geosci. Remote Sens., 43(1), 144–158, 2005.
Murayama, T., Sugimoto, N., Uno, I., et al.: Ground-based network observation of Asian dust events of April 1998 in East Asia, J. Geophys. Res., 106, 18 346–18 359, 2001.
Myhre, G., Grini, A., Haywood, J. M., Stordal, F., Chatenet, B., Tanré, D., Sundet, J. K., and Isaksen, I. S. A.: Modeling the radiative impact of mineral dust during the Saharan Dust Experiment (SHADE) campaign, J. Geophys. Res., 108(D18), 8579, doi:10.1029/2002JD002566, 2003.
Nakajima, T., Higurashi, A., Takeuchi, N., and Herman, J. R.: Satellite and ground-based study of optical properties of 1997 Indonesian forest fire aerosols, Geophys. Res. Lett., 20(16), 2421–2424, 1999.
National Research Council (NRC): Climate Change Sciences: An analysis of some key questions, National Academy Press, Washington D.C., 42 pp., 2001.
Nemesure, S., Wagener, R., and Schwartz, S. E.: Direct shortwave forcing of climate by anthropogenic sulfate aerosol: Sensitivity to particle size, composition, and relative humidity, J. Geophys. Res., 100, 26 105–26 116, 1995.
Penner, J. E., Dickinson, R. E., and O'Neill, C. A.: Effects of aerosol from biomass burning on the global radiation budget, Science, 256, 1432–1434, 1992.
Penner, J. E., Charlson, R. J., Hales, J. M., et al.: Quantifying and minimizing uncertainty of climate forcing by anthropogenic aerosols, Bull. Amer. Meteorol. Soc., 75, 375–400, 1994.
Penner, J. E., Zhang, S. Y., Chin, M., et al.: A Comparison of Model- and Satellite-Derived Aerosol Optical Depth and Reflectivity, J. Atmos. Sci., 59(3), 441–460, 2002.
Pilinis, C., Pandis, S. N., and Seinfeld, J. H.: Sensitivity of direct climate forcing by atmospheric aerosols to aerosol size and composition, J. Geophys., Res., 100, 18 739–18 754, 1995.
Platnick, S., King, M. D., Ackerman, S. A., et al.: The MODIS cloud products: Algorithms and examples from Terra, IEEE Trans. Geosci. Remote Sens., 41, 459–473, 2003.
Podgorny, I. A., Conant, W. C., Ramanathan, V., and Satheesh, S. K.: Aerosol modulation of atmospheric and solar heating over the tropical Indian Ocean, Tellus, Ser. B, 52, 947–958, 2000.

Podgorny, I. A. and Ramanathan, V.: A modeling study of the direct effect of aerosols over the tropical Indian Ocean, J. Geophys. Res., 106, 24 097–24 105, 2001.

Podgorny, I. A., Li, F., and Ramanathan, V.: Large aerosol radiative forcing due to the 1997 Indonesian forest fire, Geophys. Res. Lett., 30(1), 1028, doi:10.1029/2002GL015979, 2003.

Quinn, P. K. and Coffman, D. J.: Local closure during the First Aerosol Characterization Experiment (ACE 1): Aerosol mass concentration and scattering and backscattering coefficients, J. Geophys. Res., 103, 16 575–16 596, 1998.

Quinn, P. K., Bates, T. S., Miller, T. L., Coffman, D. J., Johnson, J. E., Harris, J. M., Ogren, J. A., Forbes, G., Anderson, T. L., Covert, D. S., and Rood, M. J.: Surface Submicron Aerosol Chemical Composition: What Fraction is Not Sulfate?, J. Geophys. Res., 105, 6785–6806, 2000.

Quinn, P. K. and Bates, T. S.: North American, Asian, and Indian haze: Similar regional impacts on climate?, Geophys. Res. Lett., 30(11), 1555, doi:10.1029/2003GL016934, 2003.

Raes, F., Bates, T., McGovern, F., and van Liedekerke, M.: The 2nd Aerosol Characterization Experiment (ACE-2): General overview and main results, Tellus, 52B, 111–125, 2000.

Rajeev, K. and Ramanathan, V.: Direct Observations of Clear-Sky Aerosol Radiative Forcing from Space during the Indoex Ocean Experiment, J. Geophy. Res., 106(D15), 17 221–17 236, 2001.

Ramana, M. V., Ramanathan, V., Podgorny, I. A., Pradhan, B. B., and Shrestha, B.: The direct observations of large aerosol radiative forcing in Himalayan region, Geophys. Res. Lett., 31, L05111, doi:10.1029/2003GL018824, 2004.

Ramanathan, V., Crutzen, P. J., Kiehl, J. L., and Rosenfeld, D.: Aerosols, climate, and the hydrological cycle, Science, 294, 2119–2124, 2001a.

Ramanathan, V., Crutzen, P. J., Lelieveld, J., et al.: Indian Ocean Experiment: An integrated analysis of the climate forcing and effects of the great Indo-Asian haze, J. Geophys. Res., 106, 28 371–28 398, 2001b.

Ramanathan, V. and Crutzen, P. J.: Atmospheric Brown “Clouds”, Atmos. Environ., 37, 4033–4035, 2003.

Reddy, M. S., Boucher, O., Bellouin, N., Schulz, M., Balkanski, Y., Dufresne, J.-L., and Pham, M.: Estimates of multi-component aerosol optical depth and direct radiative perturbation in the LMDZT general circulation model, J. Geophys. Res., 110, D10S16, doi:10.1029/2004JD004757, 2005a.

Reddy, M. S., Boucher, O., Balkanski, Y., and Schulz, M.: Aerosol optical depths and di-

rect radiative perturbations by species and source type, Geophys. Res. Lett., 32, L12803, doi:10.1029/2004GL021743, 2005b.
Reddy, M. S. and Boucher, O.: A study of the global cycle of carbonaceous aerosols in the LMDZT general circulation model, J. Geophys. Res., 109(D14), D14202, doi:10.1029/2003JD004048, 2004.
Redemann, J., Russell, P. B., and Hamill, P.: Dependence of aerosol light absorption and single-scattering albedo on ambient relative humidity for sulfate aerosols with black carbon cores, J. Geophys. Res., 106, 27 485–27 495, 2001.
Reid, J. S., Kinney, J. E., Westphal, D. L., et al.: Analysis of measurements of Saharan dust by airborne and groundbased remote sensing methods during the Puerto Rico Dust Experiment (PRIDE), J. Geophys. Res., 108(D19), 8586, doi:10.1029/2002JD002493, 2003.
Remer, L. A., Gassó, S., Hegg, D., Kaufman, Y. J., and Holben, B. N.: Urban/industrial aerosol: ground based sun/sky radiometer and airborne in situ measurements, J. Geophys. Res., 102, 16 849–16 859, 1997.
Remer, L. A., Tanré, D., Kaufman, Y. J., Ichoku, C., Mattoo, S., Levy, R., Chu, D. A., Holben, B., Dubovik, O., Smirnov, A., Martins, J. V., Li, R.-R., and Ahman, Z.: Validation of MODIS aerosol retrieval over ocean, Geophys. Res. Lett., 29(12), doi:10.1029/2001GL013204, 2002.
Remer, L. A., Kaufman, Y. J., Tanre, D., Mattoo, S., Chu, D. A., Martins, J. V., Li, R.-R., Ichoku, C., Levy, R. C., Kleidman, R. G., Eck, T. F., Vermote, E., and Holben, B. N.: The MODIS aerosol algorithm, products and validation, J. Atmos. Sci., 62(4), 947–973, 2005.
Remer, L. A. and Kaufman, Y. J.: Aerosol effect on the distribution of solar radiation over the global oceans derived from five years of MODIS retrievals, Atmos. Chem. Phys. Discuss., 5, 5007–5038, 2005, SRef-ID: 1680-7375/acpd/2005-5-5007.
Rosenfeld, D. and Lensky, I. M.: Satellite-based insights into precipitation formation processes in continental and maritime convective clouds, Bull. Am. Met. Soc., 79, 2457–2476, 1998.
Ross, J. L., Hobbs, P. V., and Holben, B. N.: Radiative characteristics of regional hazes dominated by smoke from biomass burning in Brazil: Closure tests and direct radiative forcing, J. Geophys. Res., 103(D24), 31 925–31 941, 1998.
Rossow, W. B. and Schiffer, R. A.: ISCCP cloud data products, Bull. Amer. Meteor. Soc., 72, 2–20, 1991.
Rossow, W. B. and Schiffer, R. A.: Advances in understanding clouds from ISCCP, Bull. Amer.

Meteor. Soc., 80, 2261–2287, 1999.
Russell, P. B., Kinne, S. A., and Bergstrom, R. W.: Aerosol climate effects: local radiative forcing and column closure experiments, J. Geophys. Res., 102(D8), 9397–9407, 1997.
Russell, P. B., Livingston, J. M., Hignett, P., Kinne, S., Wong, J., Chien, A., Bergstrom, R., Durkee, P., and Hobbs, P. V.: Aerosol-induced radiative flux changes off the United States mid-Atlantic coast: comparison of values calculated from sun photometer and in situ data with those measured by airborne pyranometer, J. Geophys. Res., 104, 2289–2307, 1999.
Satheesh, S. K. and Ramanathan, V.: Large differences in tropical aerosol forcing at the top of atmosphere and Earth's surface, Nature, 405, 60–63, 2000.
Satheesh, S. K.: Radiative forcing by aerosols over Bay of Bengal region, Geophys. Res. Lett., 29, 2083, doi:10.1029/2002GL015334, 2002.
Satheesh, S. K. and Srinivasan, J.: Enhanced aerosol loading over Arabian Sea during pre-monsoon season: Natural or Anthropogenic?, Geophys. Res. Lett., 29(18), 1874, doi:10.1029/2002GL015687, 2002
Satheesh, S. K., Ramanathan, V., Holben, B. N., Moorthy, K., Loeb, N. G., Maring, H., Prospero, J. M., and Savoie, D.: Chemical, microphysical, and radiative effects of Indian Ocean aerosols, J. Geophys. Res., 107, 4725, doi:10.1029/2002JD002463, 2002.
Satheesh, S. K. and Lubin, D.: Short wave versus long wave radiative forcing by Indian Ocean aerosols: Role of sea-surface winds, Geophys. Res. Lett., 30(13), 1695, doi:10.1029/2003GL017499, 2003.
Sato, M., Hansen, J., Koch, D., Lacis, A., Ruedy, R., Dubovik, O., Holben, B., Chin, M., and Novakov, T.: Global atmospheric black carbon inferred from AERONET, Proc. Nat. Aca. Sci., 100, 6319–6324, 2003.
Schaaf, C. B., Gao, F., Strahler, A. H., et al.: First operational BRDF, albedo and nadir reflectance products from MODIS, Remote Sens. Environ., 83, 135–148, 2002.
Schiffer, R. A. and Rossow, W. B.: The International Satellite Cloud Climatology Project (ISCCP): The first project of the World Climate Research Programme, Bull. Amer. Meteor. Soc., 64, 779–784, 1983.
Schutz, B. E.: Spaceborne laser altimetry: 2001 and beyond, in: Book of Extended Abstracts, edited by: Plag, H. P., WEGENER-98, Norwegian Mapping Authority, Honefoss, Norway, 1998.
Seinfeld, J. H., Carmichael, G. R., Arimoto, R., et al.: ACE-Asia: Regional climatic and atmospheric chemical effects of Asian dust and pollution, Bull. Amer. Meteo. Soc., 85(3), 367–380,

2004.
Seinfeld, J. H., Kahn, R. A., Anderson, T. L., Charlson, R. J., Davies, R., Diner, D. J., Schwartz, S. E., and Wielicki, B.: Scientific objectives, measurement needs, and challenges motivating the PARAGON aerosol initiative, Bull. Amer. Meteo. Soc., 85(10), 1503–1509, 2004.
Sellers, P. J., Los, S. O., Tucker, C. J., Justice, C. O., Dazlich, D. A., Collatz, C. J., and Randall, D. A.: A revised land surface parameterization (SiB2) for atmospheric GCMs, Part II, The generation of global fields of terrestrial biospheric parameters from satellite data, J. Clim., 9, 706–737, 1996.
Sheridan, P. J. and Ogren, J. A.: Observations of the vertical and regional variability of aerosol optical properties over central and eastern North America, J. Geophys. Res., 104, 16 793–16 805, 1999.
Smirnov, A., Holben, B. N., Eck, T. F., Dubovik, O., and Slutsker, I.: Cloud screening and quality control algorithms for the AERONET database, Rem. Sens. Env., 73, 337–349, 2000.
Smith Jr., W. L., Charlock, T. P., Kahn, R., Martins, J. V., Remer, L. A., Hobbs, P. V., Redemann, J., and Rutledge, C. K.: EOS Terra aerosol and radiative flux validation: An overview of the Chesapeake Lighthouse and aircraft measurements for satellites (CLAMS) experiment, J. Atmos. Sci., 62(4), 903–918, 2005.
Sokolik, I. N., Winker, D., Bergametti, G., et al.: Introduction to special section: outstanding problems in quantifying the radiative impacts of mineral dust, J. Geophys. Res., 106, 18 015–18 027, 2001.
Spinhirne, J. D., Palm, S. P., Hart, W. D., Hlavka, D. L., and Welton, E. J.: Cloud and Aerosol Measurements from GLAS: Overview and Initial Results, Geophys. Res. Lett., in press, 2005.
Stephens, G. L., Engelen, R. J., Vaughan, M., and Anderson, T. L.: Toward retrieving properties of the tenuous atmosphere using space-based lidar measurements, J. Geophys. Res., 106, 28 143–28 157, 2001.
Stephens, G. L., Vane, D. G., Boain, R. J., Mace, G. G., Sassen, K., Wang, Z., Illingworth, A. J., O'Conner, E. J., Rossow, W. G., Durden, S. L., Miller, S. D., Austin, R. T., Benedetti, A., and Mitrescu, C.: The CloudSat mission and the A-Train, Bull. Amer. Meteo. Soc., 83, 1771–1790, 2002.
Sumanth, E., Mallikarjuna, K., Stephen, J., et al.: Measurements of aerosol optical depths and black carbon over Bay of Bengal during post-monsoon season, Geophys. Res. Lett., 31, L16115, doi:10.1029/2004GL020681, 2004.

Tahnk, W. R. and Coakley, J. A.: Aerosol optical depth and direct radiative forcing for INDOEX derived from AVHRR: Observations, Januray-March 1996–2000, J. Geophys. Res., 107, 8010, doi:10.1029/2000JD000183, 2002.

Takemura, T., Okamoto, H., Maruyama, Y., Numaguti, A., Higurashi, A., and Nakajima, T.: Global three-dimensional simulation of aerosol optical thickness distribution of various origins, J.Geophys. Res., 105, 17 853–17 873, 2000.

Takemura, T., Nakajima, T., Dubovik, O., Holben, B. N., and Kinne, S.: Single-scattering albedo and radiative forcing of various aerosol species with a global three-dimensional model, J. Clim., 15, 333–352, 2002.

Takemura, T., Nozawa, T., Emori, S., Nakajima, T. Y., and Nakajima, T.: Simulation of climate response to aerosol direct and indirect effects with aerosol transport-radiation model, J. Geophys. Res., 110, D02202, doi:10.1029/2004JD005029, 2005.

Tanré, D., Kaufman, Y. J., Herman, M., and Mattoo, S.: Remote sensing of aerosol properties over oceans using the MODIS/EOS spectral radiances, J. Geophys. Res., 102, 16 971–16 988, 1997.

Tanré, D., Haywood, J., Pelon, J., Léon, J. F., Chatenet, B., Formenti, P., Francis, P., Goloub, P., Highwood, E. J., and Myhre, G.: Measurement and modeling of the Saharan dust radiative impact: Overview of the Saharan Dust Experiment (SHADE), J. Geophys. Res., 108(D18), 8574, doi:10.1029/2002JD003273, 2003.

Tegen, I. and Fung, I.: Contribution to the atmospheric mineral aerosol load from land surface modification, J. Geophys. Res., 100(D9), 18 707–17 726, 1995.

Tegen, I., Werner, M., Harrison, S. P., and Kohfeld, K. E.: Relative importance of climate and land use in determining present and future global soil dust emission, Geophys. Res. Lett., 31, L05105, doi:10.1029/2003GL019216, 2004.

Textor, C., Schulz, M., Guibert, S., et al.: Analysis and quantification of the diversities of aerosol life cycles within AEROCOM, Atmos. Chem. Phys. Discuss., accepted, 2005.

Torres, O., Bhartia, P. K., Herman, J. R., Ahmad, Z., and Gleason, J.: Derivation of aerosol properties from satellite measurements of backscattered ultraviolet radiation: Theoretical bases, J. Geophys. Res., 103, 17 009–17 110, 1998.

Torres, O., Bhartia, P. K., Herman, J. R., Sinyuk, A., Ginoux, P., and Holben, B. N.: A Long-Term Record of Aerosol Optical Depth from TOMS Observations and Comparison to AERONET Measurements, J. Atmos. Sci., 59(3), 398–413, 2002.

Torres, O., Bhartia, P. K., Sinyuk, A., Welton, E. J., and Holben, B. N.: Total Ozone Map-

ping Spectrometer measurements of aerosol absorption from space: Comparison to SAFARI 2000 ground-based observations, J. Geophys. Res., D10S18, doi:10.1029/2004JD004611, 2005.

Tsvetsinskaya, E. A., Schaaf, C. B., Gao, F., Strahler, A. H., Dickinson, R. E., Zeng, X., and Lucht, W.: Relating MODIS-derived surface albedo to soils and rock types over Northern Africa and the Arabian Peninsula, Geophys. Res. Lett., 29(9), 1353, doi:10.1029/2001GL014096, 2002.

Turner, D. D., Ferrare, R. A., and Brasseur, L. A.: Average aerosol extinction and water vapor profiles over the southern Great Plains, Geophys. Res. Lett., 28(23), 4441–4444, doi:10.1029/2001GL013691, 2001.

Turner, D. D., Ferrare, R. A., Brasseur, L. A., Feltz, W. F., and Tooman, T. P.: Automated retrievals of water vapor and aerosol profiles from an operational Raman lidar, J. Atmos. Ocean Tech., 19, 37–50, 2002.

Twomey, S.: The influence of pollution on the shortwave albedo of clouds, J. Atmos. Sci., 34, 1149–1152, 1977.

van de Hulst, H. C.: Light scattering by small particles, John Wiley (1957), reprinted by Dover, New York, 1981.

Vogelmann, A. M., Flatau, P. J., Szczodrak, M., Markowicz, K. M., and Minnett, P. J.: Observations of large aerosol infrared forcing at the surface, Geophys. Res. Lett., 30(12), 1655, doi:10.1029/2002GL016829, 2003.

von Hoyningen-Huene, W., Schmidt, T., Schienbein, S., Kee, C. A., and Tick, L. J.: Climate-relevant aerosol parameters for South-East-Asia forest fire haze, Atmos. Environ., 33, 3183–3190, 1999.

Wang, J., Christopher, S. A., Brechtel, F., Kim, J., Schmid, B., Redemann, J., Russell, P. B., Quinn, P., and Holben, B. N.: Geostationary Satellite Retrievals of Aerosol Optical Thickness during ACE-Asia, J. Geophys. Res., 108(D23), 8657, doi:10.1029/2003JD003580, 2003a.

Wang, J., Christopher, S. A., Reid, J. S., Maring, H., Savoie, D., Holben, B. N., Livingston, J. M., Russell, P. B., and Yang, S.-K.: GOES 8 retrieval of dust aerosol optical thickness over the Atlantic Ocean during PRIDE, J. Geophys. Res., 108(D19), 8595, doi:10.1029/2002JD002494, 2003b.

Welton, E. J., Voss, K. J., Quinn, P. K., Flatau, P. J., Markowicz, K., Campbell, J. R., Spinhirne, J. D., Gordon, H. R., and Johnson, J. E.: Measurements of aerosol vertical profiles and optical properties during INDOEX 1999 using micro-pulse lidars, J. Geophys. Res., 107,

8019, doi:10.1029/2000JD000038, 2002.
Welton, E. J., Campbell, J. R., Spinhirne, J. D., and Scott, V. S.: Global monitoring of clouds and aerosols using a network of micro-pulse lidar systems, in: Lidar Remote Sensing for Industry and Environmental Monitoring, edited by: Singh, U. N., Itabe, T., and Sugimoto, N., Proc. SPIE, 4153, 151–158, 2001.
Wendisch, M., Heintzenberg, J., and Bussemer, M.: Measurement-based aerosol forcing calculations: the influence of model complexity, Meteorologische Zeitschrift, 10(1), 45–60, 2001
Wielicki, B. A., Barkstrom, B. R., Harrison, E. F., Lee, R. B. I., Smith, G. L., and Cooper, J. E.: Clouds and the Earth's radiant energy system (CERES): An Earth observing system experiment, Bull. Amer. Meteo. Soc., 77, 853–868, 1996.
Winker, D. M., Pelon, J. R., and McCormick, M. P.: The CALIPSO mission: spaceborne lidar for observation of aerosols and clouds, Proc. SPIE, 4893, 1–11, 2003.
Xu, J., Bergin, M. H., Greenwald, R., and Russell, P. B.: Direct aerosol radiative forcing in the Yangtze delta region of China: Observation and model estimation, J. Geophys. Res., 108(D2), 4060, doi:10.1029/2002JD002550, 2003.
Yu, H., Liu, S. C., and Dickinson, R. E.: Radiative effects of aerosols on the evolution of the atmospheric boundary layer, J. Geophys. Res., 107(D12), 4142, doi:10.1029/2001JD000754, 2002.
Yu, H., Dickinson, R. E., Chin, M., Kaufman, Y. J., Holben, B. N., Geogdzhayev, I. V., and Mishchenko, M. I.: Annual cycle of global distributions of aerosol optical depth from integration of MODIS retrievals and GOCART model simulations, J. Geophys. Res., 108(D3), 4128, doi:10.1029/2002JD002717, 2003.
Yu, H., Dickinson, R. E., Chin, M., Kaufman, Y. J., Zhou, M., Zhou, L., Tian, Y., Dubovik, O., and Holben, B. N.: The direct radiative effect of aerosols as determined from a combination of MODIS retrievals and GOCART simulations, J. Geophys. Res., 109, D03206, doi:10.1029/2003JD003914, 2004.
Zhang, J. and Christopher, S. A.: Longwave radiative forcing of Saharan dust aerosols estimated from MODIS, MISR, and CERES observations on Terra, Geophys. Res., Lett., 30(23), 2188, doi:10.1029/2003GL018479, 2003.
Zhang, J., Christopher, S. A., Remer, L. A., and Kaufman, Y. J.: Shortwave aerosol radiative forcing over cloud-free oceans from Terra. I: Angular models for aerosols, J. Geophys. Res., 110, D10S23, doi:10.1029/2004JD005008, 2005a.
Zhang, J., Christopher, S. A., Remer, L. A., and Kaufman, Y. J.: Shortwave aerosol radiative

forcing over cloud-free oceans from Terra. II: Seasonal and global distributions, J. Geophys. Res., 110, D10S24, doi:10.1029/2004JD005009, 2005b.

Zhou, M., Yu, H., Dickinson, R. E., Dubovik, O., and Holben, B. N.: A normalized description of the direct effect of key aerosol types on solar radiation as estimated from AERONET aerosols and MODIS albedos, J. Geophys. Res., in press, 2005.

Zwally, H. J., Schutz, B., Abdalati, W., Abshire, J., Bentley, C., Brenner, A., Bufton, J., Dezio, J., Hancock, D., Harding, D., Herring, T., Minster, B., Quinn, K., Palm, S., Spinhirne, J., and Thomas, R.: ICESat's laser measurements of polar ice, atmosphere, ocean, and land, J. Geodynamics, 34, 405–445, 2002.

Table 1. List of major intensive field experiments that are relevant to aerosol research in a variety of aerosol regimes around the globe conducted in the past decade.

Aerosol Regimes	Intensive Field Experiments			Major References
	Name	Location	Time	
Industrial Pollution from North America and West Europe	TARFOX	North Atlantic	July, 1996	Russell et al., 1999
	NEAQS	North Atlantic	July-August, 2002	Quinn and Bates, 2003
	SCAR-A	North America	1993	Remer et al., 1997
	CLAMS	East Coast of U.S.	July-August, 2001	Smith et al., 2005
	INTEX-NA, ICARTT	North America	Summer 2004	http://www-air.larc.nasa.gov/missions/intexna
	ACE-2	North Atlantic	June-July, 1997	Raes et al., 2000
	MINOS	Mediterranean region	July-August, 2001	Lelieveld et al., 2002
	LACE98	Lindberg, Germany	July-August, 1998	Ansmann et al., 2002
	Aerosols99	Atlantic	January-February, 1999	Bates et al., 2001
Brown Haze in South Asia	INDOEX	Indian subcontinent and Indian Ocean	January-April, 1998 and 1999	Ramanathan et al., 2001b
	ABC	South and East Asia	ongoing	Ramanathan and Crutzen, 2003
Pollution and dust mixture in East Asia	ACE-Asia	East Asia and Northwest Pacific	April, 2001	Huebert et al., 2003; Seinfeld et al., 2004
	TRACE-P	East Asia and Northwest Pacific	March-April, 2001	Jacob et al., 2003
	PEM-West A & B	Western Pacific off East Asia	September-October, 1991 February-March, 1994	Hoell et al., 1996; 1997
Biomass burning smoke in the tropics	BASE-A	Brazil	1989	Kaufman et al., 1992
	SCAR-B	Brazil	August-September, 1995	Kaufman et al., 1998
	LBA-SMOCC	Amazon basin	September-November 2002	Andreae et al., 2004
	SAFARI2000	South Africa and South Atlantic	August-September, 2000	King et al., 2003a
	SAFARI92	South Atlantic and South Africa	September-October, 1992	Lindesay et al., 1996
	TRACE-A	South Atlantic	September-October, 1992	Fishman et al., 1996
Mineral dusts from North Africa and Arabian Peninsula	SHADE	West coast of North Africa	September, 2000	Tanré et al., 2003
	PRIDE	Puerto Rico	June-July, 2000	Reid et al., 2003
	UAE[2]	Arabian Peninsula	August-September, 2004	http://uae2.gsfc.nasa.gov/
Remote Oceanic Aerosol	ACE-1	Southern Oceans	December, 1995	Bates et al., 1998; Quinn and Coffman., 1998

Table 2. List of products participated in the intercomparison of aerosol optical thickness.

Products	Brief Descriptions	Major References
MODIS	Terra-MODIS monthly 1°x1° data (MOD08_M3)	Kaufman et al., 1997; Tanré et al., 1997; Remer et al., 2005
MISR	MISR monthly 0.5°x0.5° data (MIL3MAE)	Diner et al., 1997; Kahn et al., 2005
MO_GO	Integration of GOCART simulations with MODIS retrievals (land and ocean)	Yu et al., 2003
MI_GO	Integration of GOCART simulations with MISR retrievals (land and ocean)	
MO_MI_GO	Integration of GOCART simulations with retrievals from MODIS over ocean and from MISR over land.	
GOCART	2001 whole-sky monthly average; resolution: 2.5°x2°, 30 vertical layers; driven by assimilated meteorology NASA/GEOS-DAS	Chin et al., 2000a, b; Ginoux et al., 2001, 2004; Chin et al., 2002, 2003, 2004
SPRINTARS	2001 whole-sky monthly average; resolution: 1.125°x1.125°, 20 layers; coupled with an atmospheric general circulation model (GCM)	Takemura et al., 2000, 2002, 2005
SPRINTARS_clr	SPRINTARS extraction of clear-sky conditions: the grid cloud fraction less than 0.2 at each model integration step.	
GISS	3-year whole-sky monthly average; resolution: 5°x4°, 20 vertical layers; coupled with GISS GCM	Koch and Hansen, 2005; Koch et al., 2005[2]; Miller et al., 2005[3]; Schmidt et al., 2005[4]
GISS_clr	Weighted by clear-sky fraction	
LMDZ-INCA	2001 whole-sky monthly average; resolution: 3.75°x2.5°, 19 vertical layers; nudged with ECMWF winds	Schulz et al., 2005[5]; Textor et al., 2005
LMDZ-LOA	2000 and 2001 whole-sky monthly average; resolution: 3.75°x2.5°, 19 vertical layers; nudged with ECMWF winds	Boucher et al., 2002; Boucher and Pham, 2002; Reddy et al., 2004, 2005a, b

Table 3. List of products participating in the intercomparison of the aerosol direct effect.

Products	Brief Descriptions	Data year	Major References
MODIS	Using Terra-MODIS AOT with a constraint by MODIS measured radiances	2001-2004	Remer and Kaufman, 2005
MODIS_A	Using Terra-MODIS AOT and AERONET measurements of size distribution and single-scattering albedo	2002	Bellouin et al., 2005[6]
CERES_A	Using CERES fluxes in combination with standard MODIS aerosol	2000-2001	Loeb and Manalo-Smith, 2005; Loeb and Kato, 2002
CERES_B	Using CERES fluxes in combination with NOAA NESDIS aerosol from MODIS radiances		
CERES_C	Using CERES fluxes in combination with MODIS aerosol with new angular models for aerosols	2000-2001	Zhang et al., 2005a, b; Christopher and Zhang, 2004
MODIS_G	Using GOCART simulations to fill AOT gaps in satellite retrievals	2001	* Aerosol single-scattering albedo and asymmetry factor are taken from GOCART simulations; * Yu et al., 2003, 2004
MISR_G			
MO_GO	Integration of MODIS and GOCART AOT		
MO_MI_GO	Integration of GOCART AOT with retrievals from MODIS (Ocean) and MISR (Land)		
POLDER	Using POLDER AOT in combination with prescribed aerosol models	1996-1997	Boucher and Tanré, 2000; Bellouin et al., 2003
SeaWiFS	Using SeaWiFS AOT and assumed aerosol models	1997-1998	Chou et al., 2002
GOCART	Offline RT calculations using monthly average aerosols with a time step of 30 min (without the presence of clouds)	2001	Chin et al., 2002; Yu et al., 2004
SPRINTARS	Online RT calculations every 3 hours (setting cloud fraction=0)	2001	Takemura et al., 2002, 2005
GISS	Online model simulations and weighted by clear-sky fraction	3-year climatology	Koch and Hansen, 2005; Koch et al., 2005[2]; Schmidt et al., 2005[4]
LMDZ-INCA	Online RT calculations every 2 hours (setting cloud fraction = 0)	2000	Balkanski et al., 2005[7]; Balkanski and Schulz, 2005[8]; Kinne et al., 2005
LMDZ-LOA	Online RT calculations every 2 hours (setting cloud fraction=0)	2000-2001	Reddy et al., 2005a, b

Table 4. Seasonal (MAM and JJA) and annual averages of aerosol optical depth (upper line) and the clear-sky TOA direct radiative effect (Wm^{-2}, bottom line) over ocean in 13 zones (light blue background – land is not included). The global averages are listed in the blue boxes in the bottom-right corners.

MODIS

MAM	JJA	ANN	MAM	JJA	ANN	MAM	JJA	ANN	MAM	JJA	ANN
0.18	0.14	0.14	0.18	0.17	0.15	0.22	0.20	0.19	0.28	0.24	0.21
−9.5	−7.3	−7.1	−9.0	−8.4	−7.4	−11.8	−11.1	−9.9	−14.7	−12.7	−11.0
0.14	0.10	0.11	0.21	0.25	0.20	0.25	0.43	0.29	0.16	0.11	0.13
−4.3	−2.9	−3.5	−7.0	−8.4	−7.0	−8.8	−17.5	−11.4	−5.2	−3.2	−4.5
0.08	0.09	0.09	0.11	0.12	0.12	0.11	0.14	0.13	0.09	0.11	0.11
−3.0	−3.7	−2.9	−4.1	−5.4	−4.7	−4.2	−6.6	−4.9	−3.6	−4.9	−4.2
				MAM	JJA	ANN			Global Average		
				0.10	0.09	0.11			0.13	0.13	0.13
				−5.3	−4.8	−6.2			−5.5	−5.7	−5.6

CERES_A

MAM	JJA	ANN	MAM	JJA	ANN	MAM	JJA	ANN	MAM	JJA	ANN
0.29	0.20	0.19	0.21	0.19	0.17	0.26	0.24	0.21	0.46	0.36	0.30
−10.8	−7.3	−6.9	−8.3	−7.1	−6.4	−9.5	−9.0	−7.7	−15.9	−12.1	−10.3
0.17	0.12	0.13	0.24	0.26	0.23	0.27	0.46	0.30	0.18	0.13	0.15
−5.1	−4.1	−4.3	−7.1	−8.2	−7.1	−7.9	−13.3	−8.9	−5.2	−3.9	−4.6
0.09	0.10	0.10	0.11	0.12	0.13	0.11	0.16	0.14	0.10	0.12	0.12
−3.4	−3.5	−3.6	−4.0	−4.5	−4.7	−3.9	−5.6	−4.9	−3.7	−4.3	−4.2
				MAM	JJA	ANN			Global Average		
				0.11	0.10	0.14			0.19	0.19	0.17
				−4.7	−3.4	−5.6			−6.1	−5.4	−5.5

GOCART

MAM	JJA	ANN	MAM	JJA	ANN	MAM	JJA	ANN	MAM	JJA	ANN
0.18	0.11	0.15	0.18	0.16	0.16	0.33	0.30	0.27	0.30	0.20	0.22
−7.0	−4.6	−5.6	−6.7	−6.8	−5.9	−8.5	−7.2	−6.4	−10.3	−8.1	−7.8
0.09	0.09	0.08	0.18	0.26	0.20	0.17	0.22	0.16	0.11	0.08	0.09
−3.1	−3.4	−3.0	−6.4	−10.4	−7.4	−5.1	−6.9	−5.0	−3.7	−3.5	−3.4
0.05	0.06	0.05	0.07	0.10	0.09	0.05	0.12	0.08	0.05	0.07	0.06
−1.8	−2.3	−1.9	−2.6	−3.5	−3.0	−1.9	−3.6	−2.6	−1.7	−2.3	−2.0
				MAM	JJA	ANN			Global Average		
				0.10	0.13	0.11			0.11	0.13	0.11
				−4.0	−4.4	−4.4			−4.0	−4.7	−4.1

Table 5. Seasonal (MAM and JJA) and annual averages of aerosol optical depth (upper line) and the clear-sky TOA direct radiative effect (Wm^{-2}, bottom line) over land in 13 zones (light blue background – only land is included). The global averages are listed in the blue boxes in the bottom-right corners.

MISR_G

MAM	JJA	ANN	MAM	JJA	ANN	MAM	JJA	ANN	MAM	JJA	ANN
0.18	0.15	0.14	0.22	0.22	0.17	0.25	0.24	0.21	0.31	0.24	0.22
−5.7	−5.7	−4.2	−7.0	−8.7	−5.8	−5.3	−5.8	−4.4	−5.4	−6.4	−4.4
0.20	0.19	0.15	0.35	0.43	0.32	0.37	0.45	0.33	0.37	0.32	0.31
−5.7	−7.0	−5.1	−6.9	−9.1	−6.9	−6.4	−7.0	−5.6	−8.0	−9.4	−7.2
			0.13	0.10	0.17	0.14	0.24	0.23	0.11	0.10	0.14
			−3.9	−3.0	−4.3	−4.1	−4.6	−5.1	−3.3	−3.1	−3.8
				MAM	JJA	ANN			Global Average		
				0.06	0.07	0.09			0.25	0.25	0.23
				−4.1	−3.0	−5.8			−5.1	−5.8	−4.9

MO_MI_GO

MAM	JJA	ANN	MAM	JJA	ANN	MAM	JJA	ANN	MAM	JJA	ANN
0.17	0.14	0.13	0.20	0.21	0.17	0.24	0.23	0.20	0.29	0.23	0.21
−5.2	−5.0	−3.9	−6.3	−7.4	−5.3	−5.4	−5.8	−4.5	−5.4	−6.4	−4.4
0.19	0.18	0.15	0.31	0.36	0.29	0.34	0.38	0.30	0.33	0.23	0.25
−5.5	−6.3	−4.7	−6.2	−7.4	−6.1	−5.6	−6.2	−5.1	−7.0	−6.5	−6.0
			0.10	0.11	0.13	0.11	0.23	0.19	0.08	0.08	0.11
			−3.0	−2.9	−3.3	−3.2	−4.5	−4.2	−2.5	−2.5	−2.9
				MAM	JJA	ANN			Global Average		
				0.07	0.07	0.09			0.22	0.23	0.20
				−3.3	−2.8	−4.8			−4.7	−5.3	−4.4

GOCART

MAM	JJA	ANN	MAM	JJA	ANN	MAM	JJA	ANN	MAM	JJA	ANN
0.14	0.11	0.11	0.19	0.19	0.17	0.30	0.25	0.23	0.28	0.23	0.22
−4.3	−4.0	−3.6	−5.8	−5.9	−4.9	−7.0	−6.3	−5.3	−5.1	−5.8	−4.4
0.15	0.13	0.11	0.29	0.34	0.28	0.33	0.34	0.28	0.34	0.18	0.25
−3.3	−4.5	−3.2	−5.1	−6.6	−5.5	−4.7	−4.9	−4.3	−6.6	−5.0	−5.6
			0.08	0.15	0.12	0.07	0.26	0.17	0.06	0.06	0.07
			−2.3	−3.1	−2.6	−2.0	−4.2	−3.0	−1.6	−1.7	−1.7
				MAM	JJA	ANN			Global Average		
				0.07	0.08	0.08			0.22	0.22	0.20
				−3.6	−3.1	−4.0			−4.4	−4.8	−4.1

Table 6. (a) Seasonal and annual average aerosol optical depths over land and ocean (60° S–60° N). Satellite retrievals are from Terra.

Products	DJF	MAM	JJA	SON	ANN
MODIS	0.170	0.200	0.200	0.181	0.188
MISR	0.188	0.209	0.212	0.189	0.199
MO_GO	0.144	0.174	0.172	0.157	0.162
MI_GO	0.130	0.155	0.161	0.141	0.147
MO_MI_GO	0.138	0.162	0.161	0.145	0.151
GOCART	0.111	0.141	0.152	0.132	0.134
SPRINTARS	0.104	0.110	0.148	0.117	0.120
GISS	0.169	0.208	0.226	0.197	0.200
LMDZ-INCA	0.113	0.140	0.174	0.130	0.139
LMDZ-LOA	0.113	0.123	0.154	0.125	0.129
SPRINTARS_clr	0.087	0.093	0.127	0.097	0.101
GISS_clr	0.079	0.113	0.131	0.102	0.106

Table 6. **(b)** Seasonal and annual average aerosol optical depths over land (60° S–60° N). Satellite retrievals are from Terra.

Products	DJF	MAM	JJA	SON	ANN
MODIS	0.223	0.308	0.319	0.267	0.279
MISR	0.199	0.245	0.254	0.200	0.225
MO_GO	0.175	0.253	0.257	0.218	0.226
MI_GO	0.154	0.207	0.212	0.170	0.186
MO_MI_GO	0.155	0.209	0.214	0.172	0.188
GOCART	0.146	0.218	0.222	0.197	0.196
SPRINTARS	0.133	0.155	0.217	0.173	0.170
GISS	0.112	0.204	0.235	0.159	0.178
LMDZ-INCA	0.136	0.201	0.290	0.192	0.205
LMDZ-LOA	0.157	0.201	0.272	0.202	0.208
SPRINTARS_clr	0.099	0.127	0.191	0.138	0.139
GISS_clr	0.075	0.160	0.191	0.119	0.138

Table 6. (c) Seasonal and annual average aerosol optical depths over ocean (60° S–60° N). Satellite retrievals are from Terra.

Products	DJF	MAM	JJA	SON	ANN
MODIS	0.150	0.160	0.156	0.150	0.154
MISR	0.184	0.196	0.196	0.185	0.190
MO_GO	0.132	0.145	0.142	0.135	0.138
MI_GO	0.122	0.136	0.142	0.130	0.132
MO_MI_GO	0.132	0.144	0.141	0.134	0.138
GOCART	0.098	0.113	0.126	0.108	0.111
SPRINTARS	0.093	0.092	0.121	0.095	0.100
GISS	0.189	0.209	0.222	0.211	0.208
LMDZ-INCA	0.107	0.117	0.128	0.106	0.114
LMDZ-LOA	0.097	0.095	0.111	0.096	0.099
SPRINTARS_clr	0.082	0.080	0.102	0.081	0.086
GISS_clr	0.080	0.096	0.110	0.096	0.095

Table 7. Summary of seasonal and annual average clear-sky DRE (Wm^{-2}) at the TOA and the surface (SFC) over global ocean derived with different methods and data: MODIS (Remer and Kaufman, 2005), MODIS_A (Bellouin et al., 2005[6]), POLDER (Boucher and Tanré, 2000; Bellouin et al., 2003), CERES_A and CERES_B (Loeb and Manalo-Smith, 2005), CERES_C (Zhang et al., 2005b; Christopher and Zhang, 2004), MODIS_G, MISR_G, MO_GO, MO_MI_GO (Yu et al., 2003, 2004), SeaWiFS (Chou et al., 2002), GOCART (Chin et al., 2001, 2002; Yu et al., 2004), SPRINTARS (Takemura et al., 2002), GISS (Koch and Hansen, 2005; Koch et al., 2005[2]), LMDZ-INCA (Balkanski et al., 2005[7]; Balkanski and Schulz, 2005[8]; Kinne et al., 2005), LMDZ-LOA (Reddy et al., 2005a, b). Mean, median, and standard error (ε) are calculated for observations and model simulations separately. The last row is the ratio of model median to observational median.

Products	DJF		MAM		JJA		SON		ANN	
	TOA	SFC	TOA	SFC	TOA	SFC	TOA	SFC	TOA	SFC
MODIS	-5.6	–	-5.5	–	-5.7	–	-5.5	–	-5.6	–
MODIS_A	-6.7	-8.7	-7.1	-9.3	-7.4	-9.8	-7.1	-9.3	-7.1	-9.3
CERES_A	-5.2	–	-6.1	–	-5.4	–	-5.1	–	-5.5	–
CERES_B	-3.8	–	-4.3	–	-3.5	–	-3.6	–	-3.8	–
CERES_C	-5.3	–	-5.4	–	-5.2	–	–	–	-5.3	–
MODIS_G	-5.5	-9.1	-5.7	-10.4	-6.0	-10.6	-5.5	-9.8	-5.7	-10.0
MISR_G	-6.4	-10.3	-6.5	-11.4	-7.0	-11.9	-6.3	-10.9	-6.5	-11.1
MO_GO	-4.9	-7.8	-5.1	-9.3	-5.4	-9.4	-5.0	-8.7	-5.1	-8.8
MO_MI_GO	-4.9	-7.9	-5.1	-9.2	-5.5	-9.5	-5.0	-8.6	-5.1	-8.7
POLDER	-5.7	–	-5.7	–	-5.8	–	-5.6	–	-5.7 -5.2*	-7.7*
SeaWiFS	-6.0	-6.6	-5.2	-5.8	-4.9	-5.6	-5.3	-5.7	-5.4	-5.9
Obs. Mean	-5.5	-8.4	-5.6	-9.2	-5.6	-9.5	-5.4	-8.8	-5.5	-8.8
Obs. Median	-5.5	-8.3	-5.5	-9.3	-5.5	-9.7	-5.4	-9.0	-5.5	-8.8
Obs. ε	0.19	0.31	0.18	0.46	0.25	0.51	0.22	0.42	0.19	0.40
GOCART	-3.6	-5.7	-4.0	-7.2	-4.7	-8.0	-4.0	-6.8	-4.1	-6.9
SPRINTARS	-1.5	-2.5	-1.5	-2.5	-1.9	-3.3	-1.5	-2.5	-1.6	-2.7
GISS	-3.3	-4.1	-3.5	-4.6	-3.5	-4.9	-3.8	-5.4	-3.5	-4.8
LMDZ-INCA	-4.6	-5.6	-4.7	-5.9	-5.0	-6.3	-4.8	-5.5	-4.7	-5.8
LMDZ-LOA	-2.2	-4.1	-2.2	-3.7	-2.5	-4.4	-2.2	-4.1	-2.3	-4.1
Mod. Mean	-3.0	-4.4	-3.2	-4.8	-3.5	-5.4	-3.3	-4.9	-3.2	-4.9
Mod. Median	-3.3	-4.1	-3.5	-4.6	-3.5	-4.9	-3.8	-5.4	-3.5	-4.8
Mod. ε	0.61	0.66	0.66	0.92	0.67	0.91	0.68	0.81	0.64	0.80
Mod./Obs.	0.60	0.49	0.64	0.49	0.64	0.51	0.70	0.60	0.64	0.55

* Bellouin et al. (2003) use AERONET retrieval of aerosol absorption as a constraint to the method in Boucher and Tanré (2000), deriving aerosol direct effects both at the TOA and the surface.

Table 8. Summary of seasonal and annual average clear-sky DRE (Wm^{-2}) at the TOA and the surface over global land derived with different methods and data: MODIS_A (Bellouin et al., 2005[6]), MODIS_G, MISR_G, MO_GO, MO_MI_GO (Yu et al., 2003, 2004), GOCART (Chin et al., 2001, 2002; Yu et al., 2004), SPRINTARS (Takemura et al., 2002), GISS (Koch and Hansen, 2005; Koch et al., 2005[2]), LMDZ-INCA (Balkanski et al., 2005[7]; Balkanski and Schulz, 2005[8]; Kinne et al., 2005), LMDZ-LOA (Reddy et al., 2005a, b). Mean, median, and standard error (ε) are calculated for observations and model simulations separately. The last row is the ratio of model median to observational median.

Products	*DJF*		*MAM*		*JJA*		*SON*		*ANN*	
	TOA	SFC	TOA	SFC	TOA	SFC	TOA	SFC	TOA	SFC
MODIS_A	-6.0	-17.9	-7.8	-19.5	-9.1	-21.8	-7.0	-19.2	-7.7	-19.9
MODIS_G	-4.1	-9.1	-5.8	-14.9	-6.6	-17.4	-5.4	-12.8	-5.5	-13.5
MISR_G	-3.9	-8.7	-5.1	-13.0	-5.8	-14.6	-4.6	-10.7	-4.9	-11.8
MO_GO	-3.5	-7.5	-5.1	-12.9	-5.8	-14.9	-4.8	-10.9	-4.8	-11.6
MO_MI_GO	-3.4	-7.4	-4.7	-11.8	-5.3	-13.5	-4.3	-9.7	-4.4	-10.6
Obs. Mean	-4.2	-10.1	-5.7	-14.4	-6.5	-16.4	-5.2	-12.7	-5.5	-13.5
Obs. Median	-3.9	-8.7	-5.1	-13.0	-5.8	-14.9	-4.8	-10.9	-4.9	-11.8
Obs. ε	0.53	2.21	0.62	1.53	0.76	1.66	0.54	1.91	0.66	1.87
GOCART	-2.9	-6.1	-4.4	-10.9	-4.8	-12.3	-4.3	-9.3	-4.1	-9.7
SPRINTARS	-1.4	-4.0	-1.5	-4.6	-2.0	-6.7	-1.7	-5.2	-1.7	-5.1
GISS	-1.6	-3.9	-3.2	-7.9	-3.6	-9.3	-2.5	-6.6	-2.8	-7.2
LMDZ-INCA	-3.0	-5.8	-4.0	-9.2	-6.0	-13.5	-4.3	-8.2	-4.3	-9.2
LMDZ-LOA	-1.3	-5.4	-1.8	-6.4	-2.7	-8.9	-2.1	-6.7	-2.0	-6.9
Mod. Mean	-2.0	-5.0	-3.0	-7.8	-3.8	-10.1	-3.0	-7.2	-3.0	-7.6
Mod. Median	-1.6	-5.4	-3.2	-7.9	-3.6	-9.3	-2.5	-6.7	-2.8	-7.2
Mod. ε	0.42	0.51	0.65	1.22	0.80	1.37	0.62	0.79	0.59	0.93
Mod./Obs.	0.41	0.62	0.63	0.61	0.62	0.62	0.52	0.61	0.57	0.61

Table 9. Summary of seasonal (MAM, JJA) and annual (ANN) average clear-sky DRE (Wm^{-2}) at the TOA in five selected oceanic zones (Z2 – midlatitude North Atlantic, Z4 – Northwest Pacific, Z6 – Tropical Atlantic, Z7 – Arabian Sea and Northern Indian Ocean, Z9 – Tropical Southeastern Pacific). Mean, median, and standard error (ε) are calculated for observations and model simulations separately. The last row is the ratio of model median to observational median.

Products	MAM					JJA					ANN				
	Z2	Z4	Z6	Z7	Z9	Z2	Z4	Z6	Z7	Z9	Z2	Z4	Z6	Z7	Z9
MODIS	-9.0	-14.7	-7.0	-8.8	-3.0	-8.4	-12.7	-8.4	-17.5	-3.7	-7.4	-11.0	-7.0	-11.4	-2.9
MODIS_A	-9.4	-13.8	-11.9	-11.8	-4.6	-9.4	-10.0	-13.2	-18.5	-5.1	-7.8	-9.7	-10.0	-11.5	-4.9
CERES_A	-8.3	-15.9	-7.1	-7.9	-3.4	-7.1	-12.1	-8.2	-13.3	-3.5	-6.4	-9.3	-7.4	-8.6	-3.6
CERES_B	-5.6	-8.7	-5.2	-5.8	-2.8	-4.4	-5.7	-5.7	-8.5	-3.0	-4.5	-6.2	-5.5	-6.5	-2.9
CERES-C	-8.5	-17.3	-8.3	-9.0	-3.4	-6.7	-11.4	-8.9	-15.4	-3.6	-6.8	-11.8	-8.3	-10.8	-3.5
MODIS_G	-7.9	-14.2	-8.6	-8.1	-3.6	-8.0	-12.5	-11.2	-12.0	-3.8	-6.4	-9.6	-8.7	-8.4	-3.7
MISR_G	-8.7	-12.8	-9.7	-7.6	-4.8	-8.6	-11.9	-12.8	-12.0	-5.9	-7.2	-9.6	-9.9	-8.0	-4.9
MO_GO	-7.8	-13.9	-8.3	-7.2	-2.8	-7.9	-11.4	-11.0	-10.8	-3.3	-6.3	-9.2	-8.5	-7.4	-3.0
MO_MI_GO	-7.8	-13.5	-8.2	-6.7	-2.8	-7.7	-11.0	-11.0	-10.5	-3.3	-6.3	-9.0	-8.4	-6.9	-3.0
Obs. Mean	-8.1	-13.9	-8.3	-8.1	-3.5	-7.6	-11.0	-10.0	-13.2	-3.9	-6.6	-9.5	-8.2	-8.8	-3.6
Obs. Median	-8.3	-13.9	-8.3	-7.9	-3.4	-7.9	-11.4	-11.0	-12.0	-3.6	-6.4	-9.6	-8.4	-8.4	-3.5
Obs. ε	0.39	0.84	0.66	0.60	0.27	0.51	0.76	0.86	1.18	0.34	0.33	0.54	0.50	0.68	0.28
GOCART	-6.8	-10.3	-6.4	-5.1	-1.8	-6.8	-8.1	-10.4	-6.9	-2.3	-5.9	-7.8	-7.4	-5.0	-1.9
SPRINTARS	-2.0	-2.5	-2.5	-3.0	-0.7	-3.4	-4.1	-3.7	-3.4	-1.3	-2.1	-2.4	-3.4	-3.2	-1.1
GISS	-5.4	-6.7	-3.9	-4.6	-1.1	-3.5	-3.6	-6.8	-6.8	-1.7	-3.9	-5.0	-3.9	-3.9	-1.6
LMDZ-INCA	-6.1	-9.0	-6.0	-7.5	-3.7	-7.5	-11.7	-9.5	-11.1	-3.2	-5.7	-8.2	-6.4	-7.5	-3.1
LMDZ-LOA	-3.4	-4.4	-3.3	-4.3	-1.0	-3.8	-5.2	-5.8	-6.0	-1.2	-3.2	-4.2	-4.0	-4.2	-1.0
Mod. Mean	-4.7	-6.6	-4.4	-4.9	-1.7	-5.0	-6.5	-7.2	-6.8	-1.9	-4.2	-5.5	-5.0	-4.8	-1.7
Mod. Median	-5.4	-6.7	-3.9	-4.6	-1.1	-3.8	-5.2	-6.8	-6.8	-1.7	-3.9	-5.0	-4.0	-4.2	-1.6
Mod. ε	0.99	1.60	0.85	0.82	0.60	0.99	1.69	1.37	1.39	0.41	0.82	1.23	0.88	0.83	0.42
Mod./Obs.	0.65	0.48	0.47	0.58	0.32	0.48	0.46	0.62	0.57	0.47	0.61	0.52	0.48	0.50	0.46

Table 10. (a) Statistical measures of seasonal and regional average clear-sky TOA DRE estimates with respect to MODIS DRE over ocean (Remer and Kaufman, 2005), including linear correlation coefficient (r), mean ratio (B), and standard deviation of B (σ_B).

Products	r	B	σ_B
MODIS_A	0.88	1.28	0.33
CERES_A	0.93	0.99	0.23
CERES_B	0.91	0.77	0.19
CERES_C	0.93	1.03	0.21
MODIS_G	0.86	1.03	0.28
MISR_G	0.68	1.20	0.42
MO_GO	0.86	0.93	0.22
MO_MI_GO	0.82	0.91	0.24
GOCART	0.80	0.71	0.20
SPRINTARS	0.57	0.32	0.14
GISS	0.72	0.53	0.20
LMDZ-INCA	0.83	0.81	0.23
LMDZ-LOA	0.82	0.41	0.11

Table 10. (b) Statistical measures of seasonal and regional average clear-sky surface DRE estimates with respect to MODIS_A DRE over ocean (Bellouin et al., 2005[6]), including linear correlation coefficient (r), mean ratio (B), and standard deviation of B (σ_B).

Products	r	B	σ_B
MO_MI_GO	0.86	0.91	0.30
MO_GO	0.88	0.94	0.30
MODIS_G	0.89	1.08	0.35
MISR_G	0.82	1.21	0.41
GOCART	0.83	0.74	0.29
SPRINTARS	0.60	0.32	0.19
GISS	0.72	0.45	0.25
LMDZ-INCA	0.76	0.63	0.30
LMDZ-LOA	0.79	0.46	0.21

Table 11. AERONET aerosol and DRE climatology. Top panel: seasonal and zone averages of AOT (upper lines) and SSA (lower lines) at 550 nm; Middle panel: seasonal and zone averages of clear-sky aerosol direct radiative effect (DRE, Wm^{-2}) at the TOA (upper lines) and at the surface (lower lines) (Zhou et al., 2005); Bottom panel: blue dots indicate AERONET stations. Light blue shadows the continents.

AOT (upper) and SSA (lower)

DJF/ MAM/ JJA/ SON	DJF/ MAM/ JJA/ SON	DJF/ MAM/ JJA/ SON	DJF/ MAM/ JJA/ SON
0.05/0.11/0.15/0.08 0.92/0.92/0.90/0.89	0.09/0.14/0.31/0.12 0.93/0.92/0.93/0.89	0.15/0.22/0.22/0.21 0.94/0.92/0.90/0.90	0.20/0.36/0.34/0.20 0.93/0.92/0.90/0.88
	0.26/0.34/0.33/0.28 0.96/0.96/0.94/0.94	0.39/0.38/0.38/0.32 0.92/0.94/0.93/0.93	
	0.14/0.11/0.32/0.47 0.91/0.90/0.89/0.92	0.11/0.10/0.27/0.43 0.89/0.88/0.85/0.88	

DRE (Wm^{-2}) at the TOA (upper) and surface (lower)

DJF/ MAM/ JJA/ SON	DJF/ MAM/ JJA/ SON	DJF/ MAM/ JJA/ SON	DJF/ MAM/ JJA/ SON
−1.9/−4.4/−5.2/−2.7 −3.6/−10.1/−14.4/−6.7	−2.8/−6.0/−11.1/−4.5 −5.2/−12.8/−23.9/−10.8	−5.0/−7.0/−6.1/−5.8 −8.4/−17.6/−21.0/−14.9	−6.4/−10.7/−8.1/−5.3 −11.9/−28.2/−30.4/−15.7
	−8.4/−10.7/−10.4/−9.2 −14.5/−20.0/−23.2/−18.1	−9.1/−9.8/−9.0/−8.1 −23.8/−23.8/−24.3/−20.1	
	−3.9/−3.4/−7.2/−11.2 −11.4/−9.4/−23.3/−30.9	−2.7/−3.0/−6.4/−9.8 −10.6/−9.0/−23.5/−33.9	

AERONET Sites

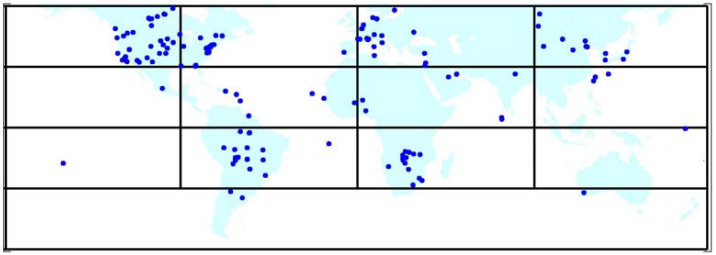

ACPD
5, 7647–7768, 2005

Table 12. Summary of the radiative efficiency E_τ ($Wm^{-2}\tau^{-1}$) in East US and mid-latitude North Atlantic.

Region	Period	Source	E_t	
			TOA	Surface
Zone 2 (land)	Summer	AERONET	-37	-84
		MODIS_A	-46	-73
		Models	-21~-37	-38~-66
	Annual	AERONET	-37	-80
		MODIS_A	-43	-69
		Models	-23~-34	-43~-55
SCAR-A (Land)	Summer	Kinne and Pueschel, 2001	-24	-65
US	Annual	Delene and Ogren (2002)	-25	n/a
Zone 2 (ocean)	Summer	MODIS	-50	
		MODIS_A	-58	-75
		CERES_A	-37	n/a
		CERES_B	-31	
		Models	-27~-42	-42~-76
TARFOX (Ocean)	Summer	Hignett et al., 1999	-30	-87
		Kinne and Pueschel, 2001	-33	-70
		Russell et al., 1999	-40~-60	-80~-90
ACE-2	Summer	Kinne and Pueschel, 2001	-36	-63

Table 13. Summary of the clear-sky radiative efficiency E_τ ($Wm^{-2}\tau^{-1}$) in Europe.

Region	Period	Source	E_t	
			TOA	Surface
Zone 3 (land)	Summer	AERONET	-29	-98
		MODIS_A	-34	-86
		Models	-13~-26	-36~-68
Almeria, Spain	Summer	Horvath et al., 2002	-11	-57
Vienna, Austria			-24	-68
Mediterranean Area	July-August, 2001	Markowicz et al., 2002	-34	-94

Table 14. Summary of the clear-sky radiative efficiency E_τ ($Wm^{-2}\tau^{-1}$) in East Asia and Northwest Pacific.

Region	Period	Source	E_τ	
			TOA	Surface
Zone 4 (ocean)	MAM	MODIS	-52	n/a
		CERES_A	-35	
		CERES_B	-31	
		MODIS_A	-50	-68
		Models	-25~-42	-45~-61
Northwest Pacific	April 2001	Seinfeld et al., 2004	-41	-71
Gosan, Korea	April, 2001	Bush and Valero, 2003	n/a	-80±11
Anmyon, Japan (ocean albedo)	Dust events (1998, 2000)	Kim et al., 2005	-26	-91
	Non-dust events (2000)		-22	-82
Gosan, Korea (ocean albedo)	Dust events (2001)		-21	-104
	Non-dust events (2001)		-29	-69
Amami-Oshima (ocean albedo)	Dust events (2001)		-12	-106
	Non-dust events (2000, 2001)		-18	-90
Zone 4 (land)	Fall	AERONET	-28	-82
		MODIS_A	-29	-66
		Models	-19~-27	-40~-54
Linan, East China (rural)	November, 1999	Xu et al., 2003	-33	-51
Dunhuang, China (desert)	April-July, 1998-2000	Kim et al., 2005	-9	-76
Yinchuan, China (urban)	September-December, 1997-2000		-16	-55
Sri-Samrong (SE Asia)	December-March, 1997-2000		-10	-63

Table 15. Summary of the clear-sky radiative efficiency E_τ ($Wm^{-2}\tau^{-1}$) in tropical North Atlantic.

Region	Period	Source	E_t	
			TOA	Surface
Zone 6 (ocean)	DJF	MODIS	-45	n/a
		CERES_A	-33	
		CERES_B	-28	
		MODIS_A	-46	-64
		Models	-16~-35	-36~-63
	JJA	MODIS	-34	n/a
		CERES_A	-32	
		CERES_B	-25	
		MODIS_A	-56	-78
		Models	-16~-41	-27~-68
West coast of North Africa	NDJ JJA	Li et al., 2004	-26 -35	-65 -85
	July 1998	Liu et al., 2003	-18	n/a
	February 1985 July, 1985	Hsu et al., 2000	-62 (1430LT) -69 (1430LT)	
Puerto Rico	June-July, 2000 (daytime average)	Christopher et al., 2003	-52	-78

Table 16. Summary of the clear-sky radiative efficiency E_τ ($Wm^{-2}\tau^{-1}$) in Arabian Sea, Northern Indian Ocean, and South Asia.

Region	Period	Source	E_τ	
			TOA	Surface
Zone 7 (ocean)	DJF	MODIS	-45	n/a
		CERES_A	-33	
		CERES_B	-26	
		MODIS_A	-44	-69
		Models	-15~-34	-39~-69
	MAM	MODIS	-35	n/a
		CERES_A	-29	
		CERES_B	-23	
		MODIS_A	-49	-76
		Models	-14~-37	-35~-77
	SON	MODIS	-36	n/a
		CERES_A	-32	
		CERES_B	-23	
		MODIS_A	-45	-71
		Models	-15~-36	-34~-63
Indian Ocean (INDOEX)	January-March, 1998, 1999	Satheesh and Ramanathan, 2000; Bush and Valero, 2002	-25~-30	-80~-86
Tropical Indian Ocean	Februray-March, 1998	Conant, 2000	n/a	-76
Tropical Indian Ocean	January-March, 1998, 1999	Podgorny et al., 2000	n/a	-82
Arabian Sea	March, 2001	Satheesh, 2002	-29	-74
Tropical Indian Ocean			-33	-52
Bay of Bengal			-16	-86
Bay of Bengal	October, 2003	Sumanth et al., 2004	-33	-60
Arabian Sea	January-March, 1996-2000	Tahnk and Coakley, 2002	-32 ~ -34	-57~ -67
Bay of Bengal			-31 ~ -32	-62 ~ -71
NH Indian Ocean			-31 ~ -33	-58 ~ -68
Nepal	Winter, 2003	Ramana et al., 2004	n/a	-73

Table 17. Summary of the clear-sky radiative efficiency E_τ ($Wm^{-2}\tau^{-1}$) in South America.

Region	Period	Source	E_t	
			TOA	Surface
Zone 10 (Land)	SON	AERONET	-25	-71
		MODIS_A	-27	-76
		Models	-10~-44	-43~-80
South America	SCAR-B	Kinne and Pueschel, 2001	-13	-72
		Ross et al., 1998	-20±7 (tropical froest) -8±9 (cerrado)	n/a
		Christopher et al., 2000	-20~-60 (depending on land cover)	
Amazon	August, 1998	Christopher and Zhang, 2002b	-26	n/a

Table 18. Uncertainty analysis of DCF at the TOA using only mean-values (regional and annual averages) of individual parameters. 20 bold numbers are required input parameters for the analysis. Green and red colors indicate with and without observational constraints, respectively. Black color indicates that the number is derived with a part of observational constraint.

	LAND				OCEAN				GLOBE		
Parameter	Mean	Uncert.	Relative Uncert.	Param. Uncert. Contrib. to DCF[a]	Mean	Uncert	Relative Uncert.	Param. Uncert. Contrib. to DCF[a]	Mean	Uncert.	Relative Uncert.
t [b]	**0.23**	**0.046**	20%	3%	**0.14**	**0.037**	26%	12%	0.17	0.04	24%
f_f [c]	**0.50**	**0.25**	50%	18%	**0.40**	**0.10**	25%	11%	0.43	0.15	34%
τ_f	0.115	0.062	54%		0.056	0.020	36%		0.074	0.033	45%
f_{af} [d]	**0.80**	**0.40**	50%	18%	**0.60**	**0.20**	33%	20%	0.660	0.260	39%
τ_a	0.092	0.068	73%		0.034	0.017	49%		0.051	0.032	62%
E_a [e]	**-19**	**6**	32%	7%	**-37**	**7**	20%	7%	-31.3	6.9	22%
DCF_{Clear}	-1.7	1.4	80%		-1.2	0.7	53%		-1.4	0.9	63%
$(1-A_c)$ [f]	**0.45**	**0.05**	11%	1%	**0.30**	**0.03**	10%	2%	0.35	0.04	
DCF [g]	-0.79	0.64	81%		-0.37	0.20	54%		-0.49	0.33	67%

(a) Parameter uncertainty contribution to DCF: contribution of this parameter (over land or ocean) to the uncertainty of global-mean DCF.
(b) Aerosol optical depth (τ): taken from MISR measurements over land (Kahn et al., 2005) and MODIS measurements over ocean (Remer et al., 2005).
(c) Fine-mode fraction of τ (f_f): over ocean, based on MODIS-AERONET comparisons (Kleidman et al., 2005); lack of observation constraint over land.
(d) Anthropogenic fraction of fine-mode τ (f_{af}): lack of observational constraint. Over ocean, the value is assigned so that the anthropogenic τ is consistent with estimate by Kaufman et al. (2005a).
(e) Forcing efficiency E_a ($Wm^{-2}\tau^{-1}$): assuming E_a=E_τ (for total aerosols). There should be some differences between E_a and E_τ because of differences in chemical composition and size of natural and anthropogenic aerosols. On the one hand, anthropogenic aerosol should be more absorptive than total aerosol (i.e., smaller single-scattering albedo) and hence has a smaller radiative efficiency. On the other hand, the smaller size may suggest a larger radiative efficiency consistent with larger backscattering and larger single-scattering albedo. E_a values over ocean are based on mean and one standard deviation of measurement-based E_τ. Over land, the measurement-based estimates are rare and the values assigned here are based on a combination of observations and models in this review.
(f) Cloud fraction Ac: mean values are based on MODIS measurements (King et al., 2003; Platnick et al., 2003). Uncertainties are assigned by considering daytime variations (Rossow and Schiffer, 1999).
(g) DCF regional: the value of DCF averaged over the land or ocean or globe, respectively.

Table 19. Summary of measurement-based clear-sky aerosol direct radiative effect estimates in the thermal infrared from the literature. The values generally refer to the clear-sky radiative efficiency E_τ at the TOA if not specified.

Region	Period	Thermal infrared effect	References	Notes
West Coast of North Africa	SHADE	+6Wm^{-2} +11Wm^{-2} (surface)	Highwood et al., 2003	10% of instantaneous solar effect
	February, 1985 July 1985	+24Wm$^{-2}\tau^{-1}$ +28Wm$^{-2}\tau^{-1}$	Hsu et al., 2000	1/3 of solar effect at 1430LT
Saharan deserts	September, 2000	+7 Wm^{-2} or 15 Wm$^{-2}\tau^{-1}$	Zhang and Christopher, 2003	Satellite overpassing time
	February, 1985 July 1985	+36 Wm$^{-2}\tau^{-1}$ +44 Wm$^{-2}\tau^{-1}$	Hsu et al., 2000	1430LT
Equator to 30N, 60W to 40E	SHADE	+1 Wm^{-2} +0.8 Wm^{-2}	Myhre et al., 2003	Clear-sky Whole-sky
West Coast of Europe	ACE-2	+1.2Wm^{-2}	Kinne and Pueschel, 2001	
Northwest Pacific	April, 2001 (ACE-Asia)	A few to 10 Wm^{-2}	Markowicz et al., 2003; Vogelmann et al., 2003	Daytime average; Depending on aerosol loading
Northwest Pacific	March, 1994	+3 Wm^{-2}	Kinne and Pueschel, 2001	Asian continental outflow
Arabian Sea	INDOEX	+1.3 Wm^{-2} +7.7 Wm^{-2} (surface) +2.7 Wm^{-2} +11 Wm^{-2} (surface)	Lubin et al., 2002	Within ABL High loading, more extended in the vertical

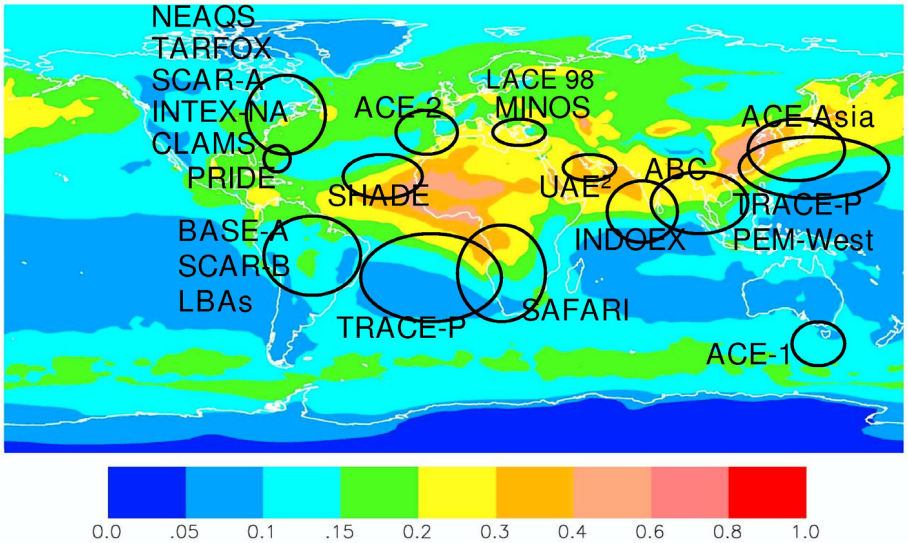

Fig. 1. Schematic of major intensive field experiments designed either mainly for aerosol research or by including aerosol characterization as part of an interdisciplinary research effort. The background represents the MODIS-MISR-GOCART integrated aerosol optical depth for 2001 (described in Sect. 3.1).

ACPD
5, 7647–7768, 2005

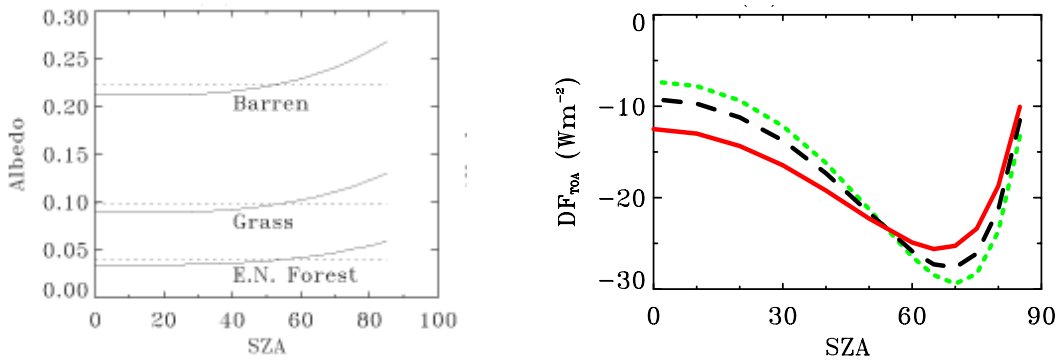

Fig. 2. Left: MODIS-derived black-sky (solid line) and white-sky albedo (dotted line) in the visible range for three land cover classifications, namely barren land, grass land, and evergreen needleleaf forest. The black-sky albedo increases with solar zenith angle (SZA) and equals the white-sky albedo at a SZA of about 55 degree. Right: Dependence of aerosol direct effect at the TOA on SZA over the grass land for prescribing white-sky albedo (green) and black-sky albedo (black), and calculating the surface reflectance based on model-calculated direct/diffuse ratio (red) (Yu et al., 2004).

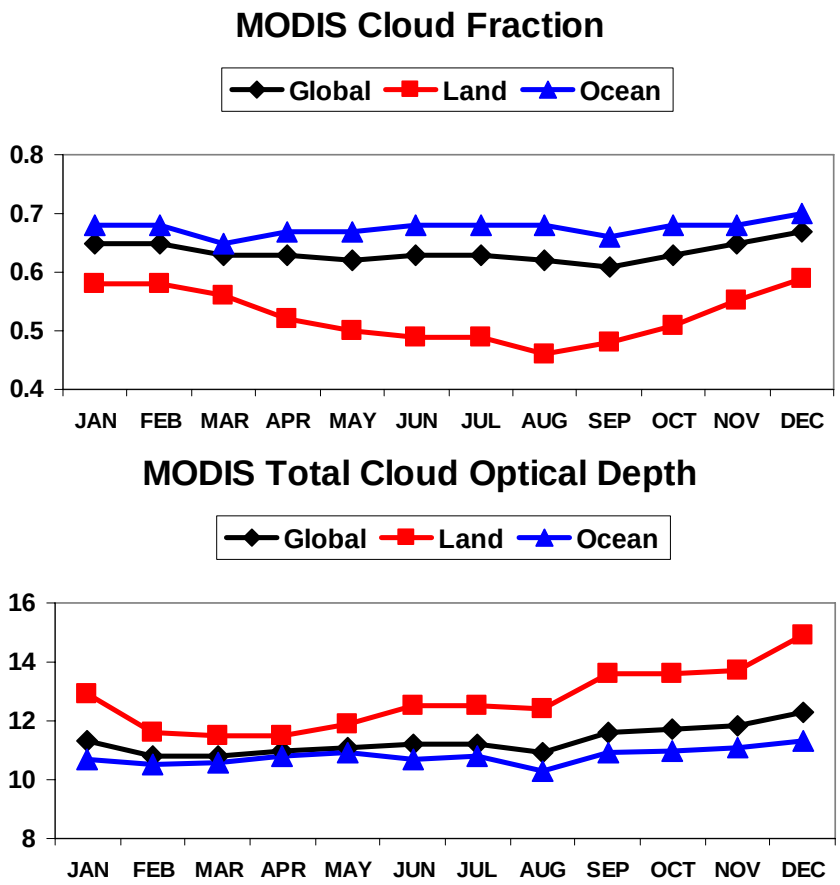

Fig. 3. Annual cycle (2001) of MODIS/Terra cloud fraction (top) and total cloud optical depth (bottom) averaged over globe, land, and ocean, respectively. (derived from MODIS Level 3 monthly 1°×1° cloud products as described in King et al., 2003b; Platnick et al., 2003).

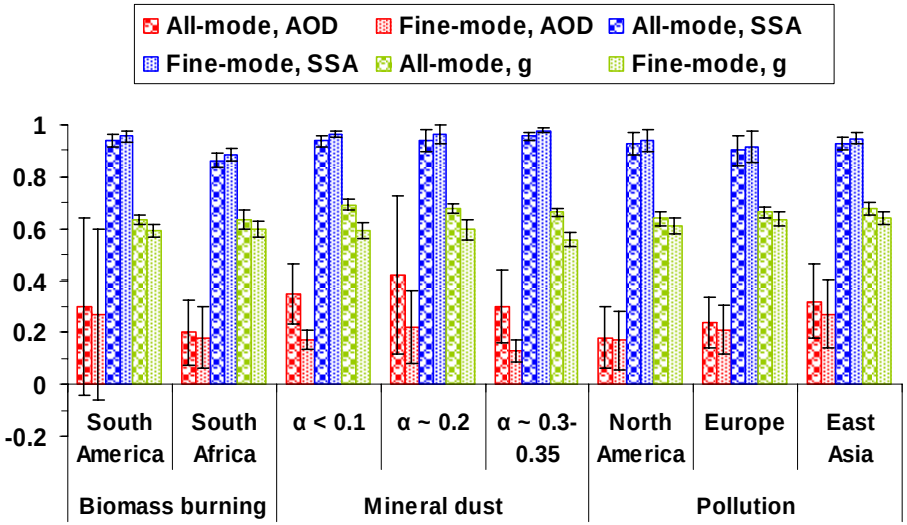

Fig. 4. (a) Mean values and standard deviations of AERONET aerosol optical depth (AOD), single-scattering albedo (SSA) and asymmetry factor (g) at 550 nm for typical aerosol types and over different geographical regions, where α is surface albedo. Standard deviation is shown as the error bar (Zhou et al., 2005).

ACPD
5, 7647–7768, 2005

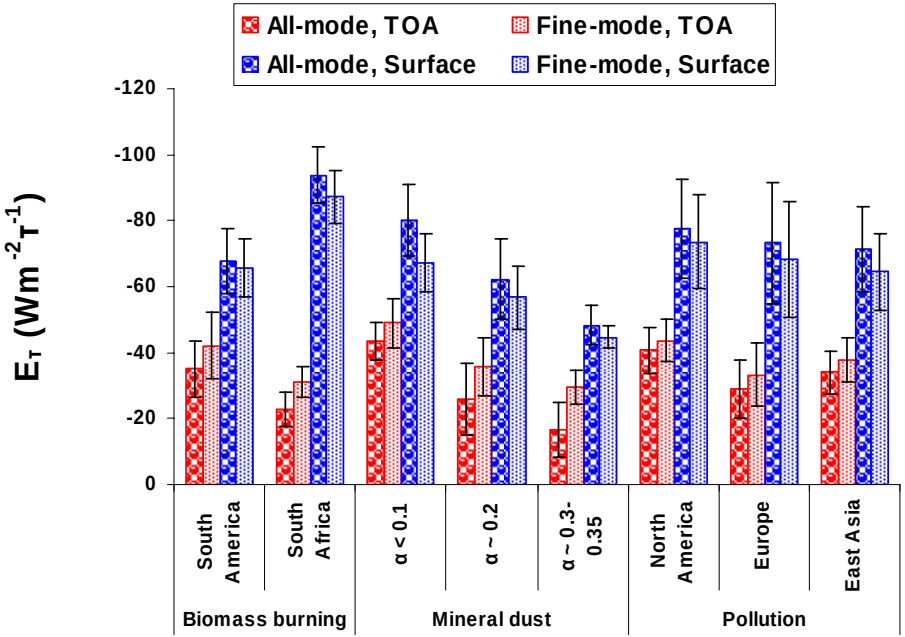

Fig. 4. (b) The clear-sky radiative efficiency E_τ (Wm$^{-2}\tau^{-1}$) at the TOA and the surface for typical aerosol types and over different geographical regions, which is calculated from AERONET aerosol climatology. α is surface albedo derived from MODIS land products (Zhou et al., 2005).

ACPD
5, 7647–7768, 2005

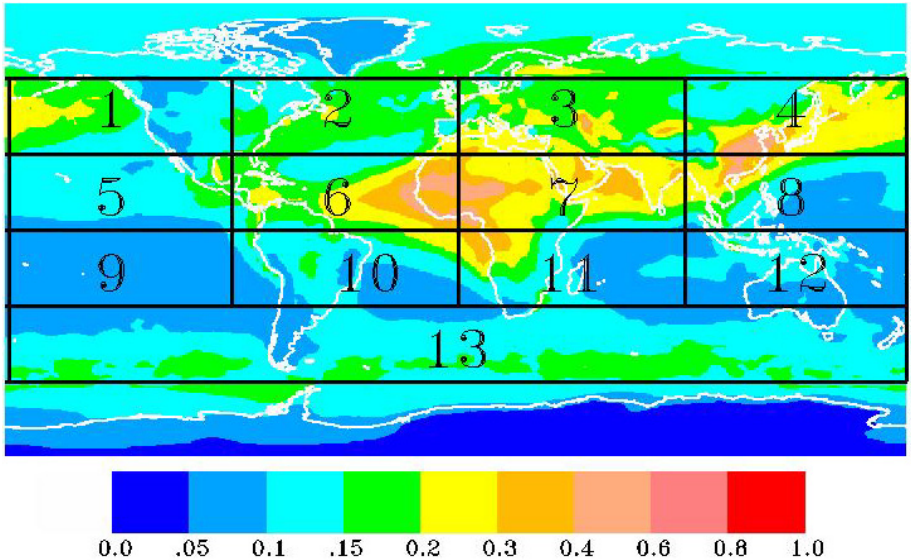

Fig. 5. Divisions of 13 zones defined for regional comparisons of aerosol and its direct effect. The background depicts the MODIS-MISR-GOCART integrated annual average aerosol optical depth at 550 nm for 2001 using the data assimilation approach as described in Yu et al. (2003).

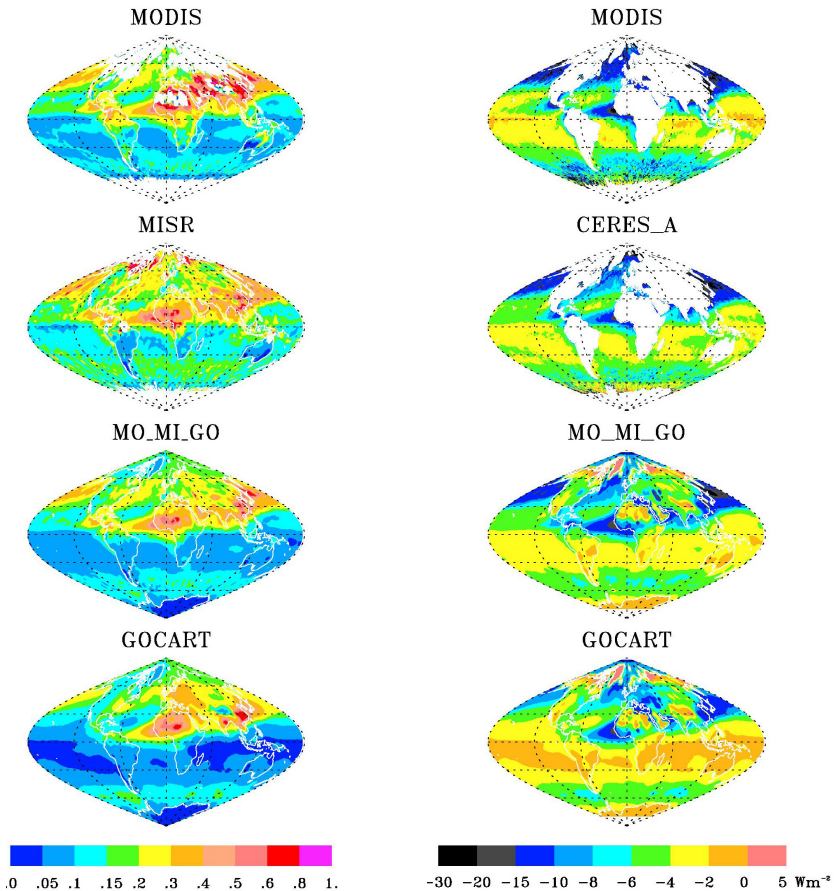

Fig. 6. Geographical patterns of seasonally (MAM) averaged aerosol optical depth at 550 nm (left panel) and the clear-sky aerosol direct solar effect (Wm^{-2}) at the TOA (right panel). Satellite retrievals are from the Terra satellite.

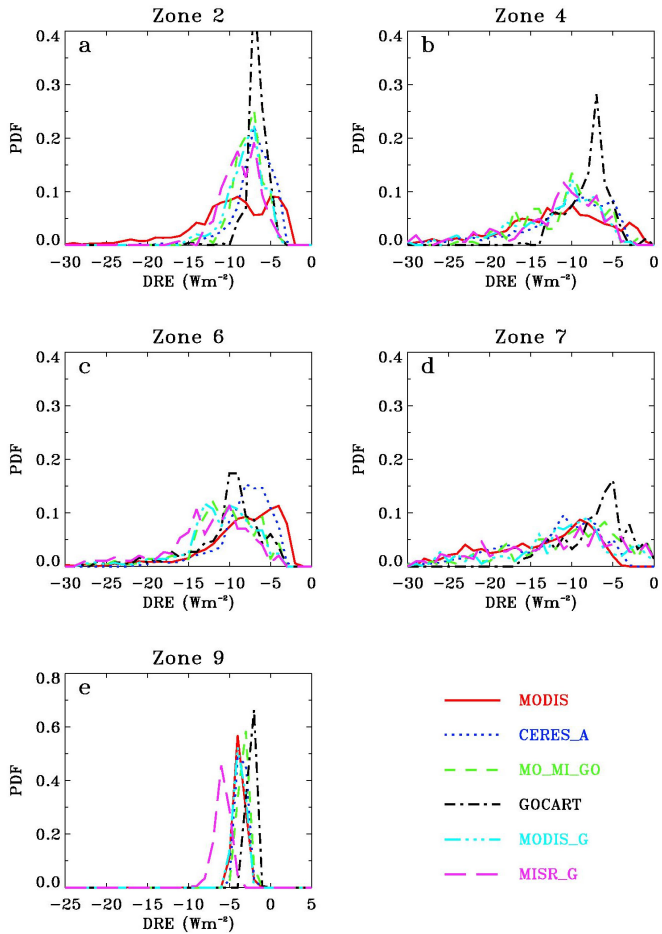

Fig. 7. Comparisons of probability density function (PDF) of clear-sky DRE estimates at the TOA over ocean in 5 different zones (see Fig. 5) for MAM.

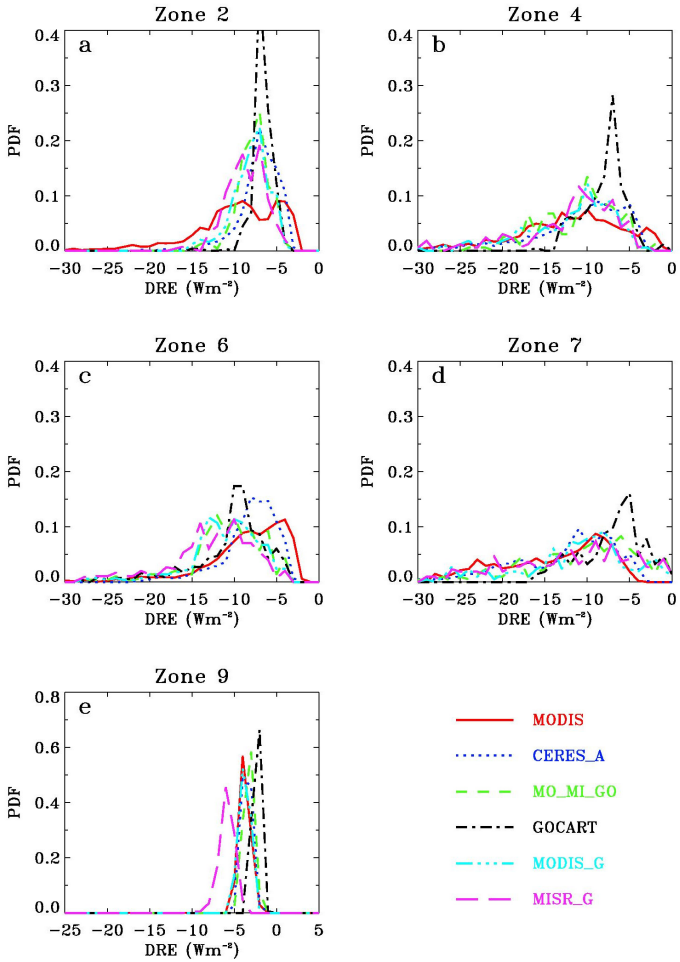

Fig. 8. Same as Fig. 7, but for JJA.

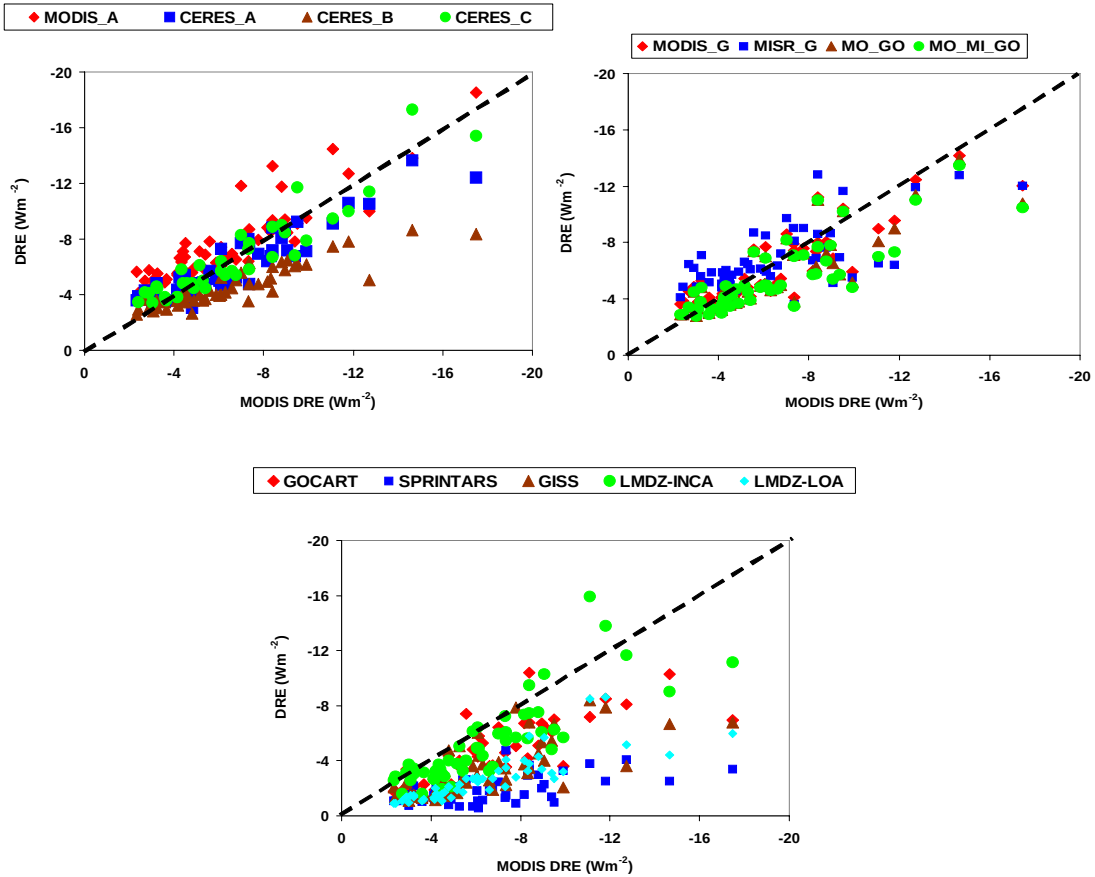

Fig. 9. (a) Scatterplots of the clear-sky and seasonal DRE estimates at the top of atmosphere (TOA) and over ocean. Each point represents a seasonal average in a particular zone.

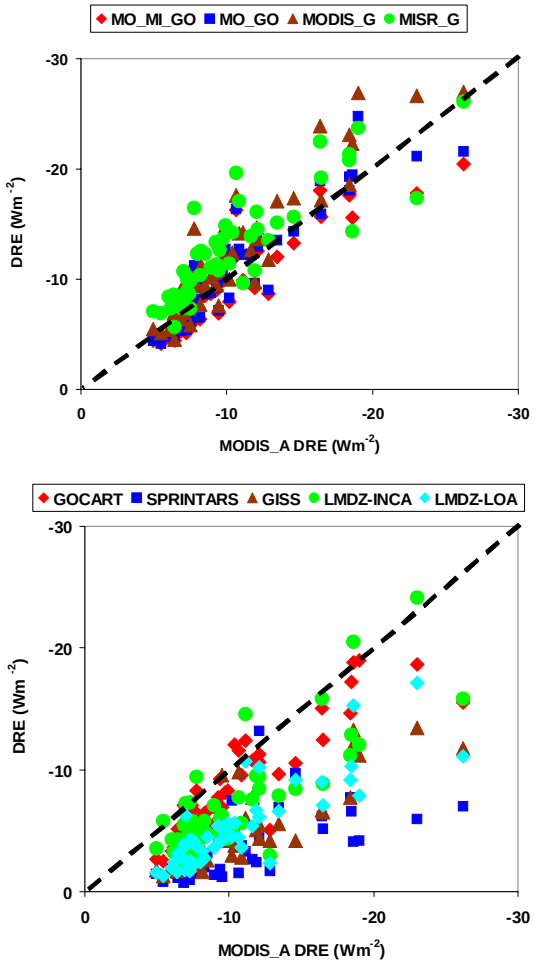

Fig. 9. (b) Scatterplots of the clear-sky and seasonal DRE estimates vs MODIS_A DRE at the surface and over ocean. Each point represents a seasonal average in a particular zone.

ACPD
5, 7647–7768, 2005

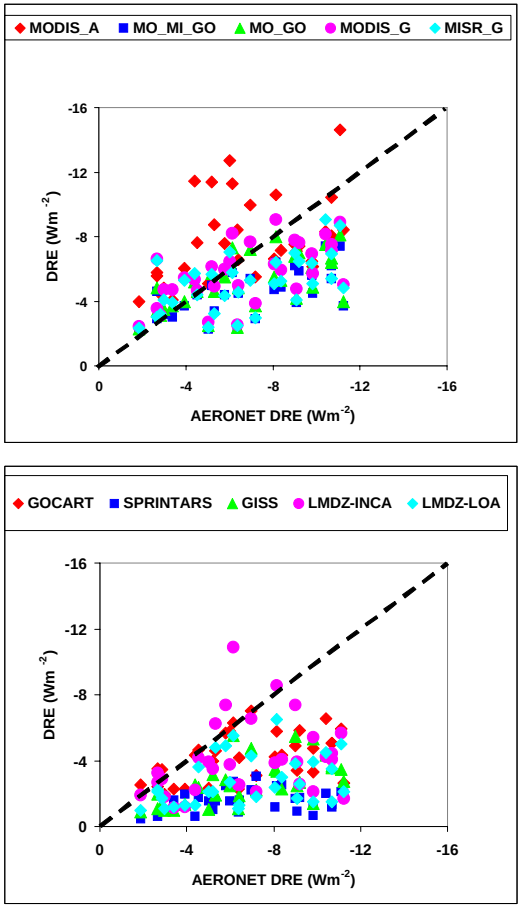

Fig. 10. (a) Scatterplots of the clear-sky and seasonal DRE estimates vs AERONET DRE at the TOA. Each point represents a seasonal average in a particular zone.

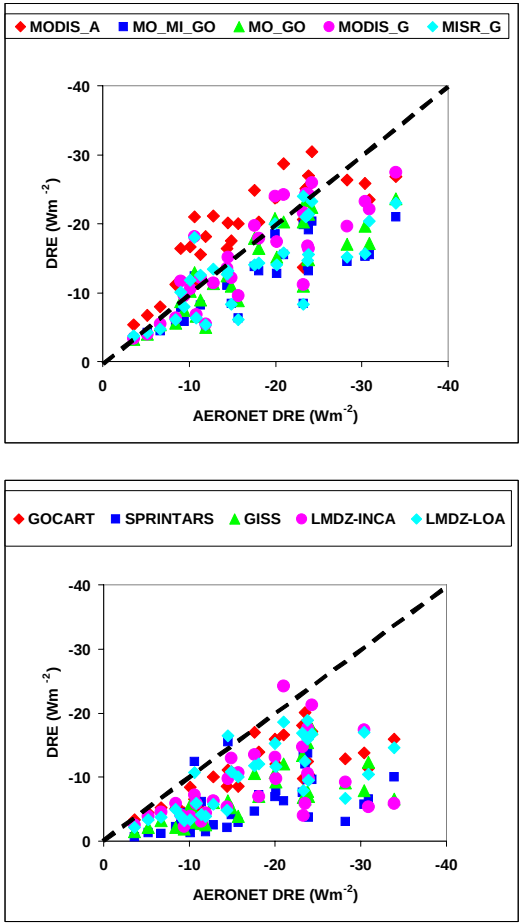

Fig. 10. (b) Scatterplots of the clear-sky and seasonal DRE estimates vs AERONET DRE at the surface. Each point represents a seasonal average in a particular zone.

ACPD
5, 7647–7768, 2005

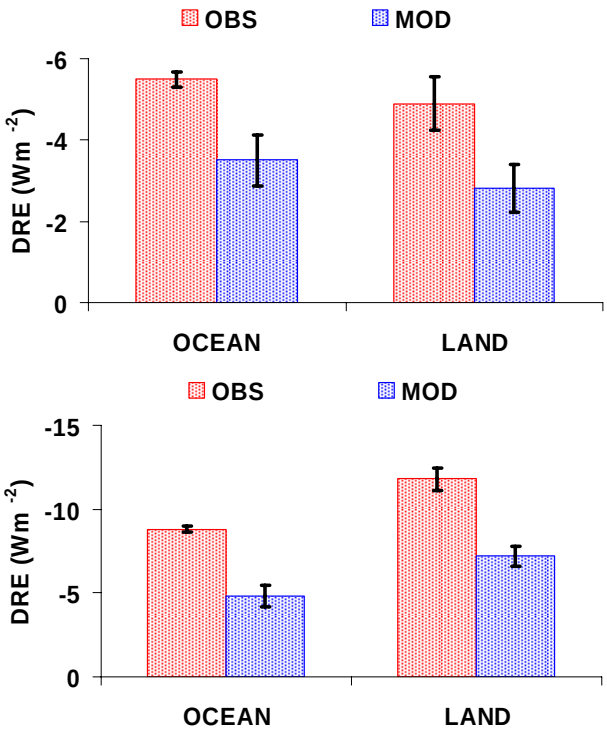

Fig. 11. Summary of observation- and model-based (denoted as OBS and MOD, respectively) estimates of clear-sky, annual average DRE at the TOA (top) and at the surface (bottom). The box and vertical bar represent median and standard error, respectively.